QUANTUM OPTICAL IMPLEMENTATION OF QUANTUM INFORMATION PROCESSING AND CLASSICAL SIMULATION OF MANY-BODY PHYSICS FROM QUANTUM INFORMATION PERSPECTIVE

by

Bin Wang

A dissertation submitted in partial fulfillment
of the requirements for the degree of
Doctor of Philosophy
(Physics)
in The University of Michigan
2008

Doctoral Committee:

Associate Professor Luming Duan, Chair
Professor Paul R. Berman
Professor Georg A. Raithel
Professor Duncan G. Steel
Assistant Professor Yaoyun Shi

To My Parents

ACKNOWLEDGEMENTS

I would like to thank my thesis advisor, Professor Luming Duan, for his support and guidance throughout my graduate study. He has always been easily accessible for questions and discussions, from which I have benefited a lot. I would also like to acknowledge all my committee members: Professor Paul Berman, Professor Duncan Steel, Professor Georg Raithel, and Professor Yaoyun Shi, for their critical reading of the manuscript.

Last but not least, I am grateful for the support from my family. I could not have possibly finished this thesis without their unselfish sacrifice.

TABLE OF CONTENTS

LIST OF FIGURES

Figure

CHAPTER I

Introduction

Quantum information processing, holding the promise to revolutionize information technology by incorporating fundamental laws of quantum mechanics into elements of information processing, has been attracting tremendous research interests over the past decade or so. The emergence of the idea of quantum information processing (QIP) can be at least dated back to the year 1982, when Feynman proposed to simulate one quantum system with another [1]. To simulate an arbitrary quantum system consisting of a large number of particles on classical computers in general is intractable, because the huge size of the Hilbert space required to describe the system grows exponentially with the number of particles in the system. Later on, interests in QIP were greatly stimulated in the mid 1990's, when ingenious quantum algorithms such as Shor's factoring [2] and Grover's Search [3] algorithms were developed. Factoring a large number or searching in an unsorted large database are classically hard mathematical problems, but with quantum algorithms their complexity can be greatly reduced. Following the discoveries of these intriguing algorithms as well as secure quantum communication protocols [4, 5, 6], great efforts have been made to pursue their physical implementations [7, 8, 9]. Nowadays, QIP has evolved into a highly interdisciplinary research field, in which problems of inter-

ests are extraordinarily diverse, including (but not limited to) designing more novel quantum computing algorithms to outperform classical computation capabilities, devising quantum communication protocols with unprecedented security level, understanding and characterizing quantum entanglement, as well as controlling quantum systems coherently to implement fault tolerant and scalable quantum information processing(QIP) devices. While it has been mainly focused on how to process information quantum mechanically, research in the field of quantum information science also sheds light on classical computation. The advancement of our understanding on quantum entanglement has led to the development of several novel algorithms for efficient classical simulation of strongly correlated quantum many-body physics [10, 11, 12, 13, 14, 15, 16, 17].

1.1 Basics of quantum information processing

To help understand fundamental principles of quantum information theory, it would be instructive to make comparison with its classical counterpart. As is well known, the primary building block of classical information is called a "bit", which takes values of either 0 or 1. Classical information is encoded as strings of bits and is processed by electric circuits constructed with classical logical gates. Naturally, the unit of quantum information is called "quantum bit", also known as "qubit". Unlike the classical bit, a qubit is a vector in a Hilbert space spanned by basis vectors $|0\rangle$ and $|1\rangle$, which can be visualized with the so-called Bloch sphere as shown in Fig. 1.1. While a classical bit is usually implemented by the voltage of either 0 or V across a capacitor, a qubit is physically represented by an effective two-level quantum system whose state can be generally expressed as a superposition of basis vectors in the form $\alpha|0\rangle + \beta|1\rangle$. Correspondingly, quantum information encoded in

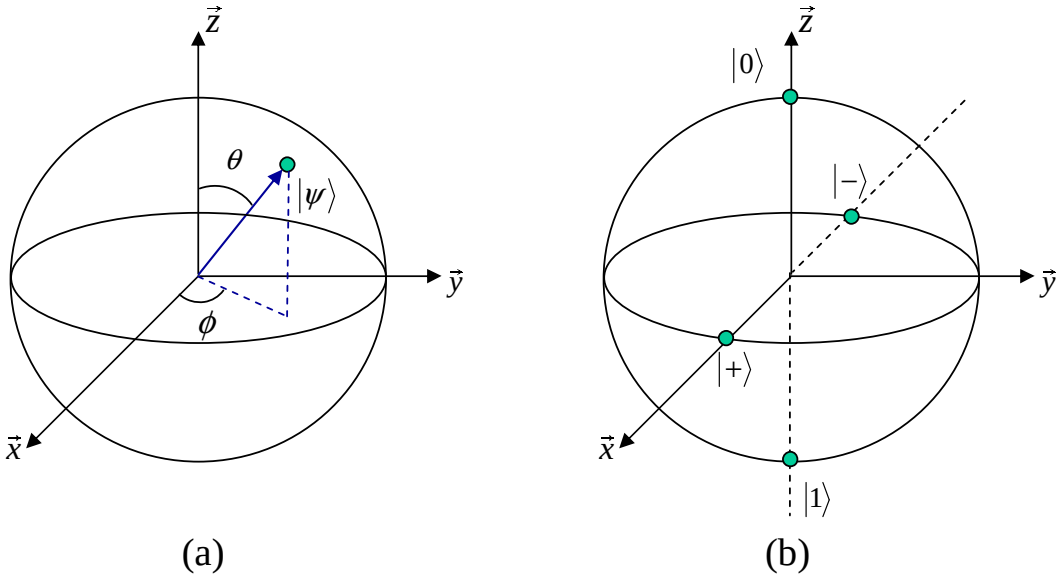

Figure 1.1: Bloch sphere representation of qubits. (a) An arbitrary qubit $|\psi\rangle = \alpha|0\rangle + \beta|1\rangle$ can be parameterized with two real numbers θ and ϕ corresponding to the polar and azimuthal angles in spherical coordinates as $|\psi\rangle = \cos\frac{\theta}{2}|0\rangle + e^{i\phi}\sin\frac{\theta}{2}|1\rangle$; (b) Bloch representations of four frequently used qubit states: $|0\rangle$ and $|1\rangle$ corresponds to spin-up and spin-down eigenvectors along z-axis; $|+\rangle$ and $|-\rangle$ corresponds to spin-up and spin-down eigenvectors along x-axis.

a string of N qubits is in general described by $\sum_{i_n=0,1} C_{i_1 i_2 \cdots i_N}|i_1\rangle \otimes |i_2\rangle \otimes \cdots |i_N\rangle$. Many intriguing features of quantum information are due to the superposition nature of quantum states together with the laws governing the measurement of a quantum state. For example, intuitively, a qubit seems to be able to contain more information than a classical bit as it could have arbitrary superposition coefficients. However, since measurement (of von Neumann type) on quantum systems induces collapse of quantum states into eigenstates of measured observables, given one copy of a qubit, one has no way to completely retrieve the magnitudes and phases of the original superposition coefficients. As a matter of fact, one qubit can only contain at most one bit of accessible classical information [18]. Besides, the superposition of quantum states also leads to quantum parallelism which is exploited in many quantum algorithms or quantum communication protocols [2, 3].

To process quantum information quantum mechanically, we also need to imple-

ment the quantum analogue of classical gates, namely quantum gates, which normally work on small number of designated qubits. Mathematically, quantum gates are represented by unitary operators (matrices). Due to their unitarity, it is not surprising that quantum gates are reversible, unlike most classical gates. A well-known example of reversible classical gates is the so-called Toffoli gate, which together with NOT and XOR gates constitutes a universal set of reversible classical gates. With a universal set of gates, one can construct any other gate and realize arbitrary algorithms. Fortunately, for quantum computation there also exist universal sets of quantum gates. For example, a continuous set of all single-qubit quantum gates and two-qubit controlled-NOT gate are sufficient to reproduce any arbitrary unitary operator exactly, thereby realizing universal quantum computing [19]. As a matter of fact, every single-qubit gate can be approximated to arbitrary accuracy with a finite number of discrete single-qubit gates. The controlled-NOT gate (see Fig. 1.2) is of great importance for QIP. Nonetheless it is only one choice from many universal controlled-unitary gates. For example, the controlled phase flip (CPF) gate is known to be equivalent to the controlled-NOT up to single-qubit unitary transformations. With current experimental technology, single-qubit rotations can be achieved with high precision relatively easily for most QIP candidate systems as compared with generic multi-qubit gates (which can not be reduced to products of single qubit gates).

Multi-qubit quantum gates are of central importance for QIP, in large part because they are indispensable for the manipulation of a precious resource in QIP called entanglement. When shared by remote parties, entanglement is especially useful for novel quantum communication protocols, such as quantum cryptography [4, 5, 6], quantum teleportation [20], and dense coding [21], etc. Entanglement,

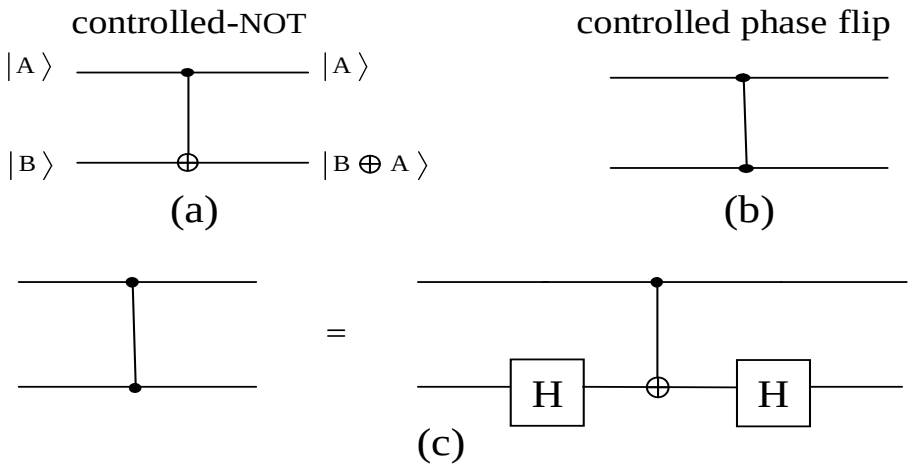

Figure 1.2: Controlled-NOT and controlled phase flip gates. (a) Controlled-NOT (CNOT) gate transforms two-qubit basis vectors according to $|00\rangle \mapsto |00\rangle$, $|01\rangle \mapsto |01\rangle$, $|10\rangle \mapsto |11\rangle$, and $|11\rangle \mapsto |10\rangle$; (b) Controlled phase flip (CPF) gate transforms two-qubit basis vectors according to $|00\rangle \mapsto |00\rangle$, $|01\rangle \mapsto |01\rangle$, $|10\rangle \mapsto |10\rangle$, and $|11\rangle \mapsto -|11\rangle$; (c) CNOT and CPF are equivalent to each other up to single-qubit Hadamard transformation (represented by the box labeled with "H"). The Hadamard gate transforms $|0\rangle$ to $|+\rangle$ and $|1\rangle$ to $|-\rangle$, and vice versa.

with no counterpart in classical physics, is a unique yet subtle phenomenon in quantum mechanics. For a bipartite or multipartite system with entanglement, states of its subsystems are correlated with each other and our knowledge about any specific subsystem is indefinite if we don't know what is going on in other subsystems. Understanding of entanglement has been a source of controversy since the birth of quantum mechanics [22, 23]. After many years of extensive study, people have not yet thoroughly understood the physics of quantum entanglement. For now, characterization and quantization of entanglement have only been achieved for limited cases [24, 25, 26, 27, 28]. The role of entanglement for generic quantum computation has not been fully revealed either. While the presence of entanglement is a necessary condition for quantum exponential speed-up compared with classical computation, it is not sufficient. Nontheless, advancement in quantum entanglement study has shed light on classical simulation of quantum many-body systems and led to the development of novel algorithms [10, 11, 12, 13, 14, 15, 16, 17].

Uncontrolled entanglement, however, could cause great trouble for implementation of QIP, inducing decoherence of qubit states [29]. In general, no QIP system can be completely isolated from its surroundings. The interaction between a quantum system and its environment generates entanglement between them, leading to leakage of quantum information from the system into the environment. In order to allow practical applications, the decoherence time of a qubit must be much longer than operation time of quantum gates. Nevertheless errors due to qubit decoherence as well as imperfect gate operations are often inevitable. In classical information processing, errors do occur too, but they can be efficiently corrected with redundant coding so that reliable performance of classical information processing is still guaranteed. But quantum error correction (QEC) is much more difficult than its classical counterpart. One reason is that errors themselves in QIP are much more complicated than classical errors which are simply bit flips. Various schemes of QEC have been proposed and extensively studied [30, 31, 32, 33, 34, 35]. Due to huge resource costs imposed by current QEC schemes, alternate paradigms to fault tolerant QIP are also being actively under pursuance [36, 37, 38].

1.2 Physical implementation of quantum information processing

Quantum information science has solid theoretical foundations as well as great potentials of practical applications. It is not hard to figure out why great efforts have been invested on construction of quantum information processors for quantum communication and computation. Quantum communication, in which usually only a few quantum computational steps are involved, is relatively easy to achieve as compared with universal quantum computing, and many quantum communication protocols can now be routinely implemented in laboratories. Nonetheless, to real-

ize long distance and high bit-rate communication, there are still great challenges to be overcome. On the other hand, for quantum computing, due to demanding requirements on reducing error rates below certain threshold, people are still working toward the goal of constructing a prototype quantum computer in laboratory. And until now, only certain quantum algorithms have been demonstrated with very limited number of qubits [39, 40, 41]. In principle, any effective two-level quantum system can be chosen as a physical qubit. However, considering practicality, only those systems satisfying the famous DiVincenzo criteria are viable choices for scalable quantum computing (5 criteria) and quantum networking (with 2 additional criteria). The criteria can be summarized as: 1. system is comprised of well characterized qubits and allows for scalability; 2. ability to initialize the state of the qubits; 3. system provides long coherence times, much longer than a gate operation time; 4. a universal set of gates is experimentally feasible; 5. qubit specific measurement capability; 6. ability to interconvert stationary and flying qubits; 7. faithful transmission of flying qubits between specified locations.

Based on the choice of physical qubit and control mechanism for QIP implementation, QIP candidate systems can be roughly divided into two categories, namely AMO and Condensed Matter systems. Trapped ions [42, 43, 44, 45], neutral atoms [46, 47, 48, 49, 50, 51, 52, 53], and photons [54, 55, 56] are common physical carriers of quantum information in AMO systems, which can usually be coherently manipulated with quantum optical techniques, while electron spins in quantum dots [57, 58, 59, 60, 61], Cooper pairs as well as current flux in superconducting circuits [8, 62, 63], and impurity spins in solids [64] are examples of physical carriers of qubits in condensed matter systems. An intriguing merit of condensed matter candidate systems is their association with the highly mature fabrication technology, which has

been developed for many years and has made great contribution to modern (classical) information technology. From this perspective, solid state systems could allow, more readily than AMO systems, highly compact and integrated construction of future quantum information processors. Nonetheless AMO systems in general provide "cleaner" environment for qubits as compared with condensed matter systems, therefore decoherence time of AMO qubits is usually longer than condensed matter qubits. As a tradeoff, gate operations on AMO qubits normally take longer time than those on condensed matter qubits. However, there is no sharp boundary for the division of condensed matter and AMO implementation of QIP. On one hand, quantum optical methods, which are considered as traditional tools for manipulations of AMO systems, are also being exploited in certain condensed matter QIP candidate systems [58, 59, 60]. On the other hand, fabrication techniques for condensed matter systems are now utilized to build new generation of traps for ions and neutral atoms on-chip [65, 66]. Moreover, interfaces between different systems are also under active pursuit. Although the exploration of QIP implementation in various quantum systems has been going on for many years, it is still not clear yet which (known or unknown) physical system(s) could finally fulfil all the stringent requirements for fault tolerance and scalability and could be adopted to build up the first prototype quantum computer in the future. In the rest of this section, we briefly introduce a few AMO candidate systems for quantum optical implementation of QIP.

Ions can be trapped relatively easily as compared with neutral atoms, by time-varying electric fields. Trapped alkaline earth ions have well-defined hyperfine manifolds of ground states with long decoherence time (on the order of 10 min), from which one can choose two levels as physical representation of qubits. The motion of ions is quantized in ion trap and can be cooled to its ground state with state-of-art quantum

optical techniques. The coupling of the motional states (environment) with internal levels (qubits) is a major source of decoherence for ion-trap based schemes. Using the quantum jump technique, a qubit can be efficiently read out with high accuracy. Single qubit operations can be readily achieved by applying the so-called Stimulated Raman Adiabatic Passage technique. Two-qubit gate has also been demonstrated with the original scheme proposed by Cirac and Zoller [42] or phase space geometric schemes [67, 68]. It is difficult to hold a large number of ions in a single linear trap for large scale QIP. To circumvent this scalability problem associated with ion-trap based system, it is proposed that one could store ions at different sections of a trap complex and then try to transport desired qubits to an operational region to get them interacting with each other [69, 70]. For now, experimentalists have demonstrated Grover's search algorithm for 4 ion qubits [41] and achieved entangled state W-state for up to eight ions [71].

Neutral atoms are relatively more insensitive to their environment as compared with ions, thereby in principle having a better qubit-scalability potential than ions. On the other hand, it is more difficult to trap and harness neutral atoms due to this property. Neutral atom qubits have long decoherence time. As with ions, initialization, detection, and single qubit rotation can be realized with standard quantum optical techniques. Cavity QED [72], either in the microwave [46] or optical [47] regime, is one of the promising candidate systems for neutral-atom based QIP. Alternate approaches for neutral atom quantum computation are based on state-dependent collision or dipole-blockade mechanisms for Rydberg atoms trapped in optical lattice systems [52, 53]. To load atoms in optical lattices, a superfluid-Mott insulator transition was proposed theoretically [73] and has been demonstrated in experiments [74].

Photons can be transported over long distance either through optical fibers or even in free space, thus they are well-suited for quantum communication and networking. Photons normally interact weakly with each other and with their environment, thereby having long decoherence time, but they could be easily absorbed. Errors in using photonic qubits mainly come from photon loss. In principle, there are many ways to encode qubits in photon pulses. One of the promising approaches is to use polarization states of single-photon pulses as qubits. For such photonic QIP schemes, single-qubit rotations can be routinely realized by using wave-plates or electro-optical crystals [55]. Entangled pair of photonic qubits and even more complicated entangled states of photons have been demonstrated based on parametric down conversion technique in nonlinear media [75, 76] as well as measurement induced entanglement generation technique with beam splitter and photon detectors [54]. It has also been proposed to use single atoms trapped in optical cavity to mediate effective interaction between photon pulses to realize photonic conditional gate operation [56]. Challenges for scalable QIP with these photon qubit based schemes are the relatively low generation rate of high quality single-photon pulses and low efficiency photon detectors.

Applications of optical cavity QED systems to quantum information processing (QIP) are mainly based on the ability to coherently convert quantum states between atomic qubits and photonic qubits. In particular, such ability has made cavity QED the most promising technique for realizing interface between different physical carriers of quantum information[77], which is indispensable for distributed QIP protocols. Over these years, many schemes for implementation of two-qubit entangling gate have been proposed for creating atom-photon, atom-atom, or photon-photon entanglements with cavity QED [48, 49, 56, 77, 78, 79]. In laboratories, the achievement of

trapping individual atoms and realizing strong atom-cavity field coupling has allowed only a few proof-of-principle demonstrations for some of these ideas [47]. In addition, optical cavity QED systems have provided an efficient approach to robust deterministic generation of single- and multiple- photon sources [80, 81, 82, 83, 84, 85, 86]. As first part of this thesis, in the following four Chapters, we will introduce optical cavity QED system in more details and present several pieces of our work on applications of such system to QIP [49, 79, 87].

1.3 Classical simulation of many-body physics from quantum information perspective

Along with the efforts in physical implementation of QIP, a great deal of attentions has also been given to foundations of quantum information theory, especially the theory of entanglement [24, 25, 26, 27, 28]. More recently the study of the entanglement properties of quantum many-body systems has already born fruits in the development of novel classical simulation techniques for quantum many-body systems [10, 11, 12, 13, 14, 15, 16, 17], i.e. generalizations of the Density Matrix Renormalization Group (DMRG) method [88, 89], as well as understanding of phase transitions in quantum spin systems [90, 91, 92, 93]. In Chapter VI, we will introduce an extension of the DMRG algorithm, namely the time evolving block decimation (TEBD) in detail [10, 11]. And by implementing such an algorithm, we have studied ground state properties of a novel effective Hamiltonian which can be engineered in optical lattice systems, and our work on this topic will presented in Chapters VII and VIII [94, 95].

Simulation of quantum many-body physics in general requires a lot of classical computing resources, which grow exponentially with the number of particles in the simulated quantum system. This fact has served as an early motivation for QIP,

although until now we are still unable to give a definite estimate on when a reliable large-scale (on the order of one hundred qubits) quantum simulator will become available. Nonetheless, certain strongly interacting quantum many-body systems can be efficiently simulated with classical computers by devising smart algorithms. As an outstanding example, DMRG has been a very powerful numerical method, which can be applied to study ground state properties of one-dimensional (1D) as well as quasi-two-dimensional strongly correlated quantum many-body systems. However, it did not perform well in simulations of quantum dynamics until very recently, when TEBD was developed. The TEBD algorithm catches the essence of entanglement scaling in 1D strongly interacting quantum systems. Unfortunately, TEBD can not be directly generalized to simulate generic two-dimensional (2D) strongly interacting systems, where more interesting physics is yet to be discovered. For example, solving 2D Hubbard model has been a long-standing goal in condensed matter physics, as it could reveal the theoretical mystery of high T_C superconductivity [96]. Fractional quantum Hall effect in 2D electron gas is another important problem remaining to be fully solved, which is critical for the study of topological quantum computation [38] besides its importance for fundamental physics. More recently, projected entangled pairs state (PEPS) [13, 17] and multiscale entanglement renormalization ansatz (MERA) [16] are proposed and developed, aiming to simulate certain classes of 2D quantum systems. It is not yet clear if one could ultimately conquer those interesting problems with classical computers by implementing the novel ideas such as PEPS or MERA. Nonetheless, stretching the capabilities of classical computers for quantum many-body systems is definitely worth a try while we are still working toward the goal of constructing a quantum computer.

1.4 Thesis Outline

In this thesis, we will present our study on theoretical proposals for various optical cavity QED implementation of QIP, as well as our numerical investigation on a strongly interacting ultracold fermionic system with the TEBD algorithm.

The main results of this thesis are summarized as follows:

- We propose a scheme for implementation of Schrodinger cat states in optical pulses with cavity QED. Our scheme can be readily extended to realize larger class of cat states targeting various QIP applications. We model the system and solve it numerically, so that we can estimate quantitatively the performance of our scheme. Our calculation shows that cat states with appreciable sizes could be realized with high fidelity.

- We propose a scheme to realize a robust conditional quantum gate acting on neutral atoms. The scheme exploits cavity aided scattering of single-photon pulses to mediate the strong interaction between the atoms. We numerically study the dynamics of the system and demonstrate that high fidelity gate operation can be achieved with finite success probability. Even with low success probability, our scheme still allows efficient fault tolerant quantum computing.

- We propose to implement a hybrid controlled-SWAP gate with a two-sided optical cavity system. We explicitly construct a photonic controlled phase flip gate to show that our scheme can be applied to realize universal photonic quantum computation. We analytically solve the model describing our system and quantitatively characterize the performance of our scheme.

- We implement an infinite lattice TEBD algorithm and apply it on a system of strongly interacting fermions in 1D optical lattice across a wide Feshbach

resonance. The system is described by a general Hubbard model with particle assisted tunnelling. Our results demonstrate that for such a system with equal spin population and repulsive on-site interaction superfluid and charge density wave could become dominant quasi-long-range orders when hole-doped below half filling. This feature is qualitatively different from the conventional repulsive-U Hubbard model in which regardless of the filling fraction superfluid and charge density wave are always suppressed and spin orders are dominant.

- With the TEBD algorithm, we numerically investigate the effect of particle assisted tunneling in a general Fermi-Hubbard model with spin-polarization and attractive on-site interaction. Our results demonstrate that FFLO type order in 1D attractive Hubbard model could be suppressed due to the presence of particle assisted tunneling. We also discuss the possible effect of particle density inhomogeneity based on local density approximation, and compare with the two-shell structure results of other groups.

In the following Chapter, we first introduce in detail the basic concepts in optical cavity QED systems as well as theoretical methods in quantum optics relevant to studies on such systems. Then in Chapters III, IV, and V, we present our theoretical proposals for Schrödinger cat state generation, robust conditional atomic gates operation, and hybrid controlled SWAP gate implementation with optical cavity QED. Chapter VI serves as an introduction to numerical methods for the second part of this thesis, where key ideas and formalism of the TEBD algorithm are explained with some details. Our TEBD study on a general Hubbard model with equal spin population and repulsive on-site interaction is presented in Chapter VII. In Chapter VIII, we present our work on the same general Hubbard model Hamiltonian but with spin-polarization and attractive on-site interaction. Finally, in Chapter IX, we

summarize the thesis and discuss possible directions for future studies.

CHAPTER II

Review of Optical Cavity QED

Trapping of neutral atoms in high finesse optical cavities constitutes one of the foremost frontiers of quantum optics. Strong coherent interactions between trapped atoms and cavity field have been achieved and opened up possibilities for various applications in quantum information processing (QIP). Before presenting our work on theoretical proposals for QIP implementation with cavity QED systems, in this chapter, we first review basic concepts associated with cavity QED experiment. Then we present an introduction to some theoretical models and methods of quantum optics relevant to cavity QED.

2.1 Basics of Optical Cavity QED

An optical cavity or optical resonator is an arrangement of mirrors that forms a standing wave cavity resonator for light waves [72]. We consider a one-dimensional optical cavity with a pair of mirrors separated by a distance l as is shown in Fig. 2.1. The cavity mirrors usually have high reflectance $\mathcal{R}$, which could be very close to unity, and small yet non-vanishing transmittance $\mathcal{T}$. Another important basic parameter to characterize the cavity mirrors is the mirror absorption loss $\mathcal{L}$, as real cavity mirrors are not perfect and they absorb photons inevitably.

With the above basic parameters, we can further characterize optical cavities by

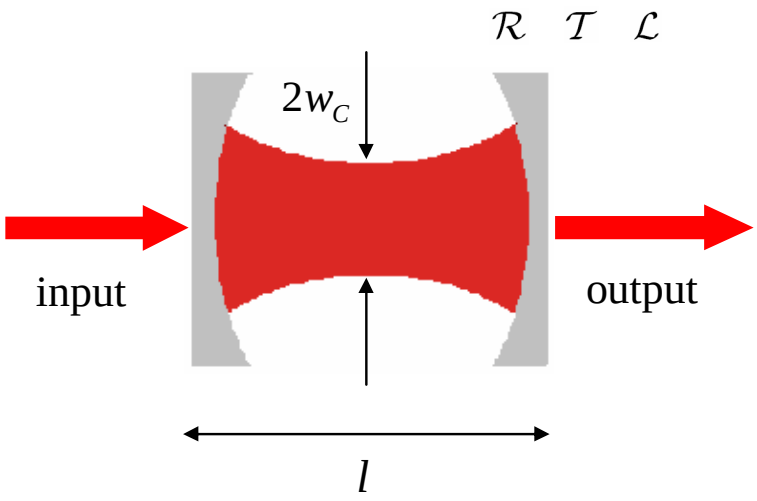

Figure 2.1: Schematic plot of an optical cavity. The cavity mirrors are characterized with its reflectance $\mathcal{R}$, transmittance $\mathcal{T}$, and absorption loss $\mathcal{L}$. The waist of the cavity's Gaussian TEM_{00} mode is given by w_C, which determines the spatial distribution of the field intensity of the corresponding mode.

defining other important parameters. The finesse of a cavity, indicating the number of bounces of a photon in the cavity, can be expressed as $\mathcal{F} = \pi\sqrt{\mathcal{R}}/(1-\mathcal{R})$. The transmission of light through cavity mirrors is periodic in light frequency and reaches its maximum when the light frequency is on resonance with a cavity mode. The so-called free spectral range is defined as the frequency difference between two adjacent transmission maxima and can be expressed as $\delta_{fsr} = \pi c/l$. Near resonance the cavity transmission can be described by a Lorentzian $\mathcal{T} \propto \kappa^2/(\kappa^2+\Delta^2)$, where $\Delta = \omega_L - \omega_C$ is the detuning between laser frequency ω_L and cavity resonance frequency ω_C. The half line-width of the Lorentzian gives the decay rate of the cavity field, which can be obtained through $\kappa = \delta_{fsr}/2\mathcal{F}$.

In optical cavity experiments, cavity mirrors are usually processed to be slightly curved to achieve stable single-mode operations. The curvature of the mirrors normally leads to Gaussian eigen-modes. For a Gaussian TEM_{00} mode, the waist w_C of the mode, i.e. the smallest radius where field strength is e^{-1} of that at the center, is given by $w_C^2 = \lambda\sqrt{l(2R-l)}/2\pi$, where λ is the wavelength of the laser sent toward

the cavity and R stands for the curvature of cavity mirrors. The spatial distribution of the TEM_{00} mode is given by $\psi(r) = \cos(kz)\exp[-(x^2+y^2)/w_C^2]$, where we have chosen the longitudinal axis of the cavity system to be z-axis and k stands for the wave vector of the laser shining on the cavity mirror along the z direction. The electromagnetic mode volume can be obtained by integrating over the spatial distribution of the cavity mode: $V_m = \int |\psi(r)|^2 dV$. For the Gaussian TEM_{00} mode, the mode volume can be readily evaluated and is given by $\pi w_C^2 l/4$. It is straightforward to understand that a smaller mode volume will lead to a stronger electromagnetic field in the cavity, thereby a stronger coupling between the cavity field and the atoms.

Given a high finesse optical cavity with a small mode volume, in order to achieve a strong atom-cavity coupling one also needs to create an appropriate optical potential to confine atoms in the cavity. Diverse approaches to the creation of such confinement potentials have been pursued, including the use of Far Off Resonant Trapping (FORT) beams [97] and the use of th cavity optical field itself [98, 99]. Trapping techniques which are compatible with strong coupling while not interfering with cavity QED interactions are crucial for the applications of cavity QED to QIP. To understand the physics of the optical confinement of an atom, let us consider an atom in an oscillating electromagnetic field created by laser beams which are far off resonance with the atomic transitions. The atom will acquire an induced electric dipole moment following the oscillating field, $\mathbf{d} = \alpha \mathbf{E}(\mathbf{r}, t)$, thereby experiencing an electric dipole potential $U = -\mathbf{d}\cdot\mathbf{E} \propto I(\mathbf{r})$, where α represents in general the dielectric polarizability tensor of the atom and $I(\mathbf{r})$ is the intensity of the optical field. Therefore, a desired trapping potential can be achieved in principle by arranging an appropriate spatial distribution of the field intensity. For a two-level atom, the potential can be analytically evaluated in the large detuning limit and it assumes

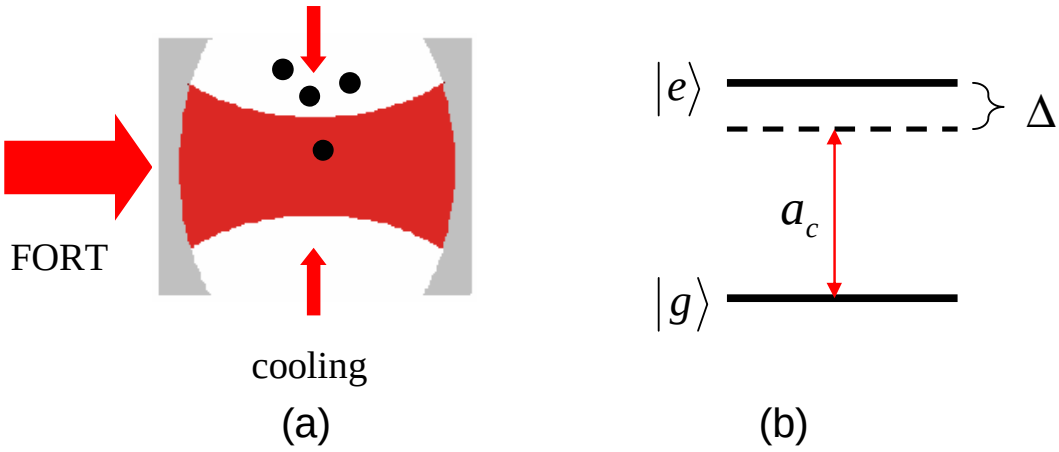

Figure 2.2: Cartoon illustration of trapping of atoms in an optical cavity and coupling between atomic transition with cavity mode. (a) Atoms are cooled and held in a MOT trap above an optical cavity. After optical trapping potential for atoms in the cavity is established with FORT beams, the atoms are released from the MOT trap. Certain number of atoms will be caught by the confining potential in the cavity and with the aid of cooling beams, they can be confined in the cavity for seconds. (b) The atomic transition between two levels $|g\rangle$ and $|e\rangle$ is strongly coupled with a cavity mode a_c. Δ measures the detuning between cavity mode a_c and the atomic resonance.

the form $U = 3\pi\gamma c^2 I/(\omega_0^3\Delta)$ [100], where γ is the spontaneous emission rate of the atom, ω_0 is the atomic resonance frequency and Δ is the large detuning between the laser frequency and ω_0. To load the atoms into cavities, in experiments the atoms are usually first cooled and held in MOT traps above a cavity. Once the trapping potential in the cavity is established, the atoms are released from the MOT trap and a certain number of atoms will be trapped in the cavity [101, 102]. See Fig. 2.2(a) for an illustration. The number of trapped atoms can be resolved by sending probing laser beams followed by detecting transmitted light signals [103].

2.2 Jaynes-Cummings Hamiltonian and Beyond

The light field in a cavity is treated as a quantized optical field, as indicated by the term "cavity QED". The quantized electromagnetic field is described by annihilation and creation operators associated with the field, for example, a_c and $a_c^\dagger$ for a cavity mode c. The field operators satisfy the standard commutation relations $[a_c, a_{c'}^\dagger] =$

$\delta_{c,c'}$, $[a_c, a_{c'}] = 0$, and $[a_c^\dagger, a_{c'}^\dagger] = 0$. An atom with two discrete orthonormal levels, $|g\rangle$ and $|e\rangle$, can interact with a mode of the quantized cavity field through electric dipole interaction if not forbidden by the selection rules (Fig. 2.2(b)). The dipole operator of the two-level atom has the general form $\mu = \mu^*\sigma_+ + \mu\sigma_-$ with $\sigma_+ = |e\rangle\langle g|$ and $\sigma_- = (\sigma_+)^\dagger = |g\rangle\langle e|$, while the electric field (here we only consider a single cavity mode strongly coupled with the atomic transition) is given by

$$\mathbf{E}(\mathbf{r}, t) = \left(\frac{\hbar\omega_c}{2\epsilon_0 V_m}\right)^{1/2} \psi(\mathbf{r})\epsilon \left[a_c + a_c^\dagger\right], \tag{2.1}$$

where ω_c is the resonant frequency of cavity mode c, V_m is the mode volume, ϵ_0 is the vacuum permittivity constant, $\psi(\mathbf{r})$ describes the spatial distribution of the electric field, and ϵ stands for the polarization vector of the field. Therefore, the electric dipole interaction Hamiltonian $H_{int} = -\mu \cdot \mathbf{E}(\mathbf{r}, t)$ can be obtained to be

$$H_{int} = -\hbar g(\sigma_+ + \sigma_-)(a_c + a_c^\dagger), \tag{2.2}$$

where we have assumed that μ is real and

$$g = \mu \cdot \epsilon \left(\frac{\omega_c}{2\hbar\epsilon_0 V_m}\right)^{1/2} \psi(r) \equiv g_0\psi(r) \tag{2.3}$$

characterizes the strength of the atom-cavity field coupling. Consider an atom locating at an antinode of the standing wave formed in the cavity, where the coupling takes its maximal value $g = g_0$. In this case, the complete Hamiltonian of the atom-cavity system is then given by:

$$H = \hbar\omega_g|g\rangle\langle g| + \hbar\omega_e|e\rangle\langle e| + \hbar\omega_c\left(a_c^\dagger a_c + \frac{1}{2}\right) - \hbar g_0(\sigma_+ + \sigma_-)(a_c + a_c^\dagger), \tag{2.4}$$

which can be transformed into an interaction picture Hamiltonian H_I according to $H_I = i\hbar\dot{U}U^\dagger + UHU^\dagger$, with

$$U = \exp\left[i\frac{\omega_e + \omega_g - \omega_c}{2}t|g\rangle\langle g| + i\frac{\omega_e + \omega_g + \omega_c}{2}t|e\rangle\langle e| + i\omega_c t\left(a_c^\dagger a_c + \frac{1}{2}\right)\right]. \tag{2.5}$$

After some straightforward algebra, one can obtain:

$$H_I = \frac{\hbar\Delta}{2}\sigma_z - \hbar g_0 \left(\sigma_+ \exp\left(i\omega_c t\right) + \sigma_- \exp\left(-i\omega_c t\right)\right)\left(a_c \exp\left(-i\omega_c t\right) + a_c^\dagger \exp\left(i\omega_c t\right)\right), \tag{2.6}$$

where $\Delta = \omega_e - \omega_g - \omega_c$ is the detuning between the cavity mode frequency and the atomic resonance frequency and $\sigma_z = [\sigma_+, \sigma_-] = |e\rangle\langle e| - |g\rangle\langle g|$ is the pseudospin-z operator for the two-level atom. After throwing away the fast-oscillating terms, i.e. $\sigma_- a_c \exp\left(-2i\omega_c t\right)$ and its hermitian conjugate, according to the well-known Rotating Wave Approximation (RWA), we finally arrive at the famous Jaynes-Cummings Hamiltonian describing the electric dipole interaction between a two-level atom and a single-mode cavity field: [104]

$$H_I = \frac{\hbar\Delta}{2}\sigma_z - \hbar g_0(a_c\sigma_+ + a_c^\dagger\sigma_-). \tag{2.7}$$

It is obvious that for an arbitrary intra-cavity photon number $n \geq 1$, only the pair of states $|g, n\rangle$ and $|e, n-1\rangle$ is coupled. Therefore, the system can be effectively viewed as a set of independent two-level systems. From this analogy, one can easily write down the eigen-frequecies of the system:

$$\omega_n^\pm = \omega_c\left(n + \frac{1}{2}\right) + \frac{1}{2}\left(\Delta \pm \sqrt{4ng_0^2 + \Delta^2}\right), \tag{2.8}$$

with the corresponding eigenvectors:

$$|+\rangle_n = \cos\phi_n|g, n\rangle - \sin\phi_n|e, n-1\rangle; \tag{2.9}$$

$$|-\rangle_n = \sin\phi_n|g, n\rangle + \cos\phi_n|e, n-1\rangle, \tag{2.10}$$

where ϕ_n is given by $\tan\phi_n = \frac{\sqrt{4ng_0^2+\Delta^2}+\Delta}{2g_0\sqrt{n}}$. The coupling between the atom and the cavity field leads to the splitting of photon number states into doublets of dressed states (except for the case when the atom is in its ground state and there is no photons

in the cavity). Therefore one can expect that the presence of a resonant atom-cavity coupling would dramatically change the transmission property of the cavity system. The vacuum-Rabi frequency $2g_0$ can actually be obtained by measuring the cavity transmission spectrum. With suitable parameters, each cavity transmission peak will be split into two peaks with one appearing below and the other above the unperturbed cavity resonance. This effect is known as normal mode splitting [105].

To describe the scattering of an optical pulse with the atom-cavity system, one has to go beyond the standard Jaynes-Cummings model as the external driving field and the cavity decay κ, as well as the atom spontaneous emission, must be taken into account. In principle, for different purposes, one could use different theoretical methods. As an example, we consider the normal mode splitting effect by adopting a non-Hermitian Hamiltonian to include the relevant relaxation rates. The effective non-Hermitian Hamiltonian under RWA can be written as

$$H = H_c + H_a - \hbar g_0(a_c\sigma_+ + a_c^\dagger\sigma_-) - i\hbar\gamma|e\rangle\langle e| - i\hbar\kappa a_c^\dagger a_c, \tag{2.11}$$

where $H_c = \hbar\omega_c(a_c^\dagger a_c + 1/2)$ and $H_a = \hbar\omega_g|g\rangle\langle g| = \hbar\omega_e|e\rangle\langle e|$ are interaction-free Hamiltonians of the cavity field and two-level atom, respectively. The solution to the eigenvalue problem of this non-Hermitian Hamiltonian gives complex eigen frequencies. The real part of the complex eigen-frequency characterizes the mode splitting, while the imaginary part describes the decay of its corresponding eigen-state. In particular, in the low excitation case when only the states $|\pm\rangle_n$ with $n = 1$ are relevant, the splitting is given by $\delta = \sqrt{4g_0^2 - (\gamma - \kappa)^2}$. To further study the transmissivity of the cavity in this case, one can add another term to the non-Hermitian Hamiltonian to account for the weak laser beam driving the cavity field $H_p = -i\hbar\eta(a_c - a_c^\dagger)$. In the case of low cavity excitation (at most one photon presents in the cavity), the

quantum state of the atom-cavity system can be expanded in the form:

$$|\Psi(t)\rangle = c_0|g,0\rangle + c_g|g,1\rangle + c_e|e,0\rangle. \tag{2.12}$$

According to the Schrödinger equation, one can write down a set of differential equations for the expansion coefficients. The equations can in general be numerically solved. Nonetheless, with some reasonable approximations, we can analytically solve the problem under certain conditions. As the cavity mirrors have high reflectance and the driving field is weak as we assumed previously, we expect that $c_0 \approx 1$ throughout the process. We further assume that the atom-cavity coupling is in resonance, while the driving laser has a detuning with respect to the cavity resonance, $\Delta_L = \omega_c - \omega_L$. In this case, after transforming the Hamiltonian to a frame rotating with the driving laser frequency ω_L and applying RWA, we obtain:

$$i\dot{c_e} = -g_0 c_g + (\Delta_L - i\gamma)c_e; \tag{2.13}$$

$$i\dot{c_g} = -g_0 c_e + (\Delta_L - i\kappa)c_g + i\eta. \tag{2.14}$$

The transmittance is proportional to the average photon number $\langle n\rangle$ in the cavity under steady-state condition ($\dot{c}_g = \dot{c}_e = 0$), therefore we can easily solve the set of linear equations and write down:

$$\mathcal{T} \propto \langle n\rangle = c_g c_g^* = \left(\frac{\eta}{\kappa}\right)^2 \left|\frac{\kappa(\gamma - i\Delta_L)}{(\Delta_L - \omega_1^+)(\Delta_L - \omega_1^-)}\right|, \tag{2.15}$$

where $\omega_1^{\pm} = \pm\sqrt{4g_0^2 - (\gamma-\kappa)^2} - i(\gamma+\kappa)$. Other interesting phenomena, such as the enhanced spontaneous emission of the trapped atoms [106, 107], etc could also be studied with similar method. In the following three chapters, we will present our work on theoretical proposals for the applications of cavity QED to QIP, along with which we will also encounter more theoretical methods for our models beyond the Jaynes-Cummings Hamiltonian.

2.3 Chapter Summary

In this chapter, we have introduced fundamental concepts of optical cavity QED, as well as basic model and methods for theoretical study on the atom-cavity system. This chapter serves as an introduction to the first part of this thesis, namely quantum optical implementation of QIP with optical cavity QED. In the following three chapters I will present our work on optical cavity QED applications to cat states engineering, robust neutral atom conditional gates implementation, and a hybrid controlled SWAP gate operation scheme.

CHAPTER III

Engineering Schrödinger Cat States of Optical Pulses with Cavity QED

In the previous chapter, we have introduced basic concepts in cavity QED as well as some relevant theoretical models and methods. In this chapter, we present a scheme for the implementation of Schrödinger cat states with optical cavity QED. We develop a numerical method to solve the dynamics of the system, which enables us to investigate the effects of possible sources of noise and characterize the performance of our scheme.

3.1 Introduction

Schrödinger's cat originally referred to a thought experiment proposed by Erwin Schrödinger [108], in which the quantum state of a macroscopic object, a cat, being either 'alive' or 'dead', gets entangled with the quantum state of a radiative two-level atom. The system of the cat and the atom is well shielded from its environment and its total state can be expressed in the form $|\psi\rangle \propto |0\rangle|\text{alive}\rangle + |1\rangle|\text{dead}\rangle$. This thought experiment was first brought up to challenge the interpretation of quantum mechanics, specifically the collapse of a superposition state upon quantum measurements. Later on, it has also invoked numerous thoughts on interesting questions of fundamental importance, such as quantum decoherence, classical-quantum boundary [109],

local reality [110], etc. Besides its impacts on our understanding of the foundations of quantum physics, Schrödinger's cat states also possess potentials for practical applications in the field of quantum communication and computation [111, 112, 113, 114] as well as high precision interferometry [115], if properly implemented in real experiments.

In the context of quantum information science, cat states are now often referred to as coherent (equal) superposition states of mesoscopic or even macroscopic systems. Here we will restrict our attention on one specific class of cat states, which are superposition states of two classically distinguishable coherent states $|\alpha\rangle$ and $|-\alpha\rangle$. In quantum optics, coherent states are one of the most important classes of states of radiation fields. One reason to justify their importance is that they can serve as an accurate description of the (low amplitude) field produced by a stabilized laser operating well above threshold. Cat states of the form $|\alpha\rangle + |-\alpha\rangle$ are called even cat states, while those of the form $|\alpha\rangle - |-\alpha\rangle$ are referred to as odd cat states. To quantify the "size" of a cat state in such form, the amplitude of its component coherent state $|\alpha|^2$ is often used. The reason why these cats have "even" and "odd" in their names can be readily seen if we expand the coherent states in the basis of Fock (number) states. For even (odd) cat states of optical field, the terms with odd (even) photon number are cancelled out, while only terms with even (odd) number of photons survive. These cat states are highly non-classical, as demonstrated by the presence of a negative value in their Wigner functions at the origin of phase space [116, 117]. It has been proposed how to implement universal quantum computation by encoding quantum information in these even and odd cat states of optical pulses and manipulating them with linear optics apparatus [111, 112]. Now an immediate question naturally arises would be how one can realize cat states in laboratories.

Significant theoretical and experimental efforts have been made to realize such cat states in different physical systems [109, 118, 119, 120]. On the experimental side, until now, cat states have been successfully generated for phonon modes of a single trapped ion [109], and for microwave photon modes confined inside a superconducting cavity [118]. Although these achievements have been quite exciting, they can not be readily applied for QIP tasks. In contrast, propagating photon pulses prepared in cat states could be of more interests for QIP applications. Very recently, by subtracting a photon from an optical beam prepared in a squeezed vacuum state, an approximate small cat ("kitten") state has been implemented [119]. The fidelity between the generated non-classical optical state and its closest cat state is reported to be about 70 percent. There is no doubt that further improvement is still necessary in order to realize well-defined cat-state optical qubits. Theoretical proposals for generating cat states of optical pulses are typically based on either the Kerr nonlinearity or postselections from non-linear detectors [122, 123, 124]. Although the Kerr nonlinearity in principle provides a method for the deterministic generation of the cat states, it is well-known that such nonlinearity in typical materials is too small to allow the cat state generation from weak coherent pulses.

In the following sections, we will present our work on a novel approach to the implementation of cat states for optical pulses with single-atom cavity QED. It has been demonstrated experimentally that a single atom can be trapped for seconds inside a high-Q optical cavity working in the strong coupling regime [125, 97, 126]. With this setup, we can generate a larger class of cat states simply by reflecting weak coherent pulses successively from a cavity mirror. With the aid of a few beam splitters, we can generate multipartite and multidimensional cat states, and the preparation of such states is a necessary step toward several distinct applications, such as loop-

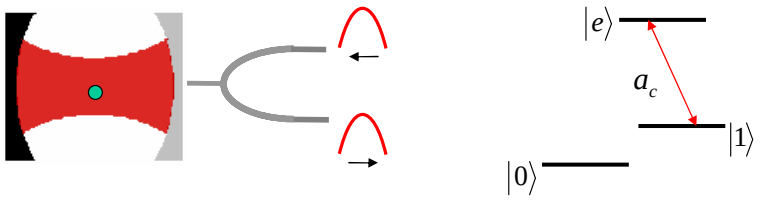

(a) (b)

Figure 3.1: Schematic setup for the generation of cat states with single-atom cavity QED and the level configuration of the trapped atom. (a) Generation of Schrödinger cat states by simply scattering a coherent optical pulse from a single-sided optical cavity with a single trapped atom. (b) The relevant level structure of the atom trapped in the cavity. The atomic transition between $|1\rangle$ and $|e\rangle$ is resonantly coupled to a cavity mode, while level $|0\rangle$ is decoupled.

hole-free detection of Bell inequalities with homodyne detections [127] and quantum coding and computation [128]. This scheme also extends an earlier photonic quantum computation scheme proposed by Duan and Kimble [56] to the continuous variable regime, eliminating the requirement of using single-photon pulses as a computation resource. To characterize the influences of various sources of experimental noise on this scheme, we develop a numerical simulation method to quantify the noise effects due to the atomic spontaneous emission, the photon pulse-shape distortion, and the cavity mode-matching inefficiency. Our numerical method enables us to find out a range of the cat-state amplitude achievable with our scheme. And the calculation shows that the generation of substantial cat states with our scheme could be within the reach of current cavity QED experimental technology.

3.2 Generation of Cat States with Optical Cavity QED

We consider an atom with three effective levels trapped inside a high-finesse one-sided optical cavity. The level configuration of the trapped atom is shown in Fig. 3.1, where $|0\rangle$ and $|1\rangle$ are levels in the ground-state manifold of the trapped atom with different hyperfine spins. The atomic transition from level $|1\rangle$ to level $|e\rangle$ is resonantly coupled to a cavity mode a_c, which is resonantly driven by an input optical pulse

prepared in a weak coherent state $|\alpha\rangle$. The atomic transition between level $|0\rangle$ and level $|e\rangle$ is decoupled from the cavity mode due to the large detuning induced by the hyperfine splitting. If the atom is prepared in level $|0\rangle$, the input pulse is resonant with the bare cavity mode a_c, and after resonant reflection it will acquire a phase of $\exp(i\pi)$ according to a standard quantum optics calculation [129]. The effective state of the pulse is then given by $|-\alpha\rangle$. However, if the atom is initially prepared in level $|1\rangle$, due to the strong atom-cavity coupling, the frequency of the dressed cavity mode is significantly detuned from the center frequency of the input pulse. In this case, one would expect intuitively that the coupling between the atom-cavity system and the input pulse does not play an important role here, and the reflection of the pulse is then similar to the reflection from a perfect mirror, which leaves the pulse shape and phase unchanged. And the pulse will remain in the same state $|\alpha\rangle$ after the reflection, given that the amplitude $|\alpha|^2$ of the input pulse is not too large. Later we will show that our numerical calculation indeed confirms the above expectations.

With this physical picture in mind, we can proceed to explain how to generate a Schrodinger cat state with the single-atom one-sided cavity setup. First we simply prepare the trapped atom in a superposition state $(|0\rangle + |1\rangle)/\sqrt{2}$, which can be routinely realized by standard quantum optical control techniques, e.g. STIRAP. Then, we send an optical pulse prepared in a coherent state $|\alpha\rangle$ toward this single-atom optical cavity. Such an optical pulse can be readily produced by stabilized laser working well above threshold. After interacting with the atom-cavity system, following the qualitative analysis presented above, one can easily check that ideally the final joint state for the atom and optical pulse will become an entangled state which is described by:

$$|\Psi_c\rangle = (|0\rangle|-\alpha\rangle + |1\rangle|\alpha\rangle)/\sqrt{2}. \tag{3.1}$$

Next, we perform projective measurement on the trapped atom in the $\{|\pm\rangle \equiv (|0\rangle \pm |1\rangle)/\sqrt{2}\}$ basis. Or, equivalently, one can apply Hadamard gate on the atom, which transforms $|0\rangle$ to $|+\rangle$ and $|1\rangle$ to $|-\rangle$, and then measure the atom in the $\{|0\rangle, |1\rangle\}$ basis. It is straightforward to check that the state of the optical pulse after the measurement on atomic state will be projected onto either an even or odd cat state, conditioned on the measurement outcome for the atom. The generated cat state can be verified experimentally by standard quantum optical homodyne detection techniques [116] or through quantum state tomography. With this technique, one can reconstruct the Wigner function of the optical field. And the non-classicality of the photonic cat state can be determined by negative values of the function in certain regions of phase space.

With some extensions to the scheme introduced above, in principle we can generate more complicated types of cat states targeting different applications. First, by bouncing a series of coherent pulses (say, n pulses), each initially in the state $|\alpha\rangle$, successively from the same single-atom cavity, one will get an entangled state of the atom-photon system with the form $\left(|0\rangle |-\alpha\rangle^{\otimes n} + |1\rangle |\alpha\rangle^{\otimes n}\right)/\sqrt{2}$, which yields entangled multi-partite cat states of optical pulses $\left(|-\alpha\rangle^{\otimes n} \pm |\alpha\rangle^{\otimes n}\right)$ (unnormalized) after carrying out projective measurement on the atomic state in the basis $\{|\pm\rangle\}$. Second, after generation of the state $(|-\alpha\rangle + |\alpha\rangle)$ for one optical pulse, one can transfer it into the state $(|\alpha\rangle + |3\alpha\rangle)$ through a simple linear optical manipulation (for instance, by interfering this pulse with another phase-locked stronger laser pulse at an unbalanced beam splitter, one can shift up each coherent component of the cat state by an amplitude of 2α). Then, if we reflect this pulse again from the same cavity, we will get a state $(|-3\alpha\rangle + |-\alpha\rangle + |\alpha\rangle + |3\alpha\rangle)$ for the pulse conditioned on that a measurement on the atomic state gives the $|+\rangle$ state outcome. It is straightforward

to extend this idea to generate the multi-dimensional cat states $\sum_{i=-n}^{n+1} |(2i-1)\,\alpha\rangle$, and such kind of states have important applications for continuous-variable quantum coding [128] and loop-hole-free detection of the Bell inequalities with efficient homodyne measurements [127].

3.3 Theoretical Model and Numerical Method

In the previous section, we have explained the physical idea for preparation of entangled atom-photon state with the form of Eq. (3.1) and described various extensions to our basic scheme. To understand and characterize our proposed implementation scheme better, however, we need a more detailed theoretical modeling for the interaction between the atom-cavity system and the input/output light pulses. First, we want to know the limit for the size of cat states allowed by our scheme. If the amplitude $|\alpha|^2$ is too large, one would expect that a single trapped atom will not be able to significantly affect the property of a strong incoming pulse, therefore the output state would be different from the state described by Eq. (3.1). Second, in reality, all experiments inevitably suffer from various kinds of noises or imperfections, such as photon loss due to the atomic spontaneous emission and the uncontrolled mirror scattering, the inherent pulse shape distortion induced by the reflection from the cavity mirror, and the random variation of the cavity mode-atom coupling rate induced by thermal motion of the trapped atom. To estimate the performance of our scheme, one must try to characterize possible influences from these sources of noise on the generation of our cat states. In this section, we will present a detailed model to describe our proposed system and a numerical method to solve the dynamics of the system according to this model.

The input pulse sent to the cavity is in coherent state, $|\alpha\rangle_{in}$, which can be explicitly

expressed as $|\alpha\rangle_{in} = \exp\left[-\frac{|\alpha|^2}{2}\right] \exp\left[\alpha \int_0^T f_{in}^*(t) a_{in}^\dagger(t) dt\right] |\text{vac}\rangle$, where $a_{in}(t)$ is a one-dimensional quantum field operator satisfying the standard Bosonic commutation relation $[a_{in}(t), a_{in}^\dagger(t')] = \delta(t - t')$, $f_{in}(t)$ describes the input pulse shape with the normalization $\int_0^T |f_{in}(t)|^2 \, dt = 1$ (T is the pulse duration), and $|\text{vac}\rangle$ represents the vacuum state for all the optical modes. The average photon number of the pulse is given by $|\alpha|^2$. This input coherent pulse drives the cavity mode a_c through the Langevin equation [129]

$$\dot{a}_c = -i[a_c, H] - \frac{\kappa}{2} a_c - \sqrt{\kappa} a_{in}(t), \tag{3.2}$$

where κ is the cavity decay rate, and the Hamiltonian H describes the atom-cavity interaction with the form

$$H = \hbar g \left(|e\rangle\langle 1| a_c + |1\rangle\langle e| a_c^\dagger \right). \tag{3.3}$$

Here, g is the atom-cavity coupling rate. The cavity output field a_{out} is connected to the input through the input-output relation

$$a_{out}(t) = a_{in}(t) + \sqrt{\kappa} a_c(t). \tag{3.4}$$

We need to find out the quantum state of the cavity output field a_{out} by solving the series of equations (3.2)-(3.4). As they are nonlinear operator equations with infinite number of modes, it is not very straightforward to solve them even numerically. For the case of a single-photon pulse input, a numerical method based on mode discretization and expansion has been developed in Refs. [56] and [130] . However, since the number of coefficients to be determined grows exponentially with the number of photons, that method does not work if the photon number of the input pulse is larger than 1, which is the case for our current problem. So, to attack this problem,

we propose a variational method based on the following observation: if the atom is in the state $|0\rangle$, the Hamiltonian (3.3) does not play a role, and Eqs. (3.2) and (3.4) become linear, from which we observe that the state $|\phi_0\rangle_{out}$ of the output field can be exactly written as $|\phi_0\rangle_{out} = \exp\left[-\frac{|\alpha|^2}{2}\right] \exp\left[\alpha \int_0^T f_{out}^{(0)*}(t) a_{in}^\dagger(t) dt\right] |\text{vac}\rangle$. The normalized shape function can be expressed as $f_{out}^{(0)}(t) = -\int \frac{\frac{\kappa}{2}+i\omega}{\frac{\kappa}{2}-i\omega} \exp\left[i\omega t\right] f_{in}(\omega) d\omega$, where $f_{in}(\omega)$ is the Fourier transform of $f_{in}(t)$. The output optical field is still in an effective single-mode coherent state, but with the mode shape function $f_{out}^{(0)}(t)$ in general different from the input pulse shape $f_{in}(t)$. If the atom is in the state $|1\rangle$, it is reasonable to make the ansatz that the output optical field is also in an effective single-mode coherent state $|\phi_1\rangle_{out} = \exp\left[-\frac{|\alpha_1|^2}{2}\right] \exp\left[\alpha_1 \int_0^T f_{out}^{(1)*}(t) a_{out}^\dagger(t) dt\right] |vac\rangle$, but probably with a different normalized mode shape function $f_{out}^{(1)}(t)$. In general, the amplitude α_1 can be different from α (actually $|\alpha_1|^2 < |\alpha|^2$) because of various relevant photon loss mechanisms. With the presence of photon loss channels, some of the photons are scattered to other directions, so we will always have an output field somehow weaker than the input. To find out the functional form of $f_{out}^{(1)}(t)$, we note that under the above ansatz, calculating the expectation value on both sides of the input-output equation (3.4) leads to

$$\alpha_1 f_{out}^{(1)}(t) = \alpha f_{in}(t) + \sqrt{\kappa} \langle a_c(t) \rangle . \tag{3.5}$$

The expectation value of the cavity mode operator $a_c(t)$ can be found by solving the corresponding master equation for the atom-cavity system density operator ρ

$$\begin{aligned} \dot{\rho} &= -\frac{i}{\hbar}[H_{eff}, \rho] + \frac{\kappa}{2}\left(2a_c \rho a_c^\dagger - a_c^\dagger a_c \rho - \rho a_c^\dagger a_c\right) \\ &+ \frac{\gamma_s}{2}\left(2\sigma_- \rho \sigma_+ - \sigma_+ \sigma_- \rho - \rho \sigma_+ \sigma_-\right), \end{aligned} \tag{3.6}$$

where $\sigma_- = |1\rangle\langle e|$ and $\sigma_+ = |e\rangle\langle 1|$ are the atomic lowering and raising operators, and the effective Hamiltonian is given by $H_{eff} = \hbar(g\sigma_+ a_c + i\sqrt{\kappa}\langle a_{in}\rangle a_c) + H.c.$ Compared

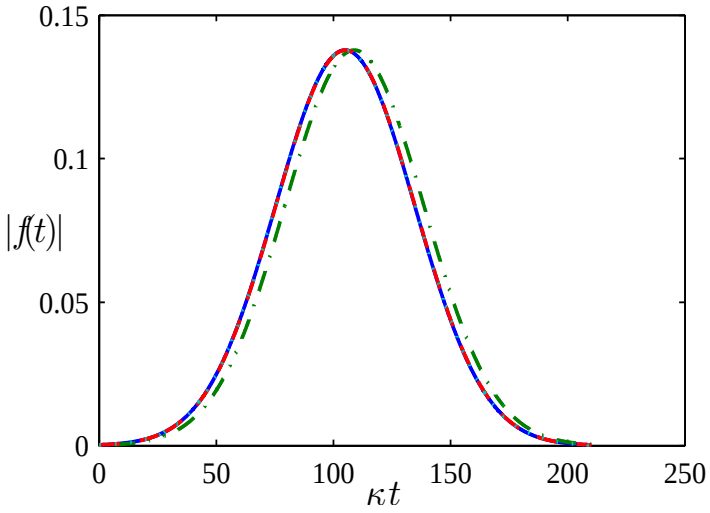

Figure 3.2: Pulse shape functions for the input and output pulses. The solid curve shows the shape function of input pulse. The dash-dotted, dashed, and dotted curves correspond to the output pulses with $g = 0$(for the atom in the level $|0\rangle$), $g/\kappa = 3$, and $g/\kappa = 6$, respectively. In the calculation, we assumed $\gamma = \kappa$ and an input pulse duration of $T = 210/\kappa$.

with the Hamiltonian (3.3), H_{eff} has two extra terms $i\hbar\sqrt{\kappa}\langle a_{in}\rangle a_c + H.c.$ to account for the driving from the input pulse. After that correction, the cavity decay and the atomic spontaneous emission loss can then be described by the last two Lindblad terms of the master equation (3.6), where γ_s denotes the atomic spontaneous emission rate. The density operator ρ can be solved from the master equation (3.6) efficiently with numerical methods. After obtaining the density matrix, we can calculate the expectation value $\langle a_c(t)\rangle = \mathrm{tr}\,(\rho a_c(t))$. Then, following Eq. (3.5), we can determine the output amplitude α_1 and its pulse shape $f^{(1)}_{out}(t)$.

With the method introduced above, we can calculate the pulse shape functions $f^{(0)}_{out}(t)$ and $f^{(1)}_{out}(t)$ of the output optical field with the atom in levels $|0\rangle$ and $|1\rangle$, respectively. For this calculation, we take a Gaussian pulse shape for the input pulse with the form $f_{in}(t) \propto \exp\left[-(t - T/2)^2/(T/5)^2\right]$, where T characterizes the pulse duration. The results are shown in Fig. 3.2, which demonstrates that the shape functions $f^{(0)}_{out}(t)$ and $f^{(1)}_{out}(t)$ of the output pulses overlap very well with $f_{in}(t)$ of the

input pulse as long as the pulse duration satisfies $T \gg 1/\kappa$. Furthermore, the global phase factors of $f_{out}^{(0)}(t)$ and $f_{out}^{(1)}(t)$ are given by -1 and 1, respectively, which confirms our previous expectation: if the atom is initially prepared in a superposition state $(|0\rangle + |1\rangle)/\sqrt{2}$, the final atom-photon state will be the desired entangled state $|\Psi_c\rangle$ as shown in Eq. (3.1), where $|-\alpha\rangle$ and $|\alpha\rangle$ are coherent states of the output mode with the mode shape function $-f_{out}^{(0)}(t) \approx f_{out}^{(1)}(t) \approx f_{in}(t)$. In the same figure, we have also shown the output shape $f_{out}^{(1)}(t)$ for different atom-photon coupling rates g. Both the phase and the amplitude of $f_{out}^{(1)}(t)$ are very insensitive to random variation of g within a certain range. For instance, even if g varies by a factor of 2 from 6κ to 3κ (which is the typical variation range of g caused by the atomic thermal motion), the change in $f_{out}^{(1)}(t)$ is negligible ($< 10^{-4}$).

To quantify the limit of the cat states that one can prepare and the possible effects due to practical sources of noise, we introduce several quantities to characterize the quality of the cat state preparation. First, the pulse shape distortion between the output and the input pulses can be characterized by their pulse shape mismatching $\xi_1 = 1 - \int f_{in}(t) f_{out}^{(1)*}(t) dt$ and $\xi_0 = 1 + \int f_{in}(t) f_{out}^{(0)*}(t) dt$ (as $f_{out}^{(0)}(t)$ has an opposite phase). With typical experimental parameters, $\xi_0 \gg \xi_1$, so ξ_0 has the dominant contribution to the imperfection of our scheme. Second, the effect of the spontaneous emission loss can be quantified by the photon loss parameter $\eta = 1 - |\alpha_1|^2 / |\alpha|^2$, which represents the fraction of the photons scattered to other directions instead of to the cavity output. Both the pulse shape distortion and the photon loss contribute to the imperfection of the generated cat state, which can be characterized by the state fidelity. The ideal cat state is given by $|\Psi_c\rangle$ in Eq. (3.1), while with noise, the real state obtained is denoted by a density matrix ρ_{real}. The fidelity, defined as

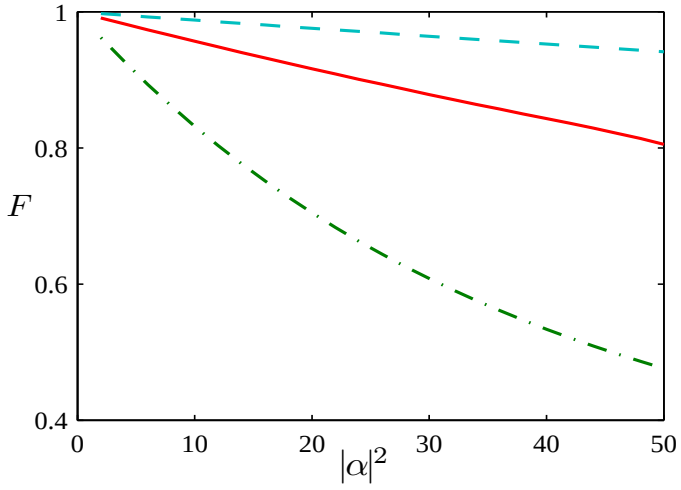

Figure 3.3: The cat state fidelity is presented as a function of the average input photon number $|\alpha|^2$ when the spontaneous emission rate is set to zero ($\gamma_s = 0$). Other parameters: $g/\kappa = 3$ and $\kappa T = 210$ for the solid curve; $g/\kappa = 6$ and $\kappa T = 210$ for the dotted curve (exactly overlapped with the solid curve); $g/\kappa = 6$ and $\kappa T = 100$ for the dash-dotted curve; $g/\kappa = 6$ and $\kappa T = 400$ for the dashed curve.

$F \equiv \langle \Psi_c | \, \rho_{\rm real} | \Psi_c \rangle$, can be expressed by ξ_0 and η as

$$F \approx \left| \frac{e^{-|\alpha|^2\left(1-\sqrt{1-\eta}\right)} + e^{-|\alpha|^2 \xi_0}}{2} \right|^2 , \tag{3.7}$$

where we've neglected the contribution of ξ_1 as $\xi_1 \ll \xi_0$.

3.4 Numerical Results and Discussion

First, let us examine the intrinsic limit to the amplitude of the cat state that one can prepare even if we neglect the influence of practical photon loss. This intrinsic limit comes from the fact that a single cavity atom can not affect the state of a strong optical field (i.e., with a large α) efficiently. For that purpose, we simply set the spontaneous emission rate $\gamma_s = 0$, and look at the state fidelity as a function of the cat state amplitude α. The result is shown in Fig. 3.3, which reveals that given a certain fidelity requirement the maximal achievable cat amplitude $|\alpha|$ depends only on the pulse duration T if we completely neglect the photon loss noise. In general, a longer input pulse duration allows the generation of a larger cat state. In particular,

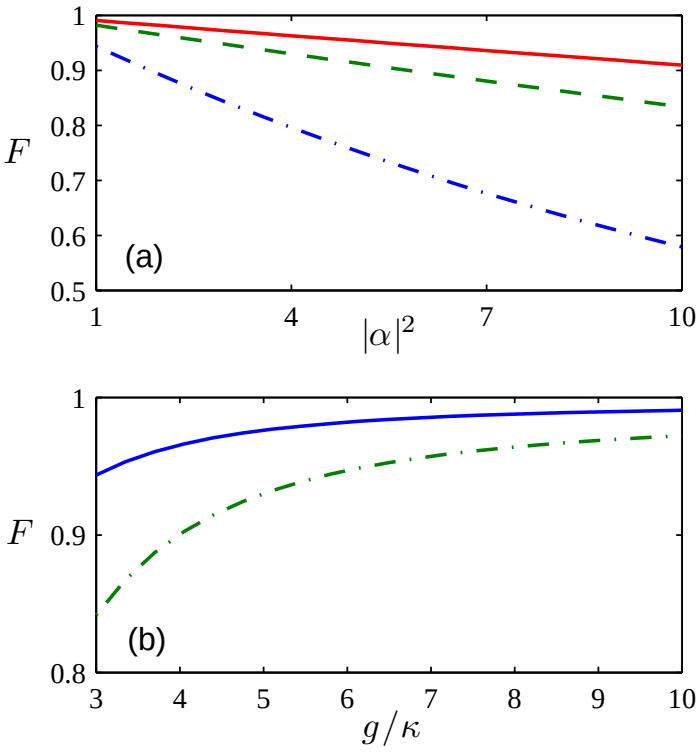

Figure 3.4: The cat state fidelity as functions of average photon number and atom-cavity coupling rate. (a) The cat state fidelity shown as a function of the average photon number α^2 of the input pulse. The dash-dotted, dashed and solid curves correspond to $g/\kappa = 3$, $g/\kappa = 6$, and $g/\kappa = 10$, respectively. (b) The fidelity shown as a function of the atom-cavity coupling rate g. The solid and dashed curves correspond to the average input photon number $|\alpha_1|^2 = 1$ and $|\alpha_1|^2 = 3$, respectively. In both calculations for (a) and (b), we have taken $\gamma = \kappa$ and $\kappa T = 210$.

the fidelity increases dramatically when we increase the pulse duration T as the shape distortion parameter ξ_0 significantly reduces for a pulse with a very narrow bandwidth.

We then take the influence of practical noise into account, and investigate under typical experimental configurations, how large the amplitude of an achievable cat-state can be. We set the spontaneous emission rate $\gamma_s = \kappa$ in our calculation. The state fidelity F is shown as a function of the cat amplitude in Fig. 3.4a, and as a function of the coupling rate in Fig. 3.4b. The fidelity increases with the coupling rate g and decreases with the cat amplitude α, as one would expect. We

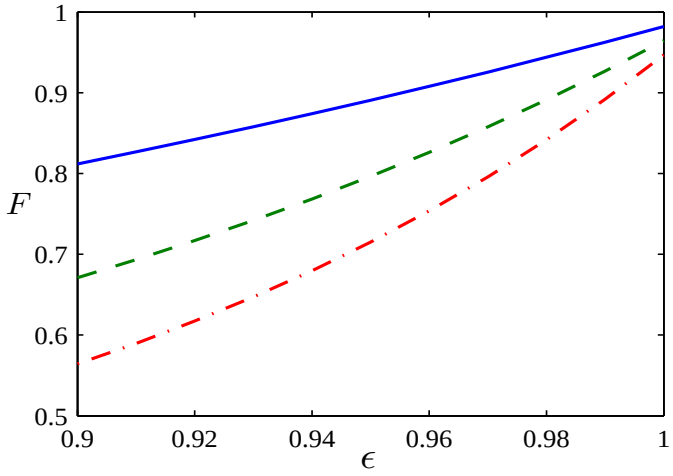

Figure 3.5: The cat state fidelity shown as a function of the mode-matching efficiency ϵ. The solid, dashed, and dash-dotted curves correspond to $|\alpha|^2 = 1$, $|\alpha|^2 = 2$, and $|\alpha|^2 = 3$, respectively. Other parameters:$\gamma = \kappa$, $g = 6\kappa$ and $\kappa T = 210$.

note that the photon loss from spontaneous decay reduces when the coupling rate g increases. Under a reasonable atom-cavity coupling rate $g \approx 10\kappa$ comparable with the experimentally achievable value with current technology, a cat state with a remarkable amplitude $\alpha \approx 3.4$ (corresponding to an entangled state of about 10 photons) could be generated with a fidelity of 90 percent.

Another source of noise for cavity QED experiments is the mode matching inefficiency between the intra-cavity field and the input-output beams. When the mode matching is not perfect, a portion of the input pulse will not be able to enter the cavity, so the state of the pulse will not be affected by the cavity-atom coupling efficiently. Independent of the atomic state, this portion of light pulse will be directly reflected without phase flip. This will degrade the fidelity of our cat-state preparation. To quantify this effect, we note that if we neglect all the other imperfections, the cat state fidelity from the mode matching inefficiency can be described by $F \approx \left|\frac{1+e^{-2|\alpha|^2(1-\epsilon)}}{2}\right|^2$, where ϵ denotes the efficiency of the mode matching. If we take into account at the same time the other sources of noise that we've considered

above, the state fidelity will have a more complicated analytic expression. In Fig. 3.5, we show the state fidelity as a function of the mode-matching efficiency ϵ. In this calculation we have also included the noise contributions from the atomic spontaneous emission and pulse shape distortion. It is shown that for a cat state with a large amplitude the fidelity could be quite sensitive to the mode-matching efficiency.

3.5 Chapter Summary

In summary, we have proposed a scheme to generate Schrödinger-cat states for propagating optical pulses, which can be readily extended to further implement and control multi-partite and high-dimensional Schrödinger-cat states. Our scheme is based on strong coupling between a single trapped atom and cavity field, which has been achieved with the state-of-the-art of the cavity technology. We have developed a efficient variational calculation method. With our method, one can solve the dynamics of the system dictated by the atom-cavity interaction together with the coupling of input and output optical field with the cavity field, thereby enabling us to quantitatively characterize the influence of various sources of practical noise on the performance of our scheme.

CHAPTER IV

Implementation of Robust Neutral Atom Gates with Optical Cavity QED

Atom-cavity system working in strong coupling regime provides us a unique platform where single atom or single photon plays central role in determining the quantum dynamics of the system. In the previous chapter, we have described an application of optical cavity QED to QIP, namely an implementation scheme for generating Schrödinger cat states for optical pulses. In the cat state generation scheme, a single trapped atom is utilized to induce conditional dynamics for coherent optical pulses. Photons sent to a cavity, on the other hand, can also be used to change the dynamics of atoms trapped in the cavity. In this chapter, we will present a novel scheme with optical cavity QED to implement robust multiqubit conditional quantum gates acting on neutral atoms. The interaction between the atoms is mediated by cavity scattering of single-photon pulses. The dominant noise in our scheme possesses a special feature, i.e. whenever an error occurs due to this noise, the error is automatically detected. It has been shown that this kind of error, even happening with high error rate, does not exclude the possibilities of efficient fault-tolerant quantum computation.

4.1 Introduction

Neutral-atom qubit systems provide intrinsic scalability since properties of individual atoms in an atomic ensemble do not differ significantly from those of single atoms. However, while the weak interactions between neutral atoms insure the scalability of qubits, they also make it difficult to realize non-trivial multiqubit gate operations. One possible way to circumvent the difficulty in achieving strong effective atom-atom interaction is to put the atoms in optical cavities and utilize the cavity field to facilitate the process [7, 47, 77, 131]. As a matter of fact, such an approach has been one of the pioneering avenues for physical implementation of QIP. Nevertheless, earlier proposals associated with this approach impose very demanding requirements on experimental technology. In particular, despite significant experimental progress made recently in transmitting and trapping single atoms in high finesse cavities [97, 132, 133, 134, 135, 136, 137, 138], no experiment has yet achieved a well defined number of atoms $N \geq 2$ each of which is strongly coupled to the cavity mode, individually addressable, and localized within the Lamb-Dicke limit, as required by the protocol of Ref. [131]. To realize a more scalable system, Chapman *et al.* proposed an architecture in which a transverse optical lattice is employed to translate atoms into and out of a high-finesse cavity for atomic entangling gate operations [132]. Transport that preserves internal state coherence has been demonstrated for both ions [139] and neutral atoms [140]. However, although the approach of Ref. [132] does solve the problem of separate addressability of many atoms confined in a tiny cavity, there remain significant obstacles to achieving Lamb-Dicke confinement and strong coupling for any scheme that has yet been proposed.

To overcome these difficulties and to provide several new capabilities for quantum

logic, we propose a scheme for atomic quantum gates, in which atom-atom interactions are catalyzed by single photons in a fashion that is robust to various sources of practical noise. More specifically, a scheme for implementing controlled phase-flip gate $U_{12} = \exp(i\pi|00\rangle_{12}\langle 00|)$ on two neutral atoms localized in an optical cavity is proposed. In this scheme the desired gate operation can be achieved by scattering a single-photon pulse from the cavity in which the atoms are trapped [56, 87]. Although it requires both atoms to be strongly coupled with the cavity mode, this scheme is insensitive to uncertainties in their individual atom-cavity coupling rates, thereby obviating the demanding requirement for Lamb-Dicke localization. Various sources of photon loss, including, for instance, atomic spontaneous emission, photon collection and detection inefficiency, and any vacuum component in the scatterred pulse, constitute the dominant noise in this scheme. However such noise only affects the success probability of the gate operation, as once a photon-loss error occurs during the process, it will be automatically detected. Although photon loss probability could be significant in experiments, the special feature of the gate error induced by it still allows efficient quantum information processing. As shown in Refs. [141, 142], given nearly perfect single-qubit gates and imperfect entangling gate with signalled error, one can nevertheless achieve efficient quantum computation even if the associated failure probability of the entangling gate is close to unity. Moreover, this scheme can be readily extended to achieve Toffoli gate for N local atoms in a single step and to realize nonlocal gates on remote atoms trapped in different cavities. The direct N-qubit Toffoli gate could lead to more efficient construction of quantum circuits, and the nonlocal gates on remote atoms mediated by photon pulses naturally integrate local quantum computation with quantum networking.

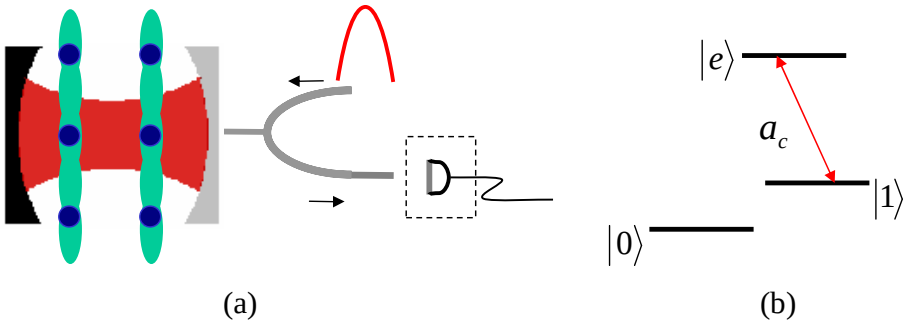

Figure 4.1: Schematic setup for implementation of controlled phase flip gate and level configuration of the trapped atoms. (A) Schematic setup for implementation of the controlled phase flip (CPF) gate on two neutral atoms inside a single-sided cavity through the photon-scattering interaction. Any pair of atoms can be transmitted into the cavity for a collective gate operation aided by a transverse optical lattice potential as suggested in Refs. [132] and [144]. For a more robust implementation of the gate, we add a single-photon detector to detect the output photon pulse as illustrated inside the dashed box. (B) The relevant level structure of the atoms and the coupling configuration.

4.2 Implementation Scheme of Robust Neutral Atom Gates

To explain physical idea behind our implementation scheme, we first consider two atoms trapped in a single-sided cavity. To have a scalable architecture, one can follow Ref. [132] to assume that there are transverse optical lattice potentials to move the target atoms into and out of the cavity [143]. Each atom has three relevant levels as shown in Fig. 4.1. Qubits are represented by different hyperfine levels $|0\rangle$ and $|1\rangle$ in the ground-state manifold of the trapped atoms. The atomic transition from $|1\rangle$ to an excited level $|e\rangle$ is resonantly coupled to a cavity mode a_c. The state $|0\rangle$ is decoupled due to the large hyperfine splitting.

To perform a collective quantum gate on the two atoms, we reflect a single-photon pulse from the cavity. This single-photon pulse, with its state denoted as $|p\rangle$, is resonant with the bare cavity mode a_c. If the photon pulse is sufficiently long so that its bandwidth $\Delta\Omega$ is much smaller than the cavity decay rate κ, reflection of the pulse from a resonant cavity with no atom-cavity coupling will leave the pulse shape almost unchanged (the longer the pulse duration, the smaller the pulse shape

distortion), but will flip its global phase, as we will characterize later in this chapter in greater detail. For the case that both of the atoms are in the $|0\rangle$ state, this is precisely the nature of the resonant reflection since there is negligible atom-cavity coupling and hence no shift of the resonant frequency of the cavity mode. After reflection, the atom-photon state $|0\rangle_1 |0\rangle_2 |p\rangle$ evolves into $-|0\rangle_1 |0\rangle_2 |p\rangle$, where the subscripts $1, 2$ denote the two intracavity atoms. However, if either or both of the atoms are in the state $|1\rangle$, the effective frequency of the dressed cavity mode will be shifted due to the atom-cavity coupling, which is described by the Hamiltonian

$$H = \hbar \sum_{i=1,2} g_i \left(|e\rangle_i \langle 1| a_c + |1\rangle_i \langle e| a_c^\dagger \right). \tag{4.1}$$

If the coupling rates $g_i \gg (\Delta\Omega, \kappa, \gamma_s)$, where γ_s is the rate of spontaneous decay of $|e\rangle$, then the frequency shift will have a magnitude comparable with g_i, so that the incident single-photon pulse will be reflected by an off-resonant cavity. Hence, both the shape and global phase will remain unchanged for the reflected pulse. Due to this property, the component states $|0\rangle_1 |1\rangle_2 |p\rangle$, $|1\rangle_1 |0\rangle_2 |p\rangle$, and $|1\rangle_1 |1\rangle_2 |p\rangle$ are likewise unaffected by reflection process. The net effect of these two subprocesses is that the reflection of a single-photon pulse from the cavity actually performs a controlled phase-flip gate (CPF) $U_{12} = \exp\left(i\pi |00\rangle_{12} \langle 00|\right)$ on the two atoms while leaving the photon state unchanged and unentangled with the atoms. Hence, in the ideal case the reflected photon can be utilized to catalyze subsequent gate operations.

However, in a realistic setting our scheme can be performed in a more robust fashion by detecting the output pulse with a single-photon detector. By this means, gate errors due to all sources of photon loss, including atomic spontaneous emission, cavity mirror absorption and scattering, imperfection in the photon source, and photon collection and detection inefficiencies, are always signaled by the absence of a photon count at the detector. As a result, these dominant sources of noise only

lead to probabilistic signaled errors, which yield a finite failure probability of the gate but have no contribution at all to the gate infidelity if the operation succeeds (i.e., if a photon count is registered). For this class of errors, efficient quantum computation is possible even with an arbitrarily small gate success probability p [141]. Compared with deterministic gates, the required extra computational overhead due to the small gate success probability p scales efficiently (polynomially) both with $1/p$ and the computational scale characterized by the number of qubits n [141]. Because of this robustness, the input single-photon pulse can also be replaced by a simple weak coherent pulse $|\alpha\rangle$ with the mean photon number $|\alpha|^2 \ll 1$. This replacement greatly eases the requirement for photon sources, while it does not give any essential problem in terms of scaling. Nonetheless, the individual gate efficiency (the success probability) is indeed significantly reduced by a factor of $|\alpha|^2$.

Before going to the detailed theoretical characterization of the gate fidelity and efficiency, we next present some extensions to the above scheme. First, our scheme can be readily extended to perform a Toffoli gate on N atoms in a single time step. If one reflects a single-photon pulse from a cavity with N atoms trapped inside, the pulse will have a flip of its global phase if and only if all the atoms are in the $|0\rangle$ state. So, this reflection performs a Toffoli gate $U_{12\cdots N} = \exp\left(i\pi \left|00\cdots0\right\rangle_{12\cdots N}\left\langle 00\cdots0\right|\right)$ on all the trapped atoms while leaving the photon state unentangled. This direct N-qubit gate could lead to more efficient construction of circuits for quantum computation. For instance, the reflection operation in the Grover's search algorithm can be realized in a single step with the N-qubit Toffoli gate [144]. Second, the above scheme can also be extended to perform nonlocal gates on two remote atoms trapped in different cavities, as illustrated in Fig. 3.2. For this purpose, one uses a single-photon (or weak coherent) pulse which is in an equal superposition state $\left(|h\rangle + |v\rangle\right)/\sqrt{2}$ of

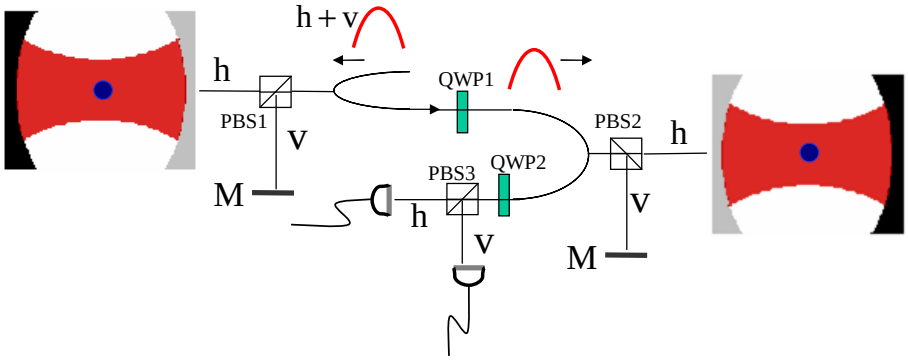

Figure 4.2: Schematic of the setup for implementation of nonlocal gates on two atoms 1 and 2 trapped in distant cavities. Not shown are circulators (e.g., Faraday devices) to redirect the output beams along paths distinct from the inputs. See the text for further explanation.

the h and v polarization components. With a polarization beam splitter (PBS1), the h and v components of the pulse are "bounced" back from the atom-cavity system and a mirror M, respectively, with the reflection from M leaving the incident pulse unchanged. The overall reflection from the cavity and the mirror M actually performs the gate operation $U_{1p} = \exp\left(i\pi \left|0h\right\rangle_{1p} \left\langle 0h\right|\right)$ on atom 1 and the photon pulse p, so that there is a phase flip only when the atom is in the state $|0\rangle$ and the photon is in the polarization $|h\rangle$. The pulse is reflected successively from the two cavity setups, with a quarter-wave plate (QWP1) inserted into the optical path between the two reflections which performs a Hardmard rotation on the photon's polarization $|h\rangle \rightarrow (|h\rangle + |v\rangle)/\sqrt{2}$, $|v\rangle \rightarrow (|v\rangle - |h\rangle)/\sqrt{2}$. The photon is detected by two single-photon detectors D1 and D2 after the reflections, which corresponds to a measurement of its polarization in the basis $\{|v\rangle \pm |h\rangle\}/\sqrt{2}$ (after the QWP2 and the PBS3; see Fig. 4.2). For a detection event in D2, a phase flip operation σ_1^z is performed on the atom 1, while no operation is applied if D1 clicks. The net effect of these operations is the desired CPF gate $U_{12} = \exp\left(i\pi \left|00\right\rangle_{12} \left\langle 00\right|\right)$ on the two atoms $1, 2$ localized in two remote cavities. Among other applications, this nonlocal gate and its extension to multiple atom-cavity systems provide a convenient avenue for

quantum networking. Similar to the case of a single cavity as described above, in this distributed setting any noise leading to photon loss is always signaled by the absence of a photon count from either D1 or D2.

4.3 Theoretical Model and Numerical Method

We now present a more detailed theoretical model for our scheme and characterize the influence of some practical sources of noise. The input single-photon pulse with a normalized shape function $f_{in}(t)$ and a duration T can be described by the state $|p\rangle = \int_0^T f_{in}(t)\, a_{in}^{\dagger}(t)\, dt\, |vac\rangle$, where $|vac\rangle$ denotes the vacuum state and $a_{in}^{\dagger}(t)$ is the one-dimensional optical field operator satisfying the commutation relation $\left[a_{in}(t), a_{in}^{\dagger}(t')\right] = \delta(t-t')$ [129]. The cavity mode a_c is driven by the input field $a_{in}(t)$ through the Langevin equation [129]

$$\dot{a}_c = -i[a_c, H] - (\kappa/2)\, a_c - \sqrt{\kappa} a_{in}(t), \tag{4.2}$$

where κ is the cavity decay rate and the Hamiltonian H is given in Eq. (4.1) for the case of two atoms; generalization to multiple atoms is straightforward. To account for atomic spontaneous emission with a rate γ_s, we add an effective term $(-i\gamma_s)\,|e\rangle\langle e|$ to the Hamiltonian H. The output field $a_{out}(t)$ of the cavity is connected with the input through the input-output relation $a_{out}(t) = a_{in}(t) + \sqrt{\kappa} a_c$.

In the case of single-photon input, there is an alternative, yet more convenient way to attack the problem [56, 130]. Instead of dealing with Langevin equations for operators, we can try to use the Hamiltonian approach by (1) writing down an effective Hamiltonian for the whole system consisting of the trapped atoms, the cavity field as well as the effective one-dimensional free-space field; (2) expanding the state of the system with restricted set of basis vectors; and (3) directly apply the Schrödinger equation to obtain differential equations for the expansion coefficients. In

the following, we briefly outline this approach step by step. The effective Hamiltonian for our system can be written as ($\hbar = 1$):

$$\begin{aligned} H_{eff} &= \sum_{l=1}^{N} \left(\Delta - i\frac{\gamma_s}{2}\right) |e\rangle_l\langle e| + \sum_{l=1}^{N} g_l \left(|e\rangle_l\langle 1|a_c + h.c.\right) \\ &+ i\sqrt{\frac{\kappa}{2\pi}} \int_{-\infty}^{+\infty} d\omega \left[b(\omega)a_c^\dagger - b^\dagger(\omega)a_c\right] + \int_{-\infty}^{+\infty} d\omega \left[\omega b^\dagger(\omega)b(\omega)\right], \quad (4.3) \end{aligned}$$

where $\Delta = \omega_e - \omega_1 - \omega_c$ is the detuning of cavity resonant frequency ω_c from the atomic resonant frequency corresponding to the transition between $|1\rangle$ and $|e\rangle$ and $b(\omega)$ ($b^\dagger(\omega)$) is annihilation (creation) operator for the effective one-dimensional free-space mode with frequency ω. The free-space mode operators satisfy the standard Bosonic commutation relation $\left[b(\omega), b^\dagger(\omega')\right] = \delta(\omega - \omega')$. Theoretically, there are infinite number of free space modes coupled with the cavity field. Nonetheless, in practice, it suffices to only consider the modes lies in a finite bandwidth $[\omega_c - \omega_b, \omega_c + \omega_b]$ where ω_b is the cut-off frequency chosen artificially. To attack the problem numerically, we also need to discretize the originally coninuous modes within frequency range. Choosing M discrete modes uniformly, we have a frequency increment of $\delta\omega = 2\omega_b/M$ between two adjacent modes. The continuous mode operators in the effective Hamiltonian should now be replaced by the descretized ones according to $b(\omega) \rightarrow b_{\omega_j}/\sqrt{\delta\omega}$ and the corresponding integrations are replaced by summations according to $\int d\omega \rightarrow \sum_{j=1}^{M} \delta\omega$. We note that to get reliable numerical results, the cut-off frequency as well as the number of discretized mode need to be chosen carefully so that ω_b is sufficiently large as compared with cavity decay rate κ while $\delta\omega$ is sufficiently small as compared with inverse of the pulse duration $1/T$. Next we expand the quantum state of the whole system into the form (for simplicity we show

the case with only two atoms):

$$|\Psi\rangle = \left(\sum_{\{q_1,q_2\}=0,1} c_{q_1,q_2}|q_1,q_2\rangle_a|1\rangle_c + \sum_{q_1=0,1} c_{q_1,e}|q_1,e\rangle_a|0\rangle_c + \sum_{q_2=0,1} c_{e,q_2}|e,q_2\rangle_a|0\rangle_c \right) \otimes |vac\rangle_f + \sum_{\{q_1,q_2\}=0,1} \left(|q_1,q_2\rangle_a|0\rangle_c \otimes \sum_{j=1}^{M} c^j_{q_1,q_2} b^\dagger_{\omega_j}|vac\rangle_f \right), \quad (4.4)$$

where the subscripts a, c, and f denote the state of atoms, cavity field, and free-space field respectively. The efficient expansion works thanks to the condition that at most one photon presents in the system. As indicated by the expression, the single-photon could be found in the cavity mode a_c, or in the free-space modes b_ω, or to be absorbed by one of the trapped atoms. Then, it is straightforward for one to obtain a set of differential equations of expansion coefficients according to Schrödinger equation $i\frac{d}{dt}|\Psi\rangle = H_{eff}|\Psi\rangle$. For the two-atom case, there are in total a number of $(4M+8)$ equations, from which one can easily determine the $(4M+8)$ expansion coefficients numerically. In general, the number of equations (or expansion coefficients) for N-atom case is given by $2^{N-1}\times(2M+N+2)$, where the number of discretized modes M is normally much larger than the number of trapped atoms N.

Once the dynamics of the system is solved, we can use the following two quantities to characterize the performance of our atomic gate scheme. (1) Due to various sources of photon loss, photons in the cavity may be lost with then no photon count at the detectors. Hence, we calculate the success probability of a photon count at the detector to characterize the efficiency of the scheme. (2) Even if a photon emerges (neglecting dark counts), there may still be imperfections of the atomic gate mainly due to the shape distortion of the photon pulse after reflection from the cavity, which can be characterized through the gate fidelity. Without loss of the photon, the final atom-photon state can in general be written as $|\Psi_{out}\rangle = \sum_{i_1 i_2} c_{i_1 i_2}\,|i_1 i_2\rangle_a\,|p\rangle_{i_1 i_2}$, where $\sum_{i_1 i_2} c_{i_1 i_2}\,|i_1 i_2\rangle_a$ $(i_1, i_2 = 0, 1)$ is the general form for the input state of the two

atoms. The output photon state $|p\rangle_{i_1 i_2}$ corresponds to the atomic component $|i_1 i_2\rangle_a$, and is given by $|p\rangle_{i_1 i_2} = \int_0^T f_{i_1 i_2}^{out}(t)\, a_{out}^{\dagger}(t)\, dt\, |vac\rangle$ with a shape function $f_{i_1 i_2}^{out}(t)$. Ideally, the output state $\left|\Psi_{out}^{id}\right\rangle$ would have the shape functions $f_{00}^{out}(t) = -f_{in}(t)$ and $f_{i_1 i_2}^{out}(t) = f_{in}(t)$ (for $i_1, i_2 \neq 0$), which realizes a perfect CPF gate U_{12} on the atoms. Hence to characterize the gate imperfection, we calculate the fidelity $F \equiv \left|\left\langle \Psi_{out}^{id} \left| \Psi_{out} \right\rangle\right|^2$, which is directly extendable to any number of atoms. In the following calculation of the fidelity F, we choose the input state $\left[\left(|0\rangle + |1\rangle\right)/\sqrt{2}\right]^{\otimes N}$ for the case of N atoms.

4.4 Numerical Results and Discussion

The results from our calculations are summarized in Fig. 4.3. First, Fig. 4.3A shows the component pulse shape $f_{i_1 i_2}^{out}(t)$ corresponding to a Gaussian input $f_{in}(t)$ for the case of two atoms. Only the component $f_{00}^{out}(t)$ has a notable phase distortion; all others are basically indistinguishable from the input. To account for random variation in the coupling rates g_i, we have also calculated $f_{i_1 i_2}^{out}(t)$ for g_i varying from 2κ to 6κ. The output pulse shapes are nearly identical for g_i varying in this range, which is typical of current experiments. Figure 4.3B shows the corresponding fidelity F of the CPF (or Toffoli) gate from the shape distortion noise with the atom number $N = 2, 3, 4, 5$. The fidelity F improves with increase of the pulse duration T since the shape distortion is reduced for longer pulses. F also increases with the atom number N, which is a bit surprising but actually reasonable: for the N-atom state $\left[\left(|0\rangle + |1\rangle\right)/\sqrt{2}\right]^{\otimes N}$, the fraction of the component $|0\rangle^{\otimes N}$ goes down as $1/2^N$, and the pulse shape distortion noise comes dominantly from this component. Because the component $|0\rangle^{\otimes N}$ dominates the contribution to the gate infidelity, F is also very insensitive to variation of the coupling rates g_i. We have verified that there is no

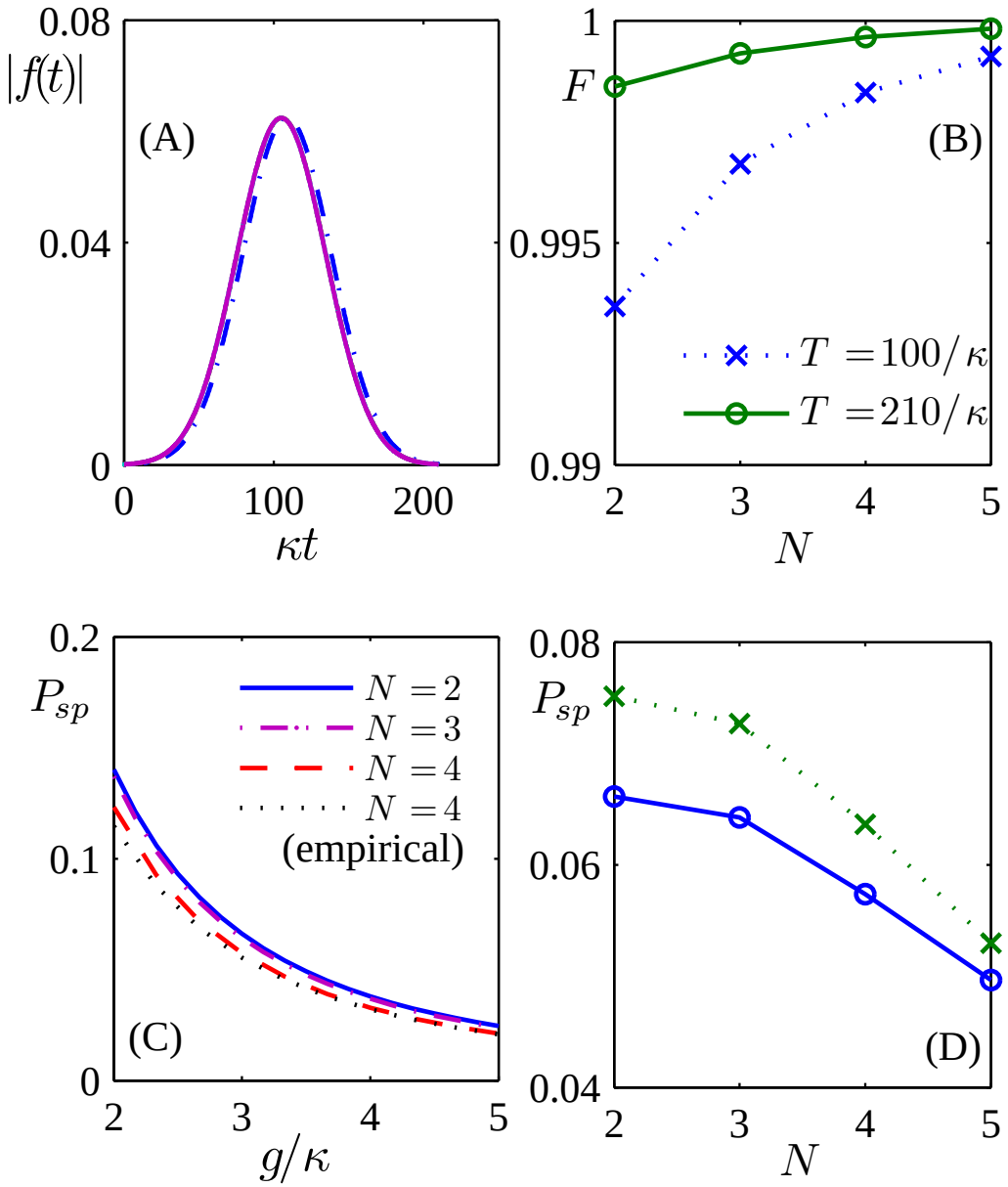

Figure 4.3: (A) The shape functions $|f(t)|$ for the input pulse (solid curve) and the reflected pulses with the atoms in different component states $|i_1 i_2\rangle_a$. The shape function for the atom in the state $|00\rangle_a$ is shown by the dash-dot curve. With the coupling rate g in a typical range from 2κ to 6κ, the shape functions for the atoms in all the other component states are indistinguishable from that of the input pulse (the solid curve). We have assumed a Gaussian shape for the input pulse with $f_{in}(t) \propto \exp\left[-(t-T/2)^2/(T/5)^2\right]$, where t ranges from 0 to T and $T = 210/\kappa$ for this example. (B) The gate fidelity versus the number of atoms with the pulse duration $T = 100/\kappa$ and $T = 210/\kappa$, respectively. (C) The photon loss probability P_{sp} due to atomic spontaneous emission shown as a function of the coupling rate g in units of κ with the atom number N=2,3,4. The dotted curves shows P_{sp} calculated from the empirical formula given in the text for N=4. (D) Comparison of the photon loss P_{sp} for a constant coupling rate $g = 3\kappa$ and for a time varying rate $g_i(t) = 3\kappa(1 + \sin(\nu t + \phi_i)/3)$ for the ith atom, where $\nu = \kappa/6$ corresponds to a typical atom's axial oscillation frequency in the trap, and ϕ_i are taken as random numbers accounting for the atoms' random initial positions. $g_i(t)$ is chosen so that its maximum and minimum differ by a factor of 2, which exceeds that in current experiments [135]. Other parameters for Figs. (A) and (B) are $\gamma_s = \kappa$ and $g = 3\kappa$, and for Figs. (C) and (D), $\gamma_s = \kappa$ and $T = 210\kappa$.

notable change of F in Fig. 4.3B for g_i varying from 2κ to 6κ.

Any source of photon loss has no contribution to the gate fidelity but instead influences gate efficiency (success probability). A fundamental source of photon loss is atomic spontaneous emission. Figure 4.3C shows the failure probability P_{sp} of the gate due to this source of noise, with the noise rate $\gamma_s = \kappa$. For N atoms with equal $g_i = g$, the probability P_{sp} can be well fit by an empirical formula $P_{sp} \approx P_{emp} \equiv \sum_{n=1}^{N} \left(N!/n!(N-n)!2^N\right) \left[1 + ng^2/\kappa\gamma_s\right]^{-1}$. The empirical P_{emp} can be understood as a probability averaged over all the Dicke-state components in the input state $\left[\left(|0\rangle + |1\rangle\right)/\sqrt{2}\right]^{\otimes N}$, with the nth Dicke-component having an effective coupling rate $\sqrt{n}g$ to the cavity mode. We have also simulated the loss probability P_{sp} when the coupling rates g_i are different and vary during the gate operation, for instance, as would be caused by the atoms' thermal motion. With some typical choice of the relevant experimental parameters, the result is shown in Figure 4.3D, which is qualitatively similar to the constant coupling rate case with an effective average over $|g_i|$. Other sources of photon loss can be similarly characterized. For instance, with a finite photon collection and detection efficiency η, the success probability of each gate will be simply reduced by a factor of η.

4.5 Chapter Summary

In summary, we have proposed a novel scheme for robust atomic gates by utilizing interactions mediated by cavity-assisted photon scattering. These gates are robust to all sources of photon loss which is typically the dominant source of error in cavity QED experimental implementations. Furthermore performance of our gate scheme is insensitive to randomness in the coupling rates caused by fluctuations in atomic position. Beyond two-atom gates as illustrated in Fig. 4.1, our scheme can also

be employed for realization of an N-atom Toffoli gate in a single step and for the implementation of nonlocal gates on distant atoms as depicted in Fig. 4.2. We have characterized the efficiency and fidelity of our scheme through exact numerical simulations which incorporate various sources of experimental noises. These results demonstrate the practicality of our scheme, current experimental technology.

CHAPTER V

Implementation of Quantum Controlled-SWAP Gate with Optical Cavity QED

In previous chapters, we have presented our theoretical work on generation of cat states and neutral atom gates with single-sided optical cavity. This chapter will be devoted to another piece of our work on exploiting optical cavity QED for QIP applications. Instead of using a single-sided cavity, the scheme we discuss in this chapter utilizes a double-sided cavity, which is more practical for real experiments. We show how to realize a universal multiqubit entangling gate, namely a quantum controlled-SWAP (CSWAP) gate, with the single-atom cavity QED system. In our scheme, a single trapped atom with four relevant levels serves as the controlling qubit. Conditioned on the atom being in $|0\rangle$ or $|1\rangle$, single-photon pulses incoming from different sides of a double-sided cavity either resonantly tunnel through or get reflected back from the cavity mirrors, leading to an effective CSWAP unitary for optical qubits. We also demonstrate the universality of CSWAP by explicitly constructing a controlled phase flip gate (CPF) with CSWAP and single-qubit gates.

5.1 Introduction

For a CSWAP gate, conditioned on the presence of state $|1\rangle_c$ of a control qubit c, two strings of target qubits $A = \{1, 2, \cdots, n\}$ and $B = \{1', 2', \cdots, n'\}$ exchange their

quantum states. In general, the (2n+1)-qubit CSWAP gate represented by a unitary operator U_{CSWAP} transforms the qubit states according to

$$\begin{aligned} & U_{CSWAP}\left(c_0\left|0\right\rangle_c + c_1\left|1\right\rangle_c\right) \otimes \left|\Psi\right\rangle_A \otimes \left|\Psi'\right\rangle_B \\ = \;& c_0\left|0\right\rangle_c \otimes \left|\Psi\right\rangle_A \otimes \left|\Psi'\right\rangle_B + c_1\left|1\right\rangle_c \otimes \left|\Psi'\right\rangle_A \otimes \left|\Psi\right\rangle_B . \end{aligned} \tag{5.1}$$

The quantum CSWAP gate is universal, in the sense that together with single-qubit gates they can realize arbitrary unitary transformations. Our scheme realizes a "hybrid" CSWAP gate, as the control qubit and target qubits are carried by an atom and series of single-photon optical pulses respectively. The hybrid CSWAP gate can be used to construct a controlled phase flip gate on optical qubits, thereby realizing universal photonic quantum computation. Compared with a recent photonic computation scheme based on single-sided cavities [56], this scheme has the advantage that it is directly built on the state-of-the-art two-sided cavities [134, 135, 136]. It can also be readily applied in quantum dot-cavity systems [147, 148, 149, 150, 151, 152]. Moreover, photons are the most viable choice for remote quantum communication as they can be transmitted over long distance in optical fibers or even in free space while preserving the encoded information. Therefore our gate scheme have a great potential for practical applications in implementing quantum networking and quantum communication protocols. In fact, the quntum CSWAP gate has been proposed as a critical element for several interesting quantum cryptographic schemes, including quantum fingerprinting [145] and quantum digital signatures [146]. The essential function of the CSWAP gate in the quantum fingerprinting and quantum digital signatures protocols is to efficiently evaluate the overlap between two strings of quantum information.

Quantum fingerprinting is a communication protocol between three parties. Two

parties, Alice and Bob, have two strings of information x and y respectively. They are not allowed to communicate directly. Instead, they follow a recipe to associate their string of information with a "fingerprint", which is normally constructed with a much fewer number of qubits than the original information, and then send their fingerprints to a third party, Richard, the referee. Richard determines if the strings held by Alice and Bob are the same or not, solely by comparing the fingerprints received from them. The ultimate goal of the three parties is to allow the referee to get with high probability the correct answer, i.e. $x = y$ or not, (or more generally, $f(x, y) = 0$ or 1), while minimizing the communication costs from Alice and Bob. To compare the fingerprints, the referee can use a CSWAP gate to efficiently measure the overlap of two quantum states $|\psi\rangle$ and $|\phi\rangle$. The quantum circuit for the referee to determine if $|\langle\psi|\phi\rangle|^2 = 1$ or $|\langle\psi|\phi\rangle|^2 \leq \delta$ is shown in Fig. 5.1, where the gate labeled with H is the Hadamard gate, which transforms $|0\rangle$ to $(|0\rangle + |1\rangle)/\sqrt{2}$ and $|1\rangle$ to $(|0\rangle - |1\rangle)/\sqrt{2}$. The whole circuit transforms the quantum states according to

$$(H\otimes I)U_{CSWAP}(H\otimes I)|0\rangle|\psi\rangle|\phi\rangle = (|0\rangle(|\psi\rangle|\phi\rangle+|\phi\rangle|\psi\rangle)+|1\rangle(|\psi\rangle|\phi\rangle-|\phi\rangle|\psi\rangle))/2. \quad (5.2)$$

After this transformation, the referee measures the control qubit and the probability for him to obtain outcome $|1\rangle$ is given by $(1 - |\langle\psi|\phi\rangle|^2)/2$, which is 0 if $x = y$ and is at least $(1 - \delta^2)/2$ if $x \neq y$. We note that although the senario and goal in quantum digital signature protocol is different from quantum fingerprinting, essentially it also exploits similar coding strategy and utilizes the CSWAP gate to compare two quantum states.

In the following sections, we will explain the basic physical idea of realizing the multi-qubit CSWAP gate on two sequences of photon pulses $1, 2, \cdots, n$ and $1', 2', \cdots, n'$ by simply scattering them from a two-sided optical cavity with a single trapped atom. We provide a detailed theoretical modeling, and with some approx-

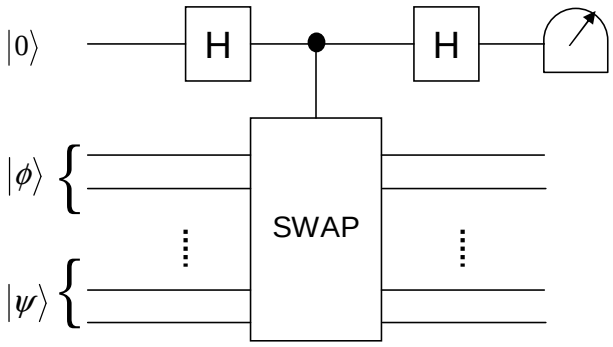

Figure 5.1: A quantum circuit measuring the overlap between two quantum states. The control qubit is initialized in the state $|0\rangle$ before each trial. It undergoes Hadamard gate transformations before and after the controlled-SWAP gate operation. At the end of each trial, the control qubit is measured in the $|0\rangle, |1\rangle$ basis. The overlap between $|\phi\rangle$ and $|\psi\rangle$ is extracted from the probabilities of measurement outcomes (0 or 1) after a number of trials.

imations we solve the model analytically. Our results demonstrate the practicality of our gate scheme under typical experimental conditions of either the atomic or the solid-state cavities. In particular, the scheme requires neither the good cavity limit nor the Lamb-Dicke condition for the localization of the trapped atom, which significantly simplifies its experimental realization.

5.2 Implementation Scheme for CSWAP Gate

In this section, we first explain the basic idea of our scheme for the implementation of the multi-qubit CSWAP gate. Consider an atom trapped in a two-sided optical cavity as shown in Fig. 5.2(a). Relevant energy levels of the trapped atom are shown in Fig. 5.2(b). The cavity supports two eigenmodes a_h and a_v with different polarizations (horizontal "h" and vertical "v", respectively). These two modes are resonantly coupled to the atomic transitions $|0\rangle \leftrightarrow |e_h\rangle$ and $|0\rangle \leftrightarrow |e_v\rangle$ respectively ($|e_h\rangle$ and $|e_v\rangle$ could be superpositions of the Zeeman states on the same excited hyperfine manifold). Level $|1\rangle$ is on a different hyperfine level in the ground-state manifold, and is decoupled from the cavity modes due to the large hyperfine splitting.

The two cavity modes a_h and a_v are resonantly driven by the "h" and "v" polarization components of the single-photon pulses incident on the cavity mirrors, respectively. Each single-photon pulse carries an optical qubit, with basis vectors being the optical polarization states "h" or "v".

If the atom is prepared in the state $|1\rangle$, the input pulses basically see an empty cavity as the atom is decoupled from the cavity modes. With such a resonant cavity, the input pulses from both sides will directly go through if their bandwidth is significantly smaller than the cavity decay rate κ (assuming that both mirrors of the cavity give rise to the same decay rate). The states of the two pulse sequences from different sides are exchanged. (See Fig. 5.2(a) for convention of the notation on cavity input and output. We assume that the pulses from different sides have the same pulse shape.) However, if the atom is prepared in the state $|0\rangle$, due to the strong atom-cavity coupling, the transmission spectrum of the dressed cavity is significantly modified, and the pulses from both sides will be reflected by the cavity mirrors if their bandwidth is significantly smaller than g^2/κ, where g is the atom-cavity coupling rate (see the following theoretical modeling). The states (pulse shape and phase) of the pulses remain unchanged after the reflection. Based on the above considerations for the two different cases, we see that if the atom is prepared in a superposition of the states $|0\rangle$ and $|1\rangle$, this cavity setup performs exactly the CSWAP gate transformation as is described by Eq. (5.1), with the atom being the control qubit and the two n-qubit pulse-sequences incident on different side mirrors being the target qubits.

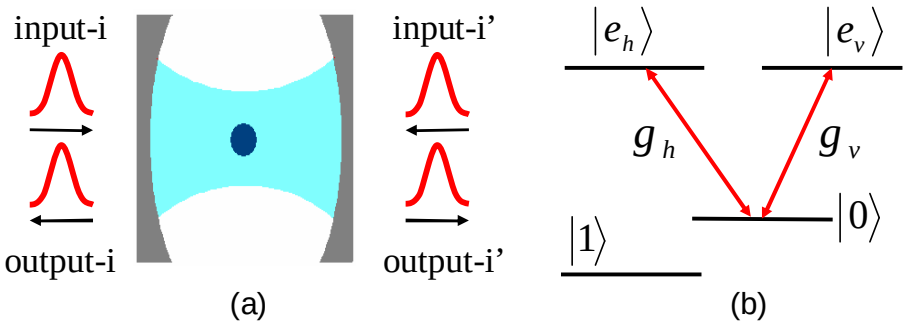

Figure 5.2: (a) Schematic setup for implementation of the multi-qubit CSWAP gate. Two pulse sequences $i, (i = 1, 2 \cdots n)$ and $i', (i' = 1', 2' \cdots n')$ are incident on and then reflected from (or transmitted through) the single-atom cavity. (b) Configuration of relevant atomic levels.

5.3 Theoretical Model and Solution

Now we proceed to present a detailed theoretical modeling of interaction between photonic pulses and an atom confined inside a two-sided optical cavity. This calculation serves for two purposes; first, we need to prove the statements made before for the principle of the CSWAP gate. In particular, we will show that the pulse will undergo reflection or transmission conditional on the atomic state if its bandwidth is much smaller than the coupling rates κ and g^2/κ. Second, we also want to characterize the influence of noise on this gate scheme. The most important noise here is the intrinsic atomic spontaneous emission, which causes loss of photons to uncontrolled directions. There could be other source of photon loss noise, such as the light absorption/scattering at the cavity mirrors. The effect of other photon loss mechanisms, however, is very similar to the atomic spontaneous emission and thus can be similarly modeled.

The interaction between the atom (or, in general, the dipole) and the cavity modes is described by the Hamiltonian in the rotating frame (see Fig. 5.2(b) for the

notations)

$$H = \sum_{\mu=h,v} g_\mu \left(\sigma_\mu^+ a_\mu + \sigma_\mu^- a_\mu^\dagger\right), \tag{5.3}$$

where $\sigma_\mu^+ \equiv |e_\mu\rangle\langle 0|$ and $\sigma_\mu^- \equiv \sigma_\mu^+$ are the atomic raising and lowering operators respectively with $\mu = h, v$ denote the polarization modes, and g_μ are the corresponding atom-cavity coupling rates. The cavity modes a_μ are driven by the corresponding input fields $a_{\mu,l}^{in}$ and $a_{\mu,r}^{in}$ from both the left and the right sides of the cavity. The Heisenberg-Langevin equations for a_μ assume the form [129]

$$\dot{a}_\mu = -ig_\mu\sigma_\mu^- - \left(\kappa_{\mu,l} + \kappa_{\mu,r}\right) a_\mu/2 + \sqrt{\kappa_{\mu,l}} a_{\mu,l}^{in} + \sqrt{\kappa_{\mu,r}} a_{\mu,r}^{in}, \tag{5.4}$$

where $\kappa_{\mu,l}$ and $\kappa_{\mu,r}$ are the cavity decay rates for mode μ of the left and right mirrors respectively. The output fields $a_{\mu,j}^{out}$ ($\mu = h, v$ and $j = l, r$) are connected with the input fields through the cavity input-output relation [129]

$$a_{\mu,j}^{out} = a_{\mu,j}^{in} + \sqrt{\kappa_{\mu,j}} a_\mu. \tag{5.5}$$

Both the input and the output fields satisfy the standard commutation relations $\left[a_{\mu,j}^{in}(t), a_{\mu',j'}^{in\dagger}(t')\right] = \left[a_{\mu,j}^{out}(t), a_{\mu',j'}^{out\dagger}(t')\right] = \delta_{\mu\mu'}\delta_{jj'}\delta(t-t')$. To solve the dynamics of the system, we also need the Heisenberg-Langevin equations for the relevant atomic operators to complete the equation set, which have the form

$$\dot{\sigma_\mu^-} = -i\left[\sigma_\mu^-, H\right] - \gamma_\mu\sigma_\mu^-/2 + \sqrt{\gamma_\mu}\sigma_\mu^z\hat{N}_\mu, \tag{5.6}$$

where γ_μ denotes the spontaneous emission rate of the atomic level $|e_\mu\rangle$, $\sigma_\mu^z \equiv |e_\mu\rangle\langle e_\mu| - |0\rangle\langle 0|$, and $\hat{N}_\mu$ is the corresponding vacuum noise operator which in needed to preserve the desired commutation relations for the atomic operators.

To characterize the CSWAP gate operation, we need to know the cavity output fields given the inputs. Equations (3)-(5) completely determine the dynamics of the system, but in general it is hard to solve this set of nonlinear operator equations.

However, we note in this scheme the atom has a rare opportunity to stay in the excited states $|e_\mu\rangle$, so the matrix elements for the components $|e_\mu\rangle\langle e_{\mu'}|$, where $\mu, \mu' = h$ or v, should be negligible. We have done some exact numerical simulation with the method specified in Refs. [49, 56, 87, 130], which also confirms this approximation. Under this approximation, $-\sigma_\mu^z$ is replaced by the state projector $P_0 = |0\rangle\langle 0|$, and the set of equations (5.3)-(5.5) become linearized [148, 153]. The linearized equations can be easily solved analytically by carrying out Fourier transformations on both sides of the equations, and the output fields are specified by the solution of the form:

$$a_{\mu,j}^{out}(\omega) = R_\mu(\omega) a_{\mu,j}^{in}(\omega) + T_\mu(\omega) a_{\mu,\bar{j}}^{in}(\omega) + m_\mu(\omega)\hat{N}_\mu(\omega), \tag{5.7}$$

where $\{j, \bar{j}\} \equiv \{l, r\}$ or $\{r, l\}$, and for simplicity we have taken $\kappa_{\mu,r} = \kappa_{\mu,l} \equiv \kappa_\mu$. The operators $a_{\mu,j}^{in}(\omega)$ and $a_{\mu,j}^{out}(\omega)$ denote the Fourier transforms of the input and the output field operators $a_{\mu,j}^{in}(t), a_{\mu,j}^{out}(t)$ with respect to time t. The reflection, the transmission, and the noise coefficients $R_\mu(\omega), T_\mu(\omega)$, and $m_\mu(\omega)$ are given respectively by

$$R_\mu(\omega) = \frac{i\omega + g_\mu^2 P_0/\left(i\omega - \gamma_\mu/2\right)}{\kappa_\mu - i\omega - g_\mu^2 P_0/\left(i\omega - \gamma_\mu/2\right)}, \tag{5.8}$$

$$T_\mu(\omega) = \frac{\kappa_\mu}{\kappa_\mu - i\omega - g_\mu^2 P_0/\left(i\omega - \gamma_\mu/2\right)}, \tag{5.9}$$

$$m_\mu(\omega) = \frac{i\sqrt{\kappa_\mu \gamma_\mu} g_\mu P_0/\left(i\omega - \gamma_\mu/2\right)}{\kappa_\mu - i\omega - g_\mu^2 P_0/\left(i\omega - \gamma_\mu/2\right)}. \tag{5.10}$$

Note that our formalism is in the rotating frame where ω measures the frequency detuning with respect to the eigen-frequency of the relevant bare cavity modes. From these expressions, we see that for an incoming pulse with its central frequency resonant with the bare cavity mode, if the pulse bandwidth $\delta\omega$ (inverse of the pulse duration) is much smaller than the rates κ_μ and g_μ^2/κ_μ, and the atomic spontaneous emission noise satisfies the condition $\gamma_\mu \ll g_\mu^2/\kappa_\mu$, we have the reflection coefficient

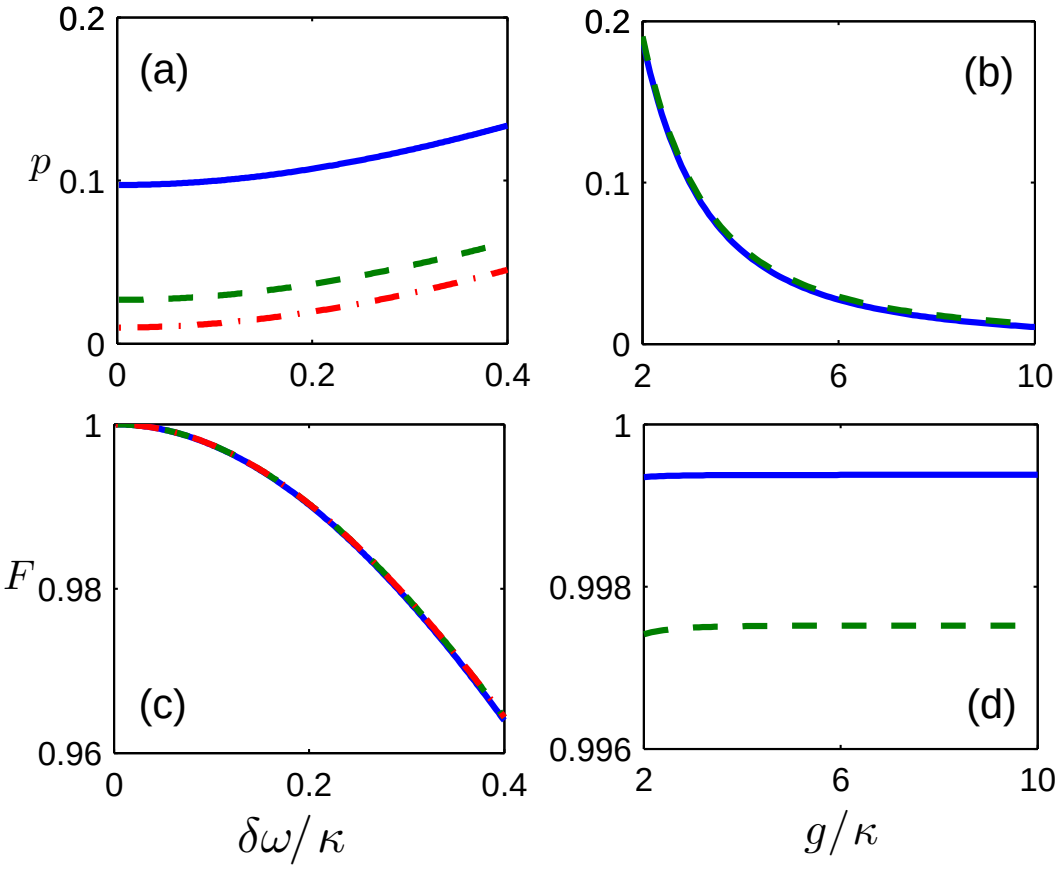

Figure 5.3: Left column: The loss probability p and the fidelity F as a function of the scaled bandwidth $\delta\omega/\kappa$, with $g = 3\kappa$ for the solid line, $g = 6\kappa$ for the dashed line, and $g = 10\kappa$ for the dash-dotted line. Right column: The loss p and the fidelity F as a function of the scaled atom-cavity coupling rate g/κ, with $\delta\omega = 0.05\kappa$ for the solid line and $\delta\omega = 0.1\kappa$ for the dashed line. In the whole figure, we take $\kappa_h = \kappa_v = \kappa$, $\gamma_h = \gamma_v = \gamma$, and $\gamma = \kappa$ for simplicity.

$R_\mu(\omega) \simeq -1$ for the atom in the state $|0\rangle$ and the transmission coefficient $T_\mu(\omega) \simeq 1$ for the atom in the state $|1\rangle$. This exactly confirms the statements that we used for the establishment of the CSWAP gate in the previous section.

To quantitatively characterize the gate performance, we need to specify the evolution from the input state to the output state. The atom is assumed to be initially in the state $|\varphi\rangle_a = (|0\rangle + |1\rangle)/\sqrt{2}$. The input state of the two single-photon pulses from two sides of the cavity can be expressed as $|\Psi\rangle_p = \sum_{\mu,\mu'} C_{\mu\mu'}|\mu\rangle_l|\mu'\rangle_r$, where $\mu, \mu' = h, v$. The qubit basis state $|\mu\rangle_j$ for a single-photon pulse is connected with the input field operator $a^{in}_{\mu,j}(\omega)$ through $|\mu\rangle_j = \int f(\omega) a^{in\dagger}_{\mu,j}(\omega) d\omega |vac\rangle$, where $|vac\rangle$

denotes the vacuum state, and $f(\omega)$ is the normalized pulse shape function in the frequency domain (which has been assumed to be the same for all the input pulses). The state of the output pulses has a similar form but with $a_{\mu,j}^{out\dagger}(\omega)$ replacing $a_{\mu,j}^{in\dagger}(\omega)$. As the output field operator $a_{\mu,j}^{out}(\omega)$ in Eq. (6) depends on the atomic projector P_0, the output state of the photons gets entangled with the atomic state, as one would expect for the CSWAP gate.

We can use two quantities to characterize the gate performance: first, due to the atomic spontaneous emission, we could lose a photon during the gate operation with one of the output modes going to the vacuum state. So we use the loss probability p to characterize the inefficiency of the gate operation. Second, even if both photons show up in the output, their pulse shapes will be slightly distorted due to the frequency-dependent reflection and transmission of the finite bandwidth input pulses. We can use the fidelity to characterize the effect of this pulse shape distortion. To be more specific, we consider a typical initial state $|\Psi_{in}\rangle = |\varphi\rangle_a \otimes |hv\rangle_{l,r}$ for the atom and the photons. In the ideal case, we should get the entangled output state $|\Psi_{out}\rangle = (|0\rangle|hv\rangle_{l,r} + |1\rangle|vh\rangle_{l,r})/\sqrt{2}$, but in real case we in general get a density matrix ρ_{out} after tracing over the noise operator. The overlap $F \equiv \langle\Psi_{out}|\,\rho_{out}|\Psi_{out}\rangle$ defines the fidelity, and we use it to characterize the gate performance. In the above characterization, we distinguish the inefficiency and the infidelity errors for the gate, as the dominant error in this scheme is the inefficiency error which allows for efficient quantum error correction.

From the solution of $a_{\mu,j}^{out}(\omega)$ in Eq. (6) and its connection with the output state, we can calculate the loss probability p and the fidelity F as defined above. Their expressions are given by $p = 1-\left(t_h^{(1)}t_v^{(1)} + r_h^{(0)}r_v^{(0)}\right)/2$ and $F = \left|\xi_h^{(0)}\xi_v^{(0)} + \xi_h^{(1)}\xi_v^{(1)}\right|^2/4$, where the superscripts (0) and (1) denotes the corresponding atomic state, $t_\mu^{(1)} =$

$\int d\omega \left| f(\omega)\, T_\mu^{(1)}(\omega) \right|^2$, $r_\mu^{(0)} = \int d\omega \left| f(\omega)\, R_\mu^{(0)}(\omega) \right|^2$, $\xi_\mu^{(1)} = \int d\omega\, |f(\omega)|^2\, T_\mu^{(1)}(\omega)/\sqrt{t_\mu^{(1)}}$, $\xi_\mu^{(0)} = \int d\omega\, |f(\omega)|^2\, R_\mu^{(0)}(\omega)/\sqrt{r_\mu^{(0)}}$. We take the pulse shape $f(\omega)$ to be a Gaussian function in the form $f(\omega) = \exp(-\omega^2/\delta\omega^2)/\left(\sqrt{\pi}\delta\omega\right)$ with a bandwidth $\delta\omega$. From these expressions, we calculate the loss probability p and the fidelity F as functions of the scaled pulse bandwidth and the atom-cavity coupling rate. The results are shown in Fig. 5.3.

Several remarks are in order from this calculation. First, the fidelity F is basically independent of the coupling rate g in the parameter regime we considered. The loss probability p depends on g, but p remains small as long as the variation in g does not reduce g close to zero. This shows that the scheme here allows random variation of the coupling rate g in a significant range. That is a valuable feature for the atomic cavity, as the thermal motion of the atom typically brings it outside of the Lamb-Dicke limit which induces significant random variation of the coupling rate g in current experiments [134, 135, 136]. Second, the scheme here does not require the good cavity limit $g > \kappa$. Independent of the ratio g/κ, the loss remains small as long as we have the strong coupling condition $g^2/\kappa\gamma \gg 1$ (or called the Purcell condition). This is a valuable feature for the solid state cavity as it is typically hard to get $g > \kappa$ for this setup although the Purcell condition $g^2/\kappa\gamma \gg 1$ can be satisfied [148, 149, 150, 151, 152]. Third, we note that in this scheme the gate infidelity is basically set by the finite pulse bandwidth $\delta\omega/\kappa$, which in principle can be arbitrarily reduced. The intrinsic noise, such as the atomic spontaneous emission (or other kinds of photon loss) only leads to the gate inefficiency errors. Finally, as some explicit parameter estimation, we have the fidelity $F = 99.75\%$ and the loss $p = 1.3\%$ with the parameters $(g, \kappa, \gamma)/2\pi = (32, 4.2, 2.6)$ MHz and $\delta\omega = 0.1\kappa$, as typical for the atomic cavity [134, 135, 136]; and $F = 99.76\%$, $p = 1.59\%$ with

$(g, \kappa, \gamma)/2\pi = (0.66, 6, 0.001)$ THz and $\delta\omega = 0.1g^2/\kappa$, as typical for a solid state cavity [149, 150, 151, 152].

5.4 Construction of Photonic Controlled Phase Flip Gate from CSWAP

As mentioned before, the multi-qubit CSWAP gate implemented by this cavity setup is ideal for the measurement of overlap of two n-qubit wave functions carried by the photon pulses. Therefore, the scheme is critical for realization of a number of quantum cryptographic protocols, such as quantum fingerprinting and quantum digital signature [145, 146]. Beyond this application, here we also want to show that the simplest version of this gate, the CSWAP on two optical qubits (denoted as CSWAP_2), also provides a critical gate, which, together with simple single-qubit rotations, realize universal photonic quantum computation. In this computational scheme, the qubits are represented by the single-photon pulses, which have the advantages of being relatively easy to scale to many qubits and to integrate into quantum networks. The atom (or the quantum dot in the solid-state cavity) only acts as an ancilla qubit which mediates strong interaction between the photons during the gate operation. To see the universality of the CSWAP_2 gate, it is enough to show that, together with single-bit rotations, it leads to the standard controlled phase flip (CPF) gate on two arbitrary photonic qubits. In Fig. 5.4(a), from the CSWAP_2 gates we give one construction of the CPF gate $U_{CPF} = e^{i\pi|hv\rangle_{12}\langle hv|}$, which flips the phase of the photons 1 and 2 if and only if they are in the state component $|hv\rangle$. The atomic qubit is initially prepared in the state $|\varphi\rangle_a = (|0\rangle + |1\rangle)/\sqrt{2}$, which is recovered after the whole operation. In this construction, we use four CSWAP_2 gates, together with a few single-bit Hadamard gates H and $e^{i\pi/2}$-phase gates (the latter adds a phase $e^{i\pi/2}$ to the state component $|1\rangle$). This construction can be fur-

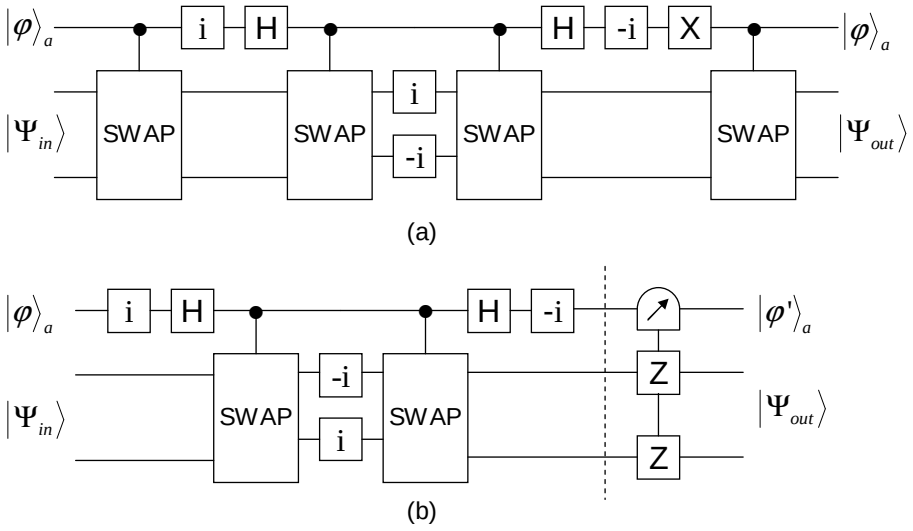

Figure 5.4: (a)A circuit to construct a controlled phase flip gate from the CSWAP gates. (b)An alternative circuit which uses only two CSWAP gates, but with feed-forward of a measurement on the atomic qubit (see the text for explanation).

ther simplified if we use feed-forward from a measurement on the atomic qubit. In Fig. 5.4(b), we give a simplified circuit which uses only two CSWAP_2 gates. After the operation represented by the left side of this circuit, we perform a measurement on the atomic qubit in the basis $\{|0\rangle, |1\rangle\}$, and upon the outcome "1", we add a $\sigma_z = |h\rangle\langle h| - |v\rangle\langle v|$ (single qubit Z-gate) to each of the photonic qubits. One can verify that the whole operation also performs the gate U_{CPF} on the two photonic qubits. These constructions prove that the CSWAP_2 gates, combined with single-bit rotations, realize universal quantum computation on photon pulses.

5.5 Chapter Summary

In summary, we have proposed a scheme to realize multi-qubit controlled-SWAP gates, which have critical application for implementation of both quantum cryptographic protocols and universal photonic quantum computation. Our scheme is directly based on state-of-the-art two-sided optical cavity QED technology. A single trapped four-level atom confined in the two-sided cavity serves as the controlling

qubit for our proposed CSWAP gate while optical qubits carried by single-photon pulses and incident from different side of the cavity are the target qubits. The optical pulses either resonantly tunnel through the cavity or directly refelcted back by the mirrors, conditional on the atomic state being in $|0\rangle$ or $|1\rangle$, which effectively realizes the CSWAP unitary transformation. With appropriate approximations, we manage to analytically solve the dynamics of the system, thereby being able to quantify the performance of our scheme under practical noises. Our results indicate that the scheme is insensitive to random variations of atom-cavity coupling constant induced by thermal motion of the trapped atom and its realization should be within the reach of current experimental technology. We also demonstrate explicitly how to construct controlled phase flip gate on photonic qubits from the proposed hybrid CSWAP gate and single qubit gates.

CHAPTER VI

Time Evolving Block Decimation Algorithm

In previous chapters, we have been focusing on physical implementation schemes for QIP with quantum optical means. Although our schemes and many other proposals seem to be promising to be realized, there remain tremendous challenges which need to be addressed before we can get a working prototype quantum computer in laboratories, which could support the execution of nontrivial quantum algorithms. While working toward this ultimate goal, we have also been making progress in deepening our understanding on theoretical foundations of quantum information science, especially the physics of quantum entanglement[24, 25, 26, 27, 28]. Although it has not been thoroughly understood yet, quantum entanglement is believed to play a central role in determining the computational power of quantum computers.

For one dimensional stongly interacting quantum many-body systems with local interactions, although entanglement does present, they can nevertheless be efficiently simulated with algorithms running on classical computers [88, 89, 155, 156]. For systems in higher dimension, however, efficient classical algorithms only exist under very limited situations (certain interaction Hamiltonian, certain geometry, etc). From the perspective of quantum information science, the classical simulatability of strongly interacting systems can be related to scaling laws of entanglement, i.e. how fast en-

tanglement grows with the size of the system. Recently there have been many novel algorithms proposed from this perspective [10, 11, 12, 13, 14, 15, 16, 17].

Implementing efficient classical algorithms to study strongly interacting systems is certainly of great interests for physicists. While we are not sure when, if ever, a reliable quantum computer or even a quantum simulator will be invented to solve interesting but hard physics problems for us, we want to stretch the capability of classical computers to its limit and hopefully we will still have enough room to study some interesting new physics with them. As a beginning step toward this direction, we have implemented a time evolving block decimation (TEBD) algorithm to study strongly interacting systems in one-dimension [10, 11, 15]. TEBD can be viewed as an extension to the well known density matrix renormalization group (DMRG) algorithm [88, 89]. We choose to implement this TEBD algorithm, as it could also serve as building blocks for further construction of certain two-dimensional algorithms besides its own merits. For the rest of this chapter, we will focus our attension on the TEBD algorithm, introducing its basic ideas and formalisms.

6.1 Tensor Product State Ansatz

The complexity in simulating quantum many-body physics arises in the first place due to the large Hilbert space where the quantum states of the system reside. Naively, for a system with N particles, each of which has a local dimension of d, in total one needs d^N coefficients to fully describe the quantum state of the system, which can in general be expressed as $|\Psi\rangle = \sum_{i_1=1}^{d} \cdots \sum_{i_N=1}^{d} c_{i_1 \ldots i_N} |i_1 \cdots i_N\rangle$. In order to simulate the system with classical computers, one has to devise smart algorithms to truncate the size of the Hilbert space while preserving as much as possible the physical properties of the system. To achieve such efficient truncation, one can make

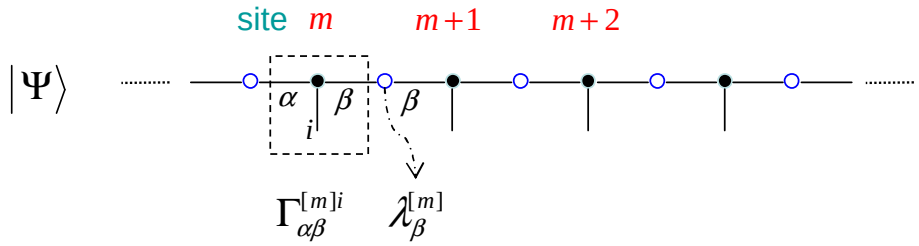

Figure 6.1: Graph illustration of the tensor product representation of quantum many-body state. A solid dot locating at site m represents $\Gamma^{[m]}$ associated with the site, while an open circle between site m and site $m+1$ represents $\lambda^{[m]}$, corresponding to the Schmidt coefficients for a bipartition of the system between sites m and $m+1$. The lines attached to the solid dots and open circles stand for the indices associated with the tensors Γ's and λ's. Connections of the lines on different tensors correspond to contraction of the corresponding indices.

various variational state ansatz for the system. For example, the essence of the so-called mean field approach is to restrict the variational state to be product state of the form $|\Psi\rangle = \sum_{i_1=1}^{d} c_{i_1}^{[1]}|i_1\rangle \cdots \sum_{i_N=1}^{d} c_{i_N}^{[N]}|i_N\rangle$, boldly reducing the number of coefficients from d^N down to Nd. This approach could lead to some qualitatively correct resutls and is being widely used. Nevertheless it is known to be prone to fail under many circumstances espeically for one-dimensional (1D) systems.

Instead of choosing product states as ansatz states, TEBD as well as some other successful 1D algorithms exploits ansatz states of the tensor product form [88, 89, 10, 11, 12, 13, 14, 15, 16, 17]. In particular, the tensor product representation of quantum states used in TEBD algorithm assumes the form:

$$|\Psi\rangle = \sum_{i_1,\ldots i_N=1}^{d} \sum_{\alpha_1,\ldots\alpha_N=1}^{\chi} \Gamma_{\alpha_1}^{[1]i_1} \lambda_{\alpha_1}^{[1]} \Gamma_{\alpha_1\alpha_2}^{[2]i_2} \lambda_{\alpha_2}^{[2]} \cdots \Gamma_{\alpha_{N-1}}^{[N]i_N} |i_1, i_2, \cdots i_N\rangle, \tag{6.1}$$

in which the description of quantum states of an N-site quantum lattice system needs about a number of $(d\chi^2 + \chi)N$ coefficients. As demonstrated in the original work of Vidal, the validity and efficiency of this tensor product representation can be justified from the perspective of entanglement theory. To see it more clearly, let us consider an arbitrary bipartition of an N-site lattice system into two subsets A and B. By applying the Schmidt decomposition, one can always put the quantum

state of the system in the following form:

$$|\Psi\rangle = \sum_{\alpha=1}^{\chi_A} \lambda_\alpha |\phi_\alpha\rangle_A \otimes |\psi_\alpha\rangle_B, \tag{6.2}$$

where $|\phi_\alpha\rangle_A$ ($|\psi_\alpha\rangle_B$) are eigenvectors of reduced density matrix $\rho_A \equiv \mathrm{tr}_B\ (|\Psi\rangle\langle\Psi|)$ ($\rho_B = \mathrm{tr}_A(|\Psi\rangle\langle\Psi|)$) with corresponding eigenvalues $|\lambda_\alpha|^2$. As a matter of fact, given any quantum state of an N-site quantum lattice system, one can carry out series of concatenated Schmidt decompositions, which finally lead to the decomposition of state expansion coefficients in the form as shown in equation (6.1). As a first step, we split the system bipartitely into subset A cosisting of site 1 and subset B consisting of the remaining $N-1$ sites and carry out the Schmidt decomposition:

$$|\Psi\rangle = \sum_{\alpha_1} \lambda_{\alpha_1}^{[1]} |\Phi_{\alpha_1}^{[1]}\rangle \otimes |\Phi_{\alpha_1}^{[2,3,\cdots N]}\rangle \equiv \sum_{\alpha_1,i_1} \Gamma_{\alpha_1}^{[1]i_1} \lambda_{\alpha_1}^{[1]} |i_1\rangle \otimes |\Phi_{\alpha_1}^{[2,3,\cdots N]}\rangle, \tag{6.3}$$

where we have expanded the Schmidt eigenvectors $|\Phi_{\alpha_1}\rangle$ for site-1 with its local basis vectors $\{|i_1\rangle, i_1 = 1, \cdots d\}$, i.e. $|\Phi_{\alpha_1}\rangle = \sum_{i_1} \Gamma_{\alpha_1}^{[1]i_1} |i_1\rangle$. To further decompose the Schmidt eigenvectors of the reduced density matrix for the remaining $(N-1)$ sites, we follow a 2-step recipe and single out site-2 from the remaining $N-2$ sites: (i) explicitly expand each eigenvector $|\Phi_{\alpha_1}^{[2,3,\cdots N]}\rangle$ with local basis vectors $\{|i_2\rangle, i_2 = 1, \cdots d\}$ for site 2 as $|\Phi_{\alpha_1}^{[2,3,\cdots N]}\rangle = \sum_{i_2} |i_2\rangle |\varphi_{\alpha_1 i_2}^{[3,\cdots N]}\rangle$; (ii) express $|\varphi_{\alpha_1 i_2}^{[3,\cdots N]}\rangle$ in terms of the eigenvalues and eigenvectors of the reduced density matrix $\rho^{[3,\cdots N]}$ as $|\varphi_{\alpha_1 i_2}^{[3,\cdots N]}\rangle = \sum_{\alpha_2} \Gamma_{\alpha_1\alpha_2}^{[2]i_2} \lambda_{\alpha_2} |\Phi_{\alpha_2}^{[3,\cdots N]}\rangle$. By iterating the recipe and singling out one site at a time in sequence through the 1D chain, we will arrive at the expression (6.1).

The maximum number of non-zero λ_α over all possible bipartitions provides a natural measure of bipartite entanglement, namely $E_\chi \equiv -\log_2(\chi)$ with $\chi \equiv \max_A \chi_A$. If the entanglement of the system is well-bounded such that E_χ scales only as order of $\log(N)$, then the total number of coefficients in the tensor product representation scales polynomially with N, thereby allowing faithful and efficient description

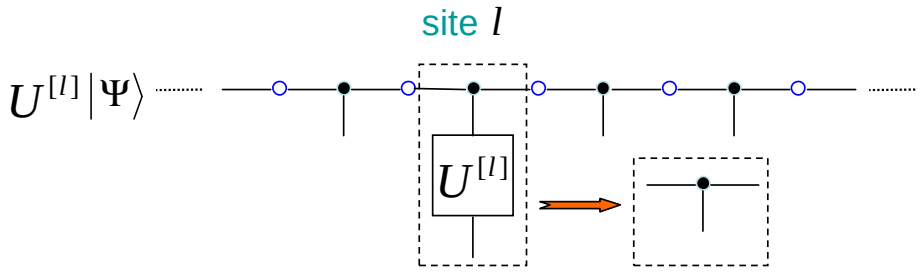

Figure 6.2: Cartoon illustration of the tensor product representation update upon action of single-site unitary gate. The action of unitary operator $U^{[l]}$ only affects the tensor $\Gamma^{[l]}$ associated with site-l.

of many-body quantum states.

6.2 Updating the Tensor Product State Representation upon Unitary Transformations

As shown in the previous section, the TEBD tensor product state representation of quantum states is directly connected with Schmidt decomposition, which endows this representation many elegant properties, allowing us to further complete the whole algorithm with ease. To simulate the dynamics of a quantum system, we need the ability to efficiently update our state decomposition after each unitary transformation. And in general, it would be sufficient for us to consider only those transformations acting only on one or two sites. We will explain why it is the case in a bit more detail later in this chapter. For now, we can understand it intuitively based on the knowledge that from single-qubit and two-qubit entangling gates one can in principle reproduce any unitary gate with an arbitrarily small error as we have learned from the quantum computation theory. Consider an arbitrary unitary operator acting on a single site l. In general the operator is represented by a $d \times d$ unitary matrix $U^{[l]}$, where d is the local Hilbert space dimension of the specific site. If we split the system into two subsets $A = [1, \cdots, l]$ and $B = [l+1, \cdots, N]$, the Schmidt decomposition form of the quantum state of the system before the unitary transformation is given by

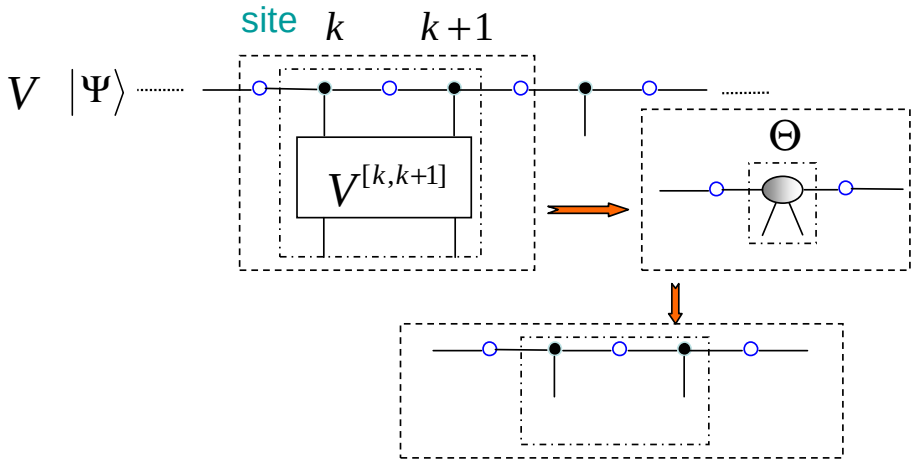

Figure 6.3: Cartoon illustration of the tensor product representation update after the action of unitary transformation targeting on two adjacent sites. The action of unitary operator $V^{[k,k+1]}$ only affects the three tensors enclosed within the dashed box. However the Schmidt decomposition (or, equivalently singular value decomposition) calculation actually involves two extra tensors $\lambda^{[k-1]}$ and $\lambda^{[k+1]}$.

$|\Psi\rangle = \sum_{\alpha_l} \lambda_{\alpha_l} |\Phi^{[A]}_{\alpha_l}\rangle |\Phi^{[B]}_{\alpha_l}\rangle$, where $|\Phi^{[A]}_{\alpha_l}\rangle = \sum_{\alpha_1,\cdots,\alpha_{l-1}} \Gamma^{[1]i_1}_{\alpha_1} \lambda^{[1]}_{\alpha_1} \cdots \Gamma^{[l]i_l}_{\alpha_{l-1}\alpha_l} |i_1 \cdots i_l\rangle$ and $|\Phi^{[B]}_{\alpha_l}\rangle = \sum_{\alpha_{l+1},\cdots,\alpha_N} \Gamma^{[l+1]i_{l+1}}_{\alpha_l \alpha_{l+1}} \lambda^{[1+1]}_{\alpha_{l+1}} \cdots \Gamma^{[N]i_N}_{\alpha_N} |i_{l+1} \cdots i_N\rangle$ as explained in the previous section. After applying $U^{[l]}$, the state is given by $U^{[l]}|\Psi\rangle = \sum_{\alpha_l} \lambda_{\alpha_l} |\Phi'^{[A]}_{\alpha_l}\rangle |\Phi^{[B]}_{\alpha_l}\rangle$, with $|\Phi'^{[A]}_{\alpha_l}\rangle \equiv I^{[1,\ldots,l-1]} \otimes U^{[l]} |\Phi^{[A]}_{\alpha_l}\rangle$. Since unitary transformations preserve the form of Schmidt decomposition, we know that the tensors $\lambda^{[l]}, \cdots, \lambda^{[N-1]}$ and $\Gamma^{[l+1]}, \cdots, \Gamma^{[N]}$ which are associated with the sites in subset B, do not change upon the action of $U^{[l]}$. On the other hand, if we partition the system into $C = [1, \cdots, l-1]$ and $D = [l, \cdots, N]$, following similar argument, we get that the tensors associated with the sites in subset C, i.e. $\lambda^{[1]}, \cdots, \lambda^{[l-1]}$ and $\Gamma^{[1]}, \cdots, \Gamma^{[l-1]}$, do not need to be updated upon the action of $U^{[l]}$ either. Therefore we arrive at a conclusion that unitary operators acting on single particle l only transform the tensor $\Gamma^{[l]}$. And it is straightforward to figure out that the new tensor $\Gamma'^{[l]}$ is given by $\Gamma'^{[l]i} = \sum_j U_{i,j} \Gamma^{[l]j}$.

Next we introduce how to update the tensor product decomposition when unitary operators are applied on two neighboring sites k and $k+1$. Following the same logic as we used above for single-qubit operations, we divide the system in two ways,

where the two neighboring target sites either locate in the left subset or right subset, and write down the state in corresponding Schmidt decompositions. Because unitary operators preserve the Schmidt decomposition forms corresponding to the two ways of partitioning, we deduce that only three tensors, namely $\Gamma^{[k]}$, $\Gamma^{[k+1]}$, and $\lambda^{[k]}$, need to be updated. To demonstrate how to update the three tensors associated with sites k and $k+1$, we divide the system into four parts, namely $L = [1, \cdots, k-1]$, sites k, $k+1$, and $R = [k+2, \cdots, N]$. The quantum state of the system can be expanded with Schmidt eigenvectors for subsystems L and R and local basis vectors for sites k and $k+1$ as

$$|\Psi\rangle = \sum \lambda^{[k-1]}_{\alpha_{k-1}} \Gamma^{[k]i_k}_{\alpha_{k-1}\alpha_k} \lambda^{[k]}_{\alpha_k} \Gamma^{[k+1]i_{k+1}}_{\alpha_k\alpha_{k+1}} \lambda^{[k+1]}_{\alpha_{k+1}} |\Phi^{[L]}_{\alpha_{k-1}} i_k i_{k+1} \Phi^{[R]}_{\alpha_{k+1}}\rangle, \tag{6.4}$$

where the summation over recurring indices is understood. Consider a $d^2 \times d^2$ unitary operator $V_{i_k i_{k+1}, i'_k i'_{k+1}}$ acting on sites k and $k+1$. It is straightforward to write down

$$\begin{aligned} |\Psi'\rangle = V|\Psi\rangle &= \sum \lambda^{[k-1]}_{\alpha_{k-1}} V_{i_k i_{k+1}, i'_k i'_{k+1}} \Gamma^{[k]i'_k}_{\alpha_{k-1}\alpha_k} \lambda^{[k]}_{\alpha_k} \Gamma^{[k+1]i'_{k+1}}_{\alpha_k\alpha_{k+1}} \lambda^{[k+1]}_{\alpha_{k+1}} |\Phi^{[L]}_{\alpha_{k-1}} i_k i_{k+1} \Phi^{[R]}_{\alpha_{k+1}}\rangle \\ &= \sum \lambda^{[k-1]}_{\alpha_{k-1}} \Theta_{(i_k\alpha_k)(i_{k+1}\alpha_{k+1})} \lambda^{[k+1]}_{\alpha_{k+1}} |\Phi^{[L]}_{\alpha_{k-1}} i_k i_{k+1} \Phi^{[R]}_{\alpha_{k+1}}\rangle, \end{aligned} \tag{6.5}$$

where $\Theta_{(i_k\alpha_k)(i_{k+1}\alpha_{k+1})} \equiv \sum V_{i_k i_{k+1}, i'_k i'_{k+1}} \Gamma^{[k]i'_k}_{\alpha_{k-1}\alpha_k} \lambda^{[k]}_{\alpha_k} \Gamma^{[k+1]i'_{k+1}}_{\alpha_k\alpha_{k+1}}$ and the summation over recurring indices are understood. At this stage, if we partition the system by cutting the link between k and $k+1$, we can proceed with the state update by carrying out Schmidt decomposition corresponding to this partition, so that we can obtain the new tensors $\Gamma'^{[k]}$, $\Gamma'^{[k+1]}$, and $\lambda'^{[k]}$. In Fig. 6.3, we illustrate the essential update procedure for the tensor product representation upon the action of unitary operator acting on two adjacent sites.

6.3 Simulating Dynamics of Quantum Systems with TEBD

6.3.1 Trotter Expansion

Now that we have learned how to efficiently describe the quantum state of 1D strongly interacting quantum lattice system as well as how to update the state description upon action of unitary operators, we are at the position to utilize the technique to simulate the dynamics of physical systems. From quantum mechanics, we know that the dynamics of a (closed) quantum system (in pure state) is determined by its Hamiltonian through the Schrödinger equation. The unitary evolution of the system can be formally expressed as

$$|\Psi(t)\rangle = \exp\left(-i \int H dt\right)|\Psi_0\rangle. \tag{6.6}$$

To carry out numerical simulation, we can discretize the evolution as $|\Psi(t_0 + \delta t)\rangle = \exp\left(-iH\delta t\right)|\Psi(t_0)\rangle$.

However, In general the unitary gate $\exp\left(-iH\delta t\right)$ can be very large ($d^N \times d^N$) even though H only contains local interactions. Therefore, in addition to efficient state representation, one also needs to find a way to efficiently decompose $U = \exp\left(-iH\delta t\right)$ into smaller gates acting on, for example, at most two sites. Fortunately, there have been extensive studies on this subject under other research context, e.g. in development of quantum monte carlo method [157]. In particular, the so-called Trotter expansion provides such an efficient decomposition, with which the propagation of numerical errors is well under control.

Consider a quantum lattice Hamiltonian with only local interactions, which has a generic form of $H = \sum_{\{i,j\}} H_{i,j}$, where the summation is over all neighboring sites $\{i, j\}$. (Note that summation over single-site terms $\sum_k H_k$ can also be cast into the form of two-site Hamiltonian as $\sum_{\{k,l\}}(H_k + H_l)/2$, where $\{k, l\}$ denotes

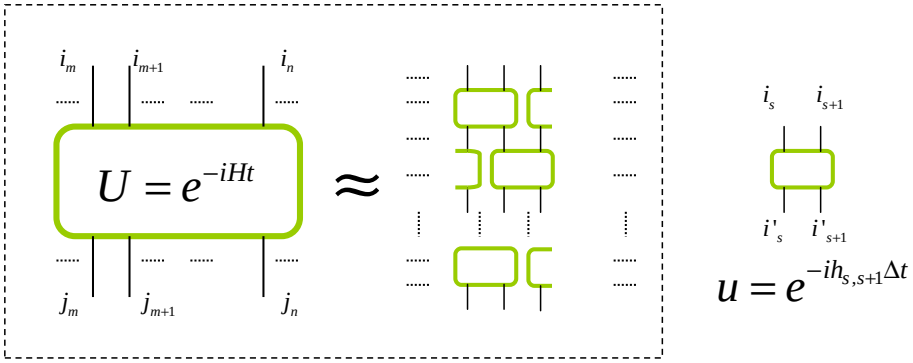

Figure 6.4: Schematic visualization of efficient decomposition of unitary time-evolution operator. Full description of the unitary evolution operator e^{-iHt} ($\hbar = 1$) in general requires $d^N \times d^N$ matrix elements. To enable efficient simulation of quantum dynamics, one can approximate the large unitary time-evolution operator with series of "small" unitary gate operators ($d^2 \times d^2$ unitary matrices) through Totter expansion.

all neighboring pairs of sites.) The unitary gate U now assumes the form $U = \exp\left(\sum_s O_{s,s+1}\right)$, with $O_{s,s+1} = -iH_{s,s+1}\delta t$. In general, since operator O's acting on different sites may not commute with each other, we can not directly decompose U into direct product of $\exp\left(O_{s,s+1}\right)$. To do the decomposition correctly, we first separate the summation over even and odd s, i.e. $\sum_s O_{s,s+1} = F + G$ with $F \equiv \sum_{\text{odd}\ \ s} O_{s,s+1}$ and $G \equiv \sum_{\text{even}\ \ s} O_{s,s+1}$. Now that the terms within F or G commute with each other, if we can further manage to separate F and G in the exponential, we are done with the decomposition. According to general theory of Trotter expansion, there are different orders of approximation to achieve the goal of efficient exponential decomposition. The first order expansion takes the simple form:

$$e^{\delta A+\delta B} = \lim_{\delta\to 0}\left(e^{\delta A}e^{\delta B} + O(\delta^2)\right). \tag{6.7}$$

By simply symmetrizing the above decomposition, one can obtain the second order expansion:

$$e^{\delta A+\delta B} = \lim_{\delta\to 0}\left(e^{\delta A/2}e^{\delta B}e^{\delta A/2} + O(\delta^3)\right). \tag{6.8}$$

Theoretically, there are various ways to construct higher order expansions. A more detailed introduction to general theory on the systematic perturbative expansion can

be found in Ref. [157]. For our purpose, a 4th order expansion would be a fairly good approximation. In particular, we adopt in our calculations an improved version of the 4th order Trotter expansion:

$$e^{\delta A+\delta B} = \lim_{\delta\to 0}\left(e^{p_2\delta A/2}e^{p_2\delta B}e^{(1-3p_2)\delta A/2}e^{(1-4p_2)\delta B}e^{(1-3p_2)\delta A/2}e^{p_2\delta B}e^{p_2\delta A/2}+O(\delta^5)\right), \tag{6.9}$$

where the parameter p_2 is given by $p_2 = (4-4^{1/3})^{-1}$. By substituting δA and δB in the 4th order expansion with F and G which are given in the previous paragraph, we can readily decompose the unitary evolution operator U.

6.3.2 Efficient Computation of Reduced Density Matrices and Correlation Functions from the Tensor Product Representation

A quantum state can not be directly monitored or accessed, instead, we extract information about the quantum state by measuring correlation functions of certain physical observables. As stated earlier in this chapter, the connection between the TEBD state representation and Schmidt decomposition leads to many elegant properties for the representation. These properties enable us to compute reduced density matrices as well as correlation functions efficiently from the tensors λ's and Γ's. In the following, we introduce how to obtain single-site and two-site reduced density matrices, $\rho^{[s]}$ and $\rho^{[s,s']}$, as well as how to obtain correlation functions of the form $\langle O^{[s]}O^{[s']}\rangle$. The reduced density matrix is defined as $\mathrm{tr}_{environment}(|\Psi\rangle\langle\Psi|)$, where the trace is nothing more than contractions of physical indices i's of tensor Γ's associated with the environment. Due to the Schmidt decomposition construction, the contractions from either end of the chain to any site s associated with a tensor $\Gamma^{[s]}_{\alpha_{s-1}\alpha_s}$ simply reduce to identity matrices $\{I_{\alpha_{s-1},\alpha'_{s-1}}\} = \delta_{\alpha_{s-1}\alpha'_{s-1}}$ and $\{I_{\alpha_s,\alpha'_s}\} = \delta_{\alpha_s\alpha'_s}$. Single-site reduced density matrix for site s is then given by

$$\rho_{i,i'} = \mathrm{tr}\left(\Gamma^{[s]i}\Gamma^{[s]i'\dagger}\right). \tag{6.10}$$

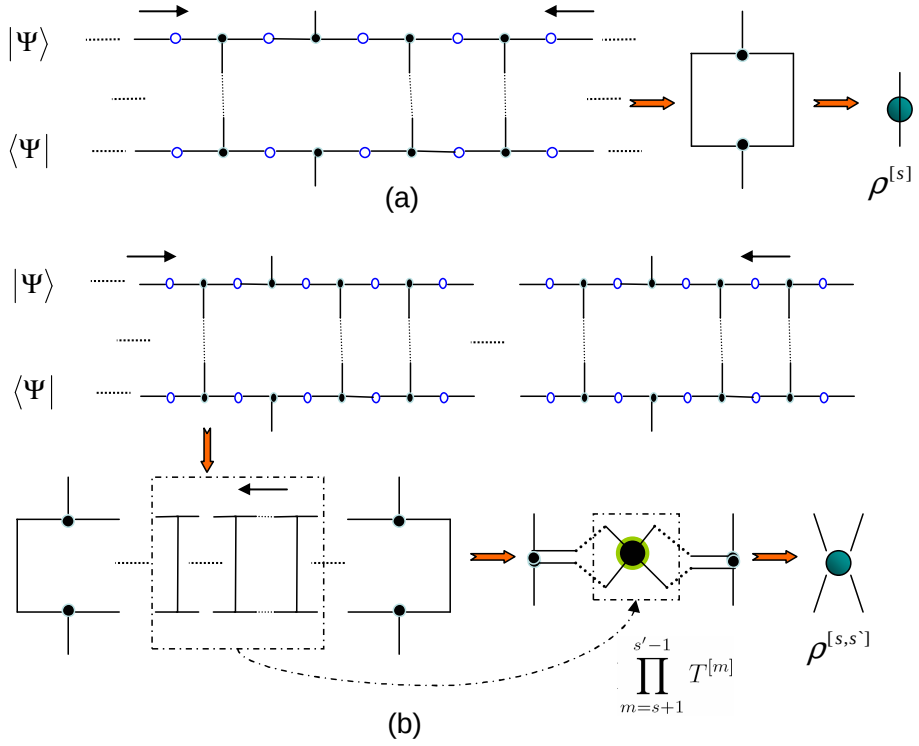

Figure 6.5: Illustration of efficient calculation for reduced density matrices. (a) Computation of single-site reduced density matrices; (b) Calculation of two-site reduced density matrices $\rho^{[s,s']}$. Thanks to the nice form of Schmidt decomposition, the contractions of the tensor network from either ends of the chain to "outer" neighbors of site s and s' are trivial and simply reduce to contraction of Schmidt coefficient tensors $\lambda^{[s-1]}$ and $\lambda^{[s']}$ with their respective conjugates.

Computation of the two-site reduced density matrix $\rho^{[s,s']}$, however, is more involved than the single-site calculation and its computational cost is related to the distance between the two relevant sites since we have to explicitly contract the tensors associated with the sites lying between them. To carry out the contraction, we first construct a $\chi^2 \times \chi^2$ matrix for each site m between site s and s' with $\Gamma^{[m]}$, $\lambda^{[m-1]}$ and $\lambda^{[m]}$ according to

$$\{T^{[m]}_{\alpha_{m-1}\alpha'_{m-1},\alpha_m\alpha'_m}\} = \sum_{i_m} \sqrt{\lambda^{[m-1]}_{\alpha_{m-1}}\lambda^{[m-1]}_{\alpha'_{m-1}}}\Gamma^{[m]i_m}_{\alpha_{m-1}\alpha_m}\Gamma^{[m]i_m*}_{\alpha'_{m-1}\alpha'_m}\sqrt{\lambda^{[m]}_{\alpha_m}\lambda^{[m]}_{\alpha'_m}}. \tag{6.11}$$

The two-site reduced density matrix can then be obtained through

$$\begin{aligned}\{\rho^{[s,s']}_{ij,i'j'}\} &= \sum_{\alpha_s,\alpha'_s,\alpha_{s'-1},\alpha'_{s'-1}} \left(\sum_{\alpha_{s-1},\alpha'_{s-1}} \Gamma^{[s]i}_{\alpha_{s-1}\alpha_s}\Gamma^{[s]i'*}_{\alpha'_{s-1}\alpha'_s}\sqrt{\lambda^{[s]}_{\alpha_s}\lambda^{[s]}_{\alpha'_s}}\right) \\ &\times \{\prod_{m=s+1}^{s'-1} T^{[m]}\}_{\alpha_s\alpha'_s,\alpha_{s'-1}\alpha'_{s'-1}} \left(\sum_{\alpha_{s'},\alpha'_{s'}} \Gamma^{[s']j}_{\alpha_{s'-1}\alpha_{s'}}\Gamma^{[s']j'*}_{\alpha'_{s'-1}\alpha'_{s'}}\sqrt{\lambda^{[s'-1]}_{\alpha_{s'-1}}\lambda^{[s'-1]}_{\alpha'_{s'-1}}}\right).\end{aligned} \tag{6.12}$$

In Fig. 6.5, we show the tensor product representations of state $|\Psi\rangle$ and its conjugate $\langle\Psi|$ as well as the contraction of them for calculation of reduced density matrix. Once obtaining reduced density matrices of the quantum lattice system, one can further compute its correlation functions according to $\mathrm{tr}(\rho^{[s]}O^{[s]})$ and $\mathrm{tr}(\rho^{[s,s']}O^{[s]}O^{[s']})$. Nevertheless, we can also directly compute them in a way similar to the density matrix calculations.

Before ending the introduction to TEBD, we note that this TEBD algorithm can be readily adapted to compute ground state properties of the system by evolving, according to imaginary time, an arbitrary initial state which has nonvanishing overlap with the true ground state. Although the imaginary time evolution is not unitary, in practice we can choose small time steps δt so that the imaginary evolution is very close to a unitary one. It turns out that this method indeed produces very accurate physical results.

6.4 Chapter Summary

In this chapter, we have introduced basic concepts of TEBD algorithm, as well as how to simulate 1D quantum systems with it. This algorithm catches the essence of entanglement scaling in 1D quantum systems and exploits Schmidt decomposition to arrive at a very elegant tensor product representation of quantum states. It allows us to efficiently update the state description upon unitary operations and compute physical properties of the evolved system, making it possible to simulate dynamics of a large class of quantum systems. Moreover, it can be readily adapted to study ground state properties of 1D strongly interacting systems, which will be the subject for the following chapters of this thesis.

CHAPTER VII

TEBD Study on Ground State Properties of Ultracold Fermions in 1D Optical Lattices with Repulsive On-site Interactions

In the previous chapter, we have introduced with some detail the TEBD algorithm, which can be used to study 1D quantum systems. In this chapter, we are going to present our study on ground state properties of a strongly interacting 1D fermionic system with TEBD. The interations in the system can be described by a general Hubbard model (GHM). Our study reveals that correlated hopping mechanism in GHM could bring in qualitatively different physics as compared with the conventional (Fermi-)Hubbard model (CHM).

7.1 Introduction

Physics of strongly interacting ultracold atoms has been attracting tremendous research interests over the past 10 years or so, during which many interesting phenomena have been predicted theoretically and observed in experiments. As a well known example, in their seminal theoretical paper, Jaksch *et al.* predicted the existence of superfluid-Mott insulator (SF-MI) transition in the system of cold bosonic atoms in an optical lattice [73], which could be used to initialize atomic qubit registers in such systems. Later, the predicted SF-MI transition was observed in experiments,

marking an important step in experimental studies on strongly interacting ultracold atoms [74]. Besides bosonic systems, ultracold fermions [158, 159] as well as mixtures of fermions and bosons have also been extensively studied recently. With advanced quantum control techniques, especially laser cooling and trapping as well as Fechbach resonance, people are facing the unprecedented opportunity to mimic condensed matter physics with ultracold atoms in controllable manners.

Many of these important ultracold atom systems can be described by variations of the fundamental Hubbard model Hamiltonians [73, 160, 161], with which very rich physics has been studied. For example, the prediction of the SF-MI transition by Jaksch *et al.* was based on a Bose-Hubbard model. More recently, with extended Bose-Hubbard model, the possible existence of supersolid order in ultracold bosonic atoms was predicted theoretically [162]. The supersolid order is a very interesting state of matter, in which at long range superfluid order and charge density wave (CDW) order are found to be coexisting. For ultracold fermions, with Fermi-Hubbard model, the Luther-Emery phase [163, 164] and the 1D analog of FFLO state [165] were predicted to be existent in 1D attractive fermionic systems with equal and unequal spin population, respectively. The Luther-Emery phase is characterized by coexistence of quasi-long range (QLR) SF and CDW orders. For spin-polarized fermions, FFLO is an exotic state of matter, where paired fermions have non-zero center-of-mass (CM) momentum as opposed to fully paired BCS state where fermion pairs have zero CM momentum.

While its 2D version remains to be an intractable theoretical problem, the 1D conventional Fermi-Hubbard model (CHM) has been extensively studied with exact Bethe ansatz method [171, 172], bosonisation approach[173], as well as efficient numerical methods such as density matrix renormalization group (DMRG) [89] and

quantum Monte Carlo (QMC) [155, 156]. In particular, it is well known that the susceptibility for SF and CDW orders are suppressed at low temperature for CHM with on-site repulsive interaction (positive-U), and the leading QLR order is given by spin density wave (SDW) at any filling fraction[96]. However, in this chapter, we show that coexistence of QLR SF and CDW orders can be observed for fermionic atoms with repulsive on-site interaction in an anisotropic optical lattice near a wide Feshbach resonance. The interactions in this strongly interacting system is described by a 1D general Hubbard model (GHM) with particle assisted tunnelling rates [160, 161]. The GHM is an effective one-band Hamiltonian that takes into account the multi-band populations and the off-site atom-molecule couplings in an optical lattice near a wide Feshbach resonance. It is interesting to note that the GHM with similar particle assisted tunnelling also arises in different physical contexts, as proposed in Ref. [166, 167, 168]. In contrast with the case of the positive-U CHM, we show that SF and CDW emerge as dominant quasi-long range orders over spin orders in the positive-U GHM when the system is significantly hole-doped below half-filling, although at or very close to half-filling, the dominant correlation in GHM is still anti-ferromagnetic spin order. This feature indicates that the particle assisted tunnelling in GHM brings in qualitatively new physics. It makes the effective interaction in GHM doping dependent, showing different behaviors with a possible phase transition in between. We get our results through numerical calculation based on the time evolving block decimation (TEBD) algorithm [10, 11, 15, 14]. We compare our numerical results with some known exact results for the positive CHM, and the remarkably precise agreement indicates that the TEBD calculation can make quantitatively reliable predictions.

7.2 Model Hamiltonian and Numerical Method

A generic Hamiltonian to describe strongly interacting two-component fermions in an optical lattice (or superlattice) is given by the following general Hubbard model:

$$\begin{aligned} H \quad &= \sum_i \left[U n_{i\uparrow} n_{i\downarrow} - \mu n_i\right] \\ &- \sum_{\langle i,j\rangle,\sigma} \left[t + \delta g \left(n_{i\bar{\sigma}} + n_{j\bar{\sigma}}\right) + \delta t n_{i\bar{\sigma}} n_{j\bar{\sigma}}\right] a^\dagger_{i\sigma} a_{j\sigma} + H.c. \end{aligned} \tag{7.1}$$

where $n_{i\sigma} \equiv a^\dagger_{i\sigma} a_{i\sigma}$, $n_i \equiv n_{i\uparrow} + n_{i\downarrow}$, μ is the chemical potential, $\langle i,j\rangle$ denotes the neighboring sites, and $a^\dagger_{i\sigma}$ is the creation operator to generate a fermion on the site i with the spin index σ. The symbol $\overline{\sigma}$ stands for $(\downarrow,\uparrow)$ for $\sigma = (\uparrow,\downarrow)$. The δg and δt terms in the Hamiltonian represent particle assisted tunnelling, for which the inter-site tunnelling rate depends on whether there is another atom with opposite spin on these two sites. The particle assisted tunnelling comes from the multi-band population and the off-site atom-molecule coupling for this strongly interacting system [160, 161]. For atoms near a wide Feshbach resonance with the average filling number $\langle n_i\rangle \leq 2$, each lattice site could have four different states, either empty (with state $|0\rangle$), or a spin $\uparrow$ or $\downarrow$ atom ($a^\dagger_{i\sigma}|0\rangle$), or a dressed molecule ($d^\dagger_i|0\rangle$) which is composed by two atoms with opposite spins. The two atoms in a dressed molecule can distribute over a number of lattice bands due to the strong on-site interaction, with the distribution coefficient fixed by solving the single-site problem. One then can mathematically map the dressed molecule state $d^\dagger_i|0\rangle$ to a double occupation state $a^\dagger_{i\downarrow} a^\dagger_{i\uparrow}|0\rangle$ by using the atomic operators $a^\dagger_{i\sigma}$ [160, 161] . After this mapping, the effective Hamiltonian is transformed to the form of Eq. (1). The GHM in Eq. (1) reduces to the conventional Hubbard model when the particle assisted tunnelling coefficients δg and δt approaching zero, as one moves far away from the Feshbach resonance. Near the resonance, δg and δt can be significant compared with the

atomic tunnelling rate t due to the renormalization from the multi-band populations and the direct neighboring coupling [160, 161].

We consider in this work an anisotropic optical lattice for which the potential barriers along the x, y directions are tuned up to completely suppress tunnelling along those directions. The system becomes a set of independent one-dimensional chains. We thus solve the GHM in one dimension through numerical analysis. For this purpose, first we transfer all the fermion operators to the hard core boson operators through the Jordan-Wigner transformation [170]. In the one-dimensional case, we can get rid of the non-local sign factor, and after the transformation the hard core boson operators satisfy the same Hamiltonian as Eq. (1). On each site we then have two hard core boson modes which are equivalent to a spin-3/2 system with the local Hilbert space dimension $d = 4$. We can therefore use the TEBD algorithm to solve this pseudo-spin system. As we have introduced in the previous chapter, the TEBD algorithm is based on the assumption that in the one-dimensional case the ground state $|\Psi\rangle = \sum_{i_1=1}^{d} \cdots \sum_{i_n=1}^{d} c_{i_1 \ldots i_n} |i_1 \cdots i_n\rangle$ of the Hamiltonian with local interactions can be written into the following matrix product form:

$$c_{i_1 \ldots i_n} = \sum_{\alpha_1, \ldots \alpha_n = 1}^{\chi} \Gamma^{[1] i_1}_{\alpha_n \alpha_1} \Gamma^{[2] i_2}_{\alpha_1 \alpha_2} \Gamma^{[3] i_2}_{\alpha_2 \alpha_3} \cdots \Gamma^{[n] i_n}_{\alpha_{n-1} \alpha_n}, \tag{7.2}$$

where $\Gamma^{[s] i_s}$ denotes the matrix associated with site-s with the matrix dimension χ. When $\chi = 1$, the assumption reduces to the mean-field approximation, and for a larger χ, the matrix product state well approximates the ground state as it catches the right entanglement structure for 1D systems [10, 11]. To use the TEBD algorithm, we just start with an arbitrary matrix product state in the form of Eq. (2) which has non-zero overlap with the real ground state, and evolve this state with the Hamiltonian (1) in imaginary time through the propagator e^{-Ht}. The state converges to the ground

state of the Hamiltonian pretty quickly. From the final ground state in the matrix product form, one can efficiently calculate the reduced density operator and various correlation functions. This calculation has a well controlled precision since at each time step to update the matrix product state, the Hilbert space truncation error can be suppressed by choosing an appropriate matrix dimension χ. In this calculation, we use the infinite lattice algorithm by assuming that the lattice is bipartite and the ground state has a translational symmetry for each sublattice [15]. This allows us to directly calculate the system in the thermodynamic limit (particle number goes to infinity while preserving particle number density).

7.3 Numerical Results and Discussion

To show that our calculation is capable of making reliable predictions, we first test our results by comparing them with some known exact results of the Hubbard model in certain cases. For the Hubbard model at half-filling $\langle n_{i\uparrow}\rangle = \langle n_{i\downarrow}\rangle = 0.5$, the ground state energy per site is known to have the analytic expression $E = -4\int_0^\infty \frac{J_0(\omega)J_1(\omega)d\omega}{\omega[1+\exp(\omega U/2)]}$ in the thermodynamic limit from the exact Bethe ansatz solution [171], where J_0 and J_1 are Bessel functions and we have chosen the tunnelling rate t as the energy unit. In Fig. 7.1 (a), we show our numerical results for the ground state energy of the Hamiltonian (1) with $\delta g = \delta t = 0$, and one can see that it agrees very well with the exact energy of the Hubbard model in particular when $U > t$. The error is in general smaller than 10^{-3} as shown in Fig. 7.1(b). In this and the following calculations, we choose the matrix dimension $\chi = 40$. We have tried larger χ which gives better precision, but we choose $\chi = 40$ to have a faster speed and its precision is enough for our purpose.

We have also tested the final state from our calculation by comparing its cor-

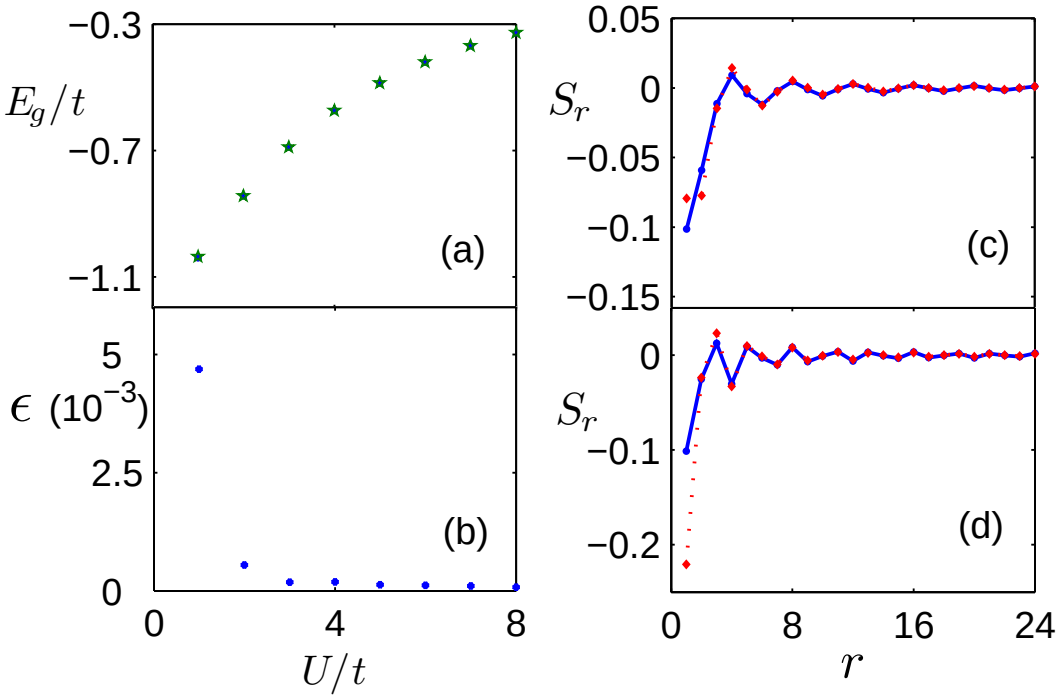

Figure 7.1: Numerical results for conventional Hubbard model compared with some known exact result. (a) Ground state energy as a function of U at half-filling (energy in the unit of t), where data points marked by solid dots are from the exact Bethe ansatz solution while those marked by pentagram are from our numerical program; (b) The relative error in the ground state energy; (c) Real-space spin correlation function at the filling fraction $\langle n_i \rangle = 0.5$ and $U = 8t$, compared with the asymptotic form in Eq. (3) (solid curve) with $K_\rho = 0.62$ and $A = 0.13$. (d) Similar to (c), except that $\langle n_i \rangle = 0.75$, and the corresponding $K_\rho = 0.60$, A =0.19.

relation functions with some known results. It is difficult to get correlations analytically from the Bethe ansatz solution, but from the bosonization approach to the one-dimensional Hubbard model, we know its correlation functions take certain asymptotic forms. For instance, one can look at the spin-spin correlation, defined as $S_r \equiv \langle \mathbf{s}_i \cdot \mathbf{s}_{i+r} \rangle$, where the spin operator for the site i is given by $\mathbf{s}_i \equiv a^\dagger_{i\alpha} \sigma_{\alpha\beta} a_{i\beta}/2$ with α and $\beta =\downarrow, \uparrow$ and σ standing for the Pauli matrices. The correlation S_r is independent of i because of the translational symmetry. The Hubbard spin correlation function has the following asymptotic form [172]

$$S_r = -\frac{1}{(\pi r)^2} + \frac{A}{r^{1+K_\rho}} \cos(2k_F r) \ln^{1/2}(r) + ..., \tag{7.3}$$

where K_ρ is the Luttinger parameter whose value has been determined before from the exact Bethe ansatz solution [171, 172], k_F is the fermi momentum related to the filling number $\langle n_i \rangle$ through $k_F = \langle n_i \rangle \pi/2$, and A is a non-universal model dependent constant. In Fig.1 (c) and (d), we compare our calculation results for S_r with this asymptotic form for filling number $\langle n_i \rangle = 0.5$ and 0.75, and the agreement is again remarkable as long as r is not too small (the expression of S_r in Eq. (3) is not accurate for small r).

With the confidence in numerics built from the above comparison, we now present our main calculation results for the repulsive GHM in Eq. (1) with $U > 0$. Apart from the spin correlation S_r defined before, we also calculate the charge-density-wave (CDW) correlation, defined as $D_r \equiv \langle n_i n_{i+r} \rangle - \langle n_i \rangle \langle n_{i+r} \rangle$, and the pair (superfluid) correlation, defined as $P_r \equiv \langle a_{i\uparrow} a_{i\downarrow} a^\dagger_{i+r\downarrow} a^\dagger_{i+r\uparrow} \rangle$. The results are shown in Fig. 7.2 for different filling fraction $\langle n_i \rangle$ and for models with different particle assisted tunnelling rates δg and δt. First at half filling with $\langle n_i \rangle = 1$, the correlation functions S_r, D_r, and P_r for the GHM with different δg and δt all look qualitatively similar to the corresponding results for the conventional Hubbard model, although with increase

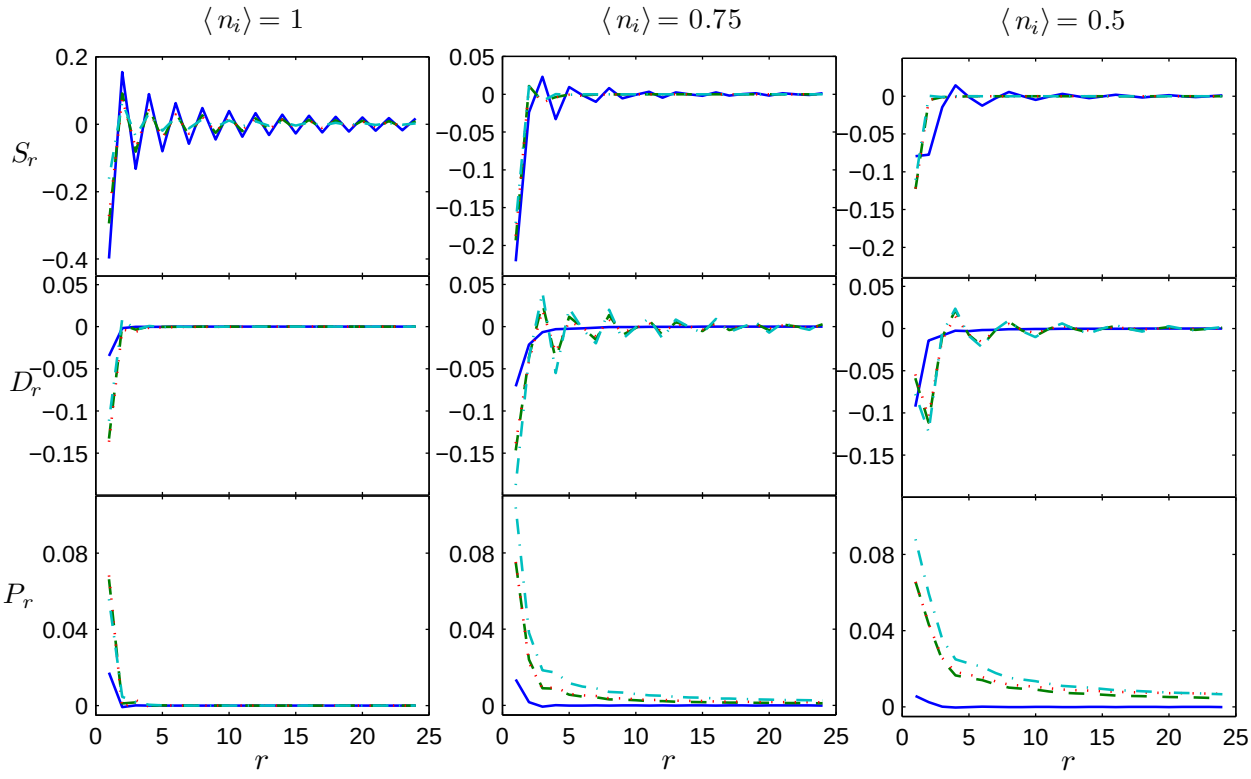

Figure 7.2: The numerical results for the spin (S_r), the CDW (D_r), and the pair (P_r) correlation functions for the GHM with different particle assisted tunnelling rates and at different filling fractions, where $\delta g = 0$ $\delta t = 0$ for solid curves, $\delta g = 3t$ $\delta t = -6t$ for dashed curves, $\delta g = 3t$ $\delta t = -3t$ for dotted curves, and $\delta g = 7t$ $\delta t = -14t$ for dash-dotted curves.

of the coefficient δg the spin correlation reduces a bit while the CDW and superfluid correlations increase slightly. Clearly, the dominant correlation in this case is in spin which suggests a quasi-long range anti-ferromagnetic order. In this and following calculations, we take $U = 8t$ for all the cases, which corresponds to a significant on-site repulsion.

Qualitatively different results show up when the system is doped with holes. At the filling fraction $\langle n_i \rangle = 0.75$, although for the Hubbard model the spin correlation is still the dominant one (the spin density wave order has been pinned to the corresponding $2k_F = 3\pi/4$), for the GHM with a noticeable δg, the superfluid and the CDW emerge as the leading quasi-long-range orders, and their correlations increase significantly and decay much slower in space compared with the spin correlation when δg grows. These features become more evident when we further increase the doping. For instance, at the right column of Fig. 7.(2), we show the correlations for the filling fraction $\langle n_i \rangle = 0.5$. The qualitative behavior is similar to the case with $\langle n_i \rangle = 0.75$, but the CDW and superfluid correlations for the GHM get significantly larger at long distance, and the contrast with the Hubbard model becomes sharper. One also note that for all these calculations, change of the coefficient δt in the GHM makes little difference to the result. This is understandable as a significant positive U suppresses the possibility of double occupation in the lattice, and the δt term in the GHM has no effect without double occupation. The δg term in the GHM, however, is critically important, which favors superfluidity in general and brings in the qualitatively different features mentioned above.

To show the spatial structure of these quasi-long range (QLR) orders, we plot in Fig. 7.3 the spin, the CDW, and superfluid correlations in the momentum space for the GHM with $\delta g = 3t$ at different filling fractions $\langle n_i \rangle$. The momentum space corre-

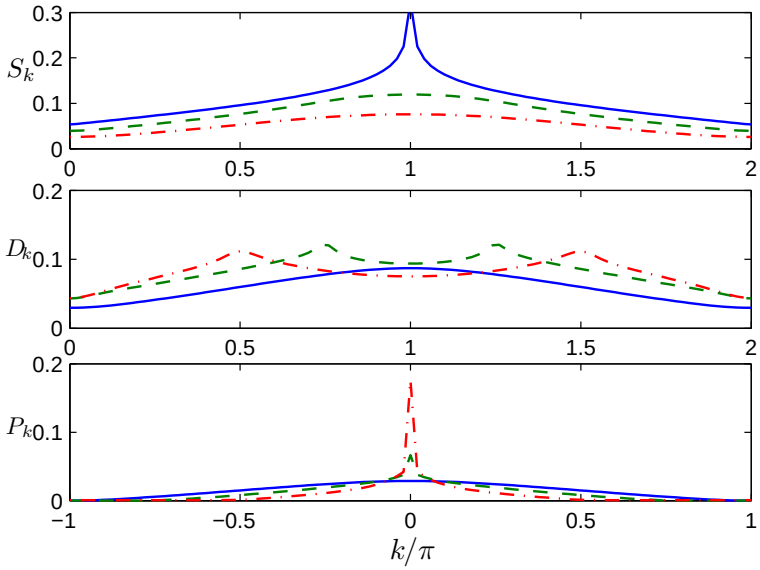

Figure 7.3: The spin, the CDW, and the pair correlation functions in momentum space for the GHM with $\delta g = 3t$ $\delta t = -3t$. The solid, dashed, and dash-dotted curves correspond to filling factor $\langle n_i \rangle = 1$, 0.75, and 0.5, respectively. For the calculation of the Fourier transformation, we have used the real space correlation functions for $N = 100$ sites.

lations are defined by the Fourier transform $X_k = 1/\sqrt{N} \sum_{r=0}^{N} X_r \cos(kr)$, where X stands for the correlations S, D, or P. From these momentum space curves, one can clearly see that this GHM at half filling has a QLR anti-ferromagnetic order (characterized by the peak at $k = \pi$), and away from half filling a QLR superfluid order (peak at $k = 0$) and CDW order (peaks at $k = 2k_F$ and $2\pi - 2k_F$, where $2k_F = 3\pi/4$ ($\pi/2$) for the filling fractions $\langle n_i \rangle = 0.75$ (0.5), respectively). The peaks in Fig. 7.3 have finite widths because these orders in 1D are only quasi-long-range with algebraic decay. Note that if we turn on small tunnelling interaction between different 1D chains, a leading QLR order, such as superfluid order, could be stabilized to a true long range order [96]. The GHM thus provides an example of a microscopic Hamiltonian that with hole doping from half filling, an anti-ferromagnetic phase could be transferred to a superfluid phase (or a CDW phase in some case depending on which order becomes more dominant with the inter-chain coupling). The correlations that characterize these QLR orders can be detected for the cold atomic gas, for instance,

through the method described in Ref. [174].

7.4 Chapter Summary

In summary, we have investigated the ground state properties of the general Hubbard model with repulsive on-site interaction in one dimension through well controlled numerical analysis. For the system with significant particle assisted tunneling rates δg and δt, we have found coexistence of quasi-long range superfluid and charge-density-wave orders when the system is hole-doped from half filling. This feature is in sharp contrast with convention Hubbard model, in which case for positive-U the charge and superfluid orders are always suppressed regardless of the filling fraction. With a combination of the Bosonlization approach and the numerical method here, it may be possible to determine the compete phase diagram for the GHM. The model here describes strongly interacting fermionic atoms in an anisotropic optical lattice. The possibility of a transition from an anti-ferromagnetic phase to a superfluid phase for the GHM with hole doping may also have interesting indications for other areas.

CHAPTER VIII

TEBD Study on Spin-polarized 1D General Hubbard Model with Attractive On-site interactions

In the previous chapter, we have presented our work on a TEBD numerical simulation of a general Hubbard model (GHM) without spin polarization, meaning that the system has equal numbers of spin-up and spin-down fermions. It has been shown that the particle assisted tunneling in the system could introduce qualitatively different physics from that described by the conventional Hubbard model (CHM). In this chapter, we further explore the spin-polarized GHM model with attractive on-site interactions (negative-U) to reveal the effects of the particle assisted tunneling. With the 1D attractive spin-polarized CHM the existence of the Fulde-Ferrell-Larkin-Ovchinnikov (FFLO) state, which is an exotic fermion pairing mechanism, has been predicted. Our TEBD calculation to be presented in this chapter shows that with the particle assisted tunneling, the FFLO order could get suppressed in GHM. We also discuss the possible effect of particle number density inhomogeneity due to the presence of an overall harmonic trap as is the case in optical lattice experiments.

8.1 Introduction

Physics of strongly interacting Fermi systems has been at the frontier of various research fields in modern physics. One outstanding example is given by the

physics of superconductivity, or more generally, fermionic superfluidity. The usual fermion pairing mechanism, namely the Cooper-pairing of fermions, is known to be responsible for the fermionic condensate and superfluidity in Fermi systems with equal spin populations. In spin-polarized systems, however, the population imbalance between the spin-up and spin-down species leads to partial pairing of fermions inevitably. The mismatching of Fermi surfaces for different spin species induces a competition between Cooper pairing and population imbalance, which could allow the observation of many interesting new phenomena. In condensed matter physics, many interesting and seemingly exotic pairing mechanisms for spin-polarized Fermi systems have been proposed theoretically [175, 176, 177]. Nonetheless most of them remain elusive from direct experimental observation in solid state systems. Very recently, the observation of fermionic superfluidity in spin-polarized ultra-cold Fermi gas experiments has opened up the possibilities of systematic study on these new phenomena under well controlled conditions and it has triggered enormous research interests [178, 179, 180, 181, 182].

The FFLO state is one specific example of the proposed exotic pairing mechanisms and has been extensively studied in condensed matter physics. Under the original research context, it was suggested that the ground state for a BCS superconductor under a constant magnetic field should become a magnetized superconductor, in which the fermion pairs have non-zero center-of-mass momentum [175, 176]. In principle, the FFLO state could be found existent in spin-polarized Fermi gas with attractive interactions. It has been suggested that spin-polarized Fermi gas in a one-dimensional (1D) optical lattice is a promising system for direct observation of the FFLO state, as the inter-chain coupling of the quasi-1D systems may help stabilize the order [96]. For a homogeneous 1D attractive Fermi gas system with unequal

spin populations, theoretical evidence of the FFLO state has been found by means of bosonization and other renormalization group techniques [183]. More recently, based on the Gaudin-Yang model under the local density approximation (LDA), the zero-temperature phase diagram of a trapped 1D spin-polarized Fermi gas system has been obtained [184, 185]. According to these mean-field studies, the ground state of the system should exhibit a two-shell structure. In the core, it is a superfluid of FFLO-type characters, while in the wings it could be either a fully paired BCS superfluid or a fully polarized normal state, depending on the magnitude of the spin polarization. There have also been many important numerical results obtained by applying the density matrix renormalization group (DMRG) [165, 186, 187] and the quantum Monte-Carlo (QMC) [188] algorithms to the 1D attractive Hubbard model in harmonic traps with spin population imbalance, indicating the possible existence of the FFLO state.

In this chapter, we present a time evolving block decimation (TEBD) numerical study on a 1D general Hubbard model (GHM) with on-site attractive interaction. We show that the FFLO superfluidity in the conventional 1D attractive Hubbard model could be affected due to the presence of the particle assisted tunneling in GHM. For fermionic atoms in an anisotropic optical lattice near a wide Feshbach resonance, the particle assisted tunneling terms arise in an effective single-band Hamiltonian, when multi-band populations and off-site atom-molecule couplings are taken into account [160, 161]. Our calculation reveals that for the spin-polarized 1D attractive GHM, the FFLO order could be enhanced at low particle assisted tunneling rates. However, at relatively high correlated tunneling rates, the FFLO order could get suppressed, while the spin density wave (SDW) orders become more dominant, especially in the case with relatively weak on-site attractive interactions. We also analyze the

density inhomogeneity effect based on LDA. For the conventional Hubbard model, we find that in the low density case (half-filling at the trap center and decreasing all the way to zero toward the edge), one will get a two-shell structure with a FFLO superfluid core, as predicted by previous theoretical studies. While all previous studies agree that at the center the system should be found in an FFLO state, the results obtained with different methods are somehow different on the state of matter in the wings. According to mean-field calculations, it could be either a fully paired superfluid (Luther-Emery liquid) or a fully polarized normal state in the wings depending on the overall degree of polarization, while with the DMRG simulation, only a fully polarized state has been found. Although our calculation does not exclude the possibility of finding fully paired superfluidity in the wings, it is indicated that the critical polarization below which one can find a fully paired superfluid in the wings could be much smaller than what the mean-field studies have predicted. Furthermore, we investigate the effects of correlated tunneling on the shell structure of the inhomogeneous system. We find that in the case with strong on-site attraction the shell structure is very similar to that for the conventional Hubbard model. In the case with weak on-site interaction, however, the shell structure could be completely different. More specifically, the new structure is found to have a SDW core, and depending on the magnitude of the polarization, in the wings one could get either a Luther-Emery liquid (with fully paired superfluidity) or a fully polarized normal state, while in between, the state of the system shows some remanence of the FFLO-type order.

8.2 Model Hamiltonian and Numerical Method

The model Hamiltonian for the system of Fermi atoms in an optical lattice near a wide Feshbach resonance assumes basically the same form as is given by equation (7.1) in the previous chapter, except that now we explicitly distinguish the chemical potential term for spin-up and spin-down species so that population imbalance can be introduced into the system. The general Hubbard Hamiltonian for our numerical study can be written as [160, 161]:

$$\begin{aligned} H \quad &= \sum_i \left[U n_{i\uparrow} n_{i\downarrow} - \mu_\uparrow n_{i\uparrow} - \mu_\downarrow n_{i\downarrow}\right] \\ &- \sum_{\langle i,j\rangle,\sigma} \left[t + \delta g \left(n_{i\overline{\sigma}} + n_{j\overline{\sigma}}\right) + \delta t n_{i\overline{\sigma}} n_{j\overline{\sigma}}\right] a^\dagger_{i\sigma} a_{j\sigma} + H.c. \end{aligned} \tag{8.1}$$

where $n_{i\sigma} \equiv a^\dagger_{i\sigma} a_{i\sigma}$, $n_i \equiv n_{i\uparrow} + n_{i\downarrow}$, μ_σ is the chemical potential for spin-σ component, $\langle i, j\rangle$ denotes the neighboring sites, and $a^\dagger_{i\sigma}$ is the creation operator to generate a fermion on the site i with the spin index σ. The symbol $\overline{\sigma}$ stands for $(\downarrow, \uparrow)$ for $\sigma = (\uparrow, \downarrow)$. To calculate the ground state properties of the general Hubbard model Hamiltonian, we use an infinite lattice version of the TEBD algorithm, which has been introduced in previous chapters. The magnitude of spin polarization is controlled through the adjustments of the chemical potentials for the two spin components.

8.3 Numerical Results and Discussions

We first present our results for the half-filling case in Fig. 8.1. In our calculation, we choose a fixed polarization $p = \frac{N_\uparrow - N_\downarrow}{N_\uparrow + N_\downarrow}$ at 0.4 and examine the effect of particle assisted tunneling at a relatively strong on-site (attractive) interaction $U = -8t$. It is known that in the 1D conventional Hubbard model with attractive interaction, the ground state of the system without spin-polarization is described by a Luther-Emery

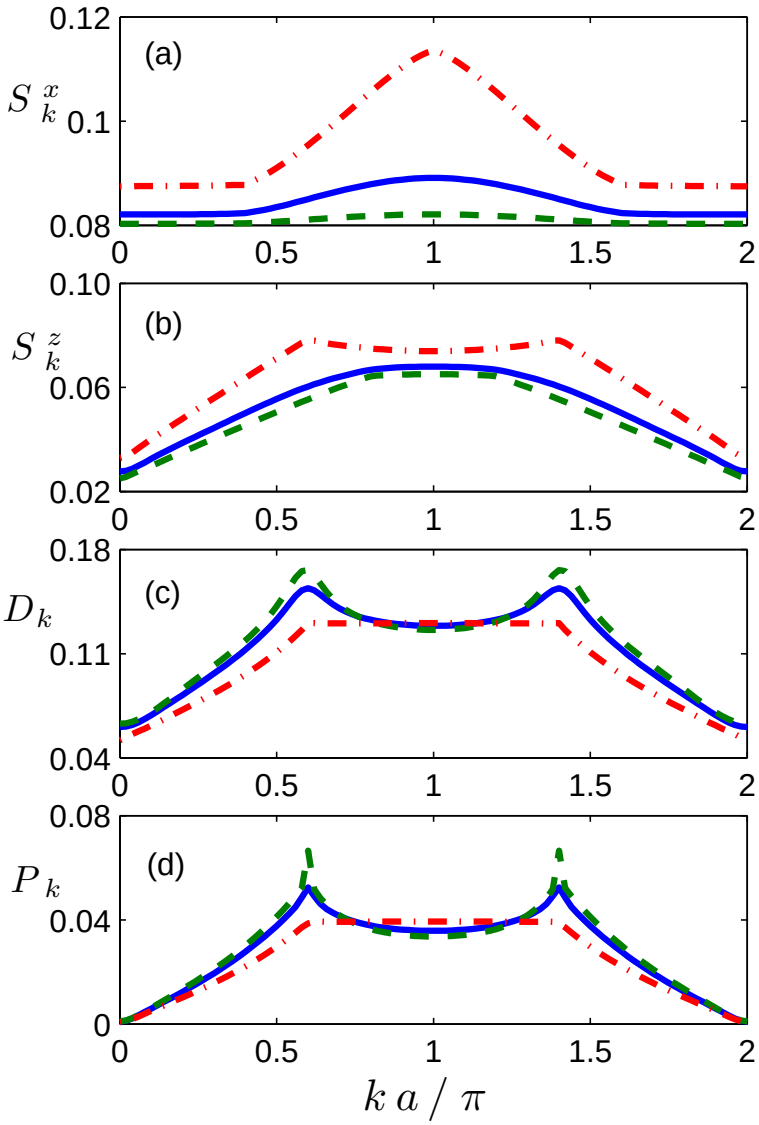

Figure 8.1: Momentum space correlation functions for the general Hubbard model at half-filling. For all plots, $U = -8t$ and the spin polarization is chosen to be the same at $p = 0.4$. The solid, dashed, and dash-dotted curves correspond to $\delta g = 0$, $0.5t$, and $-t$, respectively.

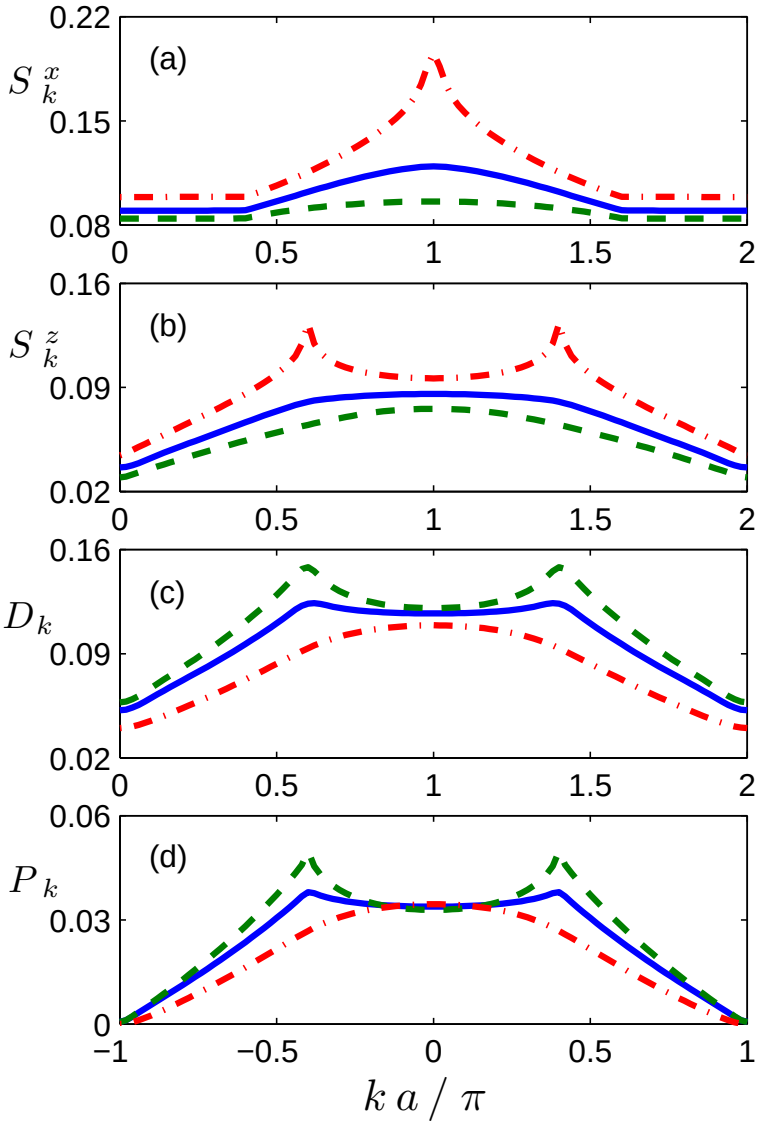

Figure 8.2: Momentum space correlation functions for the general Hubbard model at half-filling. For all plots, $U = -2t$ and the spin polarization is chosen to be the same at $p = 0.4$. The solid, dashed, and dash-dotted curves correspond to $\delta g = 0$, $0.5t$, and $-t$, respectively.

liquid while in the case with spin-polarization (even arbitrarily small) the ground state of the system becomes an FFLO-type state. The pairing (or superfluid) correlation is crucial for the characterization of the FFLO state, with the peaks of P_k locating at non-zero momentum k being its signature. Our plots agree very well with this well-known result, with the solid curves peaking at $k = \pm 0.4\pi$. Moreover, according to our results, in GHM the FFLO order is enhanced at $\delta g = 0.5t$ (sharper peaks in the P_k v.s. k plot) while it is suppressed at $\delta g = -t$. At $\delta g = -t$ (reasonably high correlated-tunneling rate), the spin correlations show tiny peaks, indicating the emergence of the SDW order. The interesting effects of the correlated hopping, however, can be understood by mapping to the unpolarized positive-U general Hubbard model below half-filling, which has been studied in our earlier work and shown to exhibit Luther-Emery like phase [94]. Fig. 8.2 is also devoted to the demonstration of the effects due to the particle assisted tunneling, but at a relatively weak on-site interaction $U = -2$. Although the effects of the correlated tunneling shown in Fig. 8.2 are quite similar to those in Fig. 8.1, nonetheless, one should be able to observe that the effects of particle assisted tunneling are more prominent at weaker on-site interaction strength.

In Fig. 8.3, we show the momentum space superfluid correlations at different polarizations and particle densities for the conventional Hubbard model ($U = -8t$). From the results shown in Fig. 8.3, we can discuss the density inhomogeneity effects due to the presence of an overall trap potential based on LDA. In each sub-plot we fix the difference in the chemical potentials $\delta\mu$ for different spin species, while varying the particle density by adjusting $\mu \equiv (\mu_\uparrow + \mu_\downarrow)/2$. We assume that the lattice sites in the trap center are half-filled. Then, according to our simulation, in the trap center, we get the FFLO state even though the polarization is very small. When the

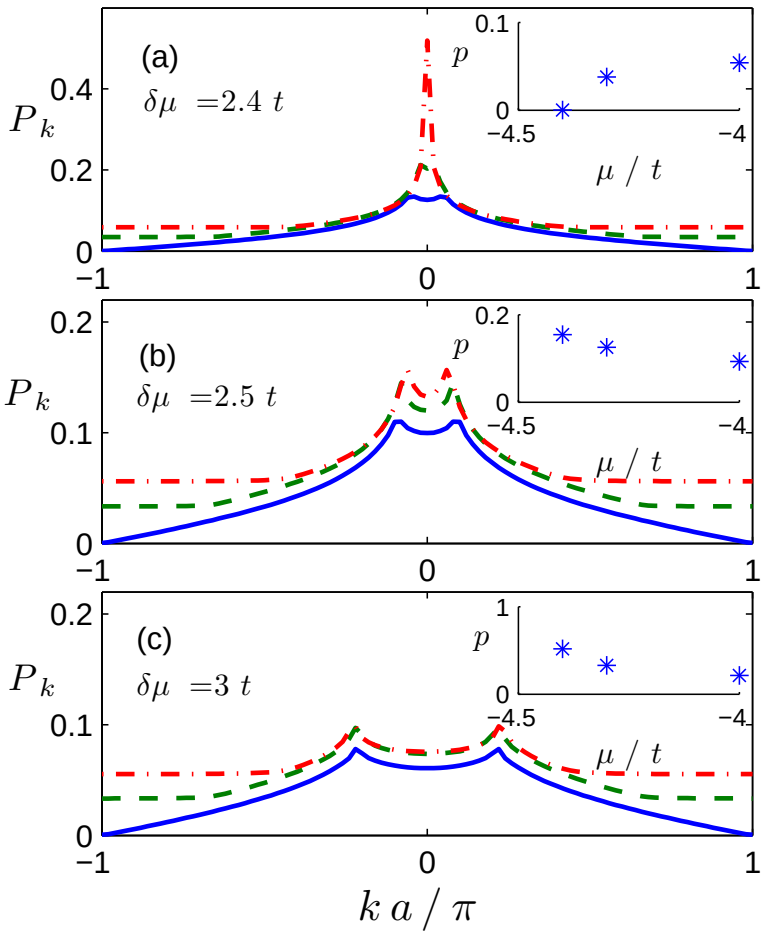

Figure 8.3: Pairing correlation functions for the conventional Hubbard model at $U = -8t$. The difference in chemical potential for spin-up and spin-down species are chosen to be $\delta\mu \equiv (\mu_\downarrow - \mu_\uparrow)/2 = 2.4t$, $2.5t$, and $3t$ for plots (a), (b), and (c), respectively. The solid, dashed, and dash-dotted line shapes in all plots correspond to $\mu \equiv (\mu_\uparrow + \mu_\downarrow)/2 = -4t$ (half-filling), $-4.3t$, and $-4.4t$, respectively. The insets show the spin polarization corresponding to each curve.

polarization in the trap center is small (e.g. in Fig. 8.3(a) when $\delta\mu = 2.4t$, $p = 0.054$ at half-filling), we can see that the spin polarization decreases all the way down to zero when moving toward the trap edge (with μ decreasing). In this case, a fully paired superfluid is found in the wings. However, if we have a higher polarization in the center (by increasing $\delta\mu$), the spin polarization is found to be increasing from the center to unity toward the edge. Therefore, in this case a fully polarized normal state will be found in the wings (although in Fig. 8.3(b) and (c) only the partially paired FFLO state is shown). We note that in previous studies with mean field calculation, it was predicted that for strong on-site interactions, there is a critical polarization as large as $p = 0.2$ below which one could get fully paired superfluid in the wings, however as reported in Ref. [165], at $U = -8t$ one does not see any fully paired superfluid toward the edge of the trap at any polarization through DMRG calculations. According to our result, when $\delta\mu = 2.5t$ (fully polarized state in the wings), the spin polarization is about 0.093 in the trap center. In this case, when moving toward the edge, we find that the particle density difference decreases although the polarization increases. This implies that the critical polarization for the observation of fully paired superfluid in the wings should be smaller than 0.093 (not tight). For the conventional Hubbard model at $U = -10$, we also carried out similar calculations and analysis. And the critical polarization is found to be smaller than 0.088.

Similar to the analysis for the trap effects on the conventional Hubbard model, we also investigate the general Hubbard model at different spin polarizations and particle number densities. In Fig. 8.4, we show our results for pairing correlation functions of GHM at $U = -10t$ and $\delta g = -t$. From the figure, one can observe that the physics here is quite similar to that of the conventional Hubbard model. In the

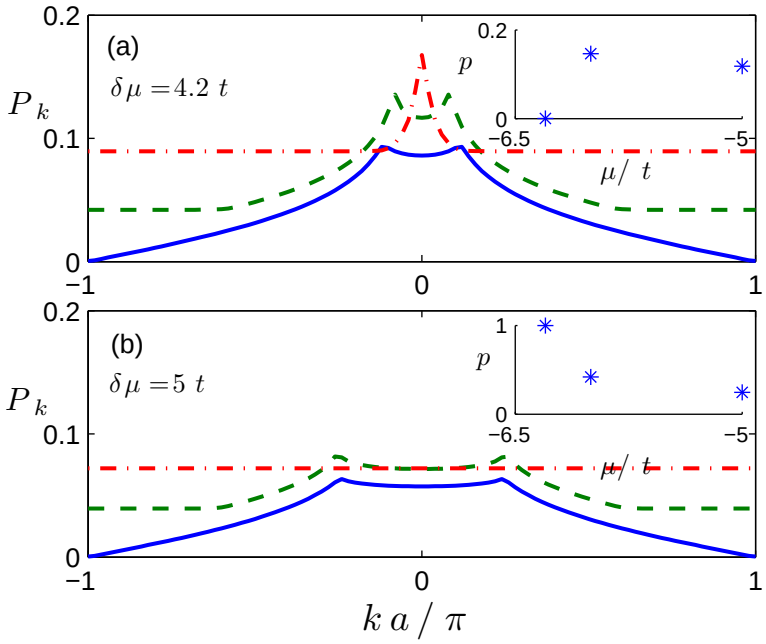

Figure 8.4: Momentum space pairing correlation functions for the general Hubbard model at $U/t = -10$, $\delta g/t = -1$ and $\delta t/t = 2$. Difference in chemical potential for spin-up and spin-down species are chosen to be $\delta\mu \equiv (\mu_\downarrow - \mu_\uparrow)/2 = 4.2t$ and $5t$ for subplots (a) and (b), respectively. The solid, dashed, and dash-dotted line shapes in all plots correspond to $\mu \equiv (\mu_\uparrow + \mu_\downarrow)/2 = -5t$ (half-filling), $-6t$, and $-6.3t$, respectively. The insets show the spin polarization corresponding to each curve.

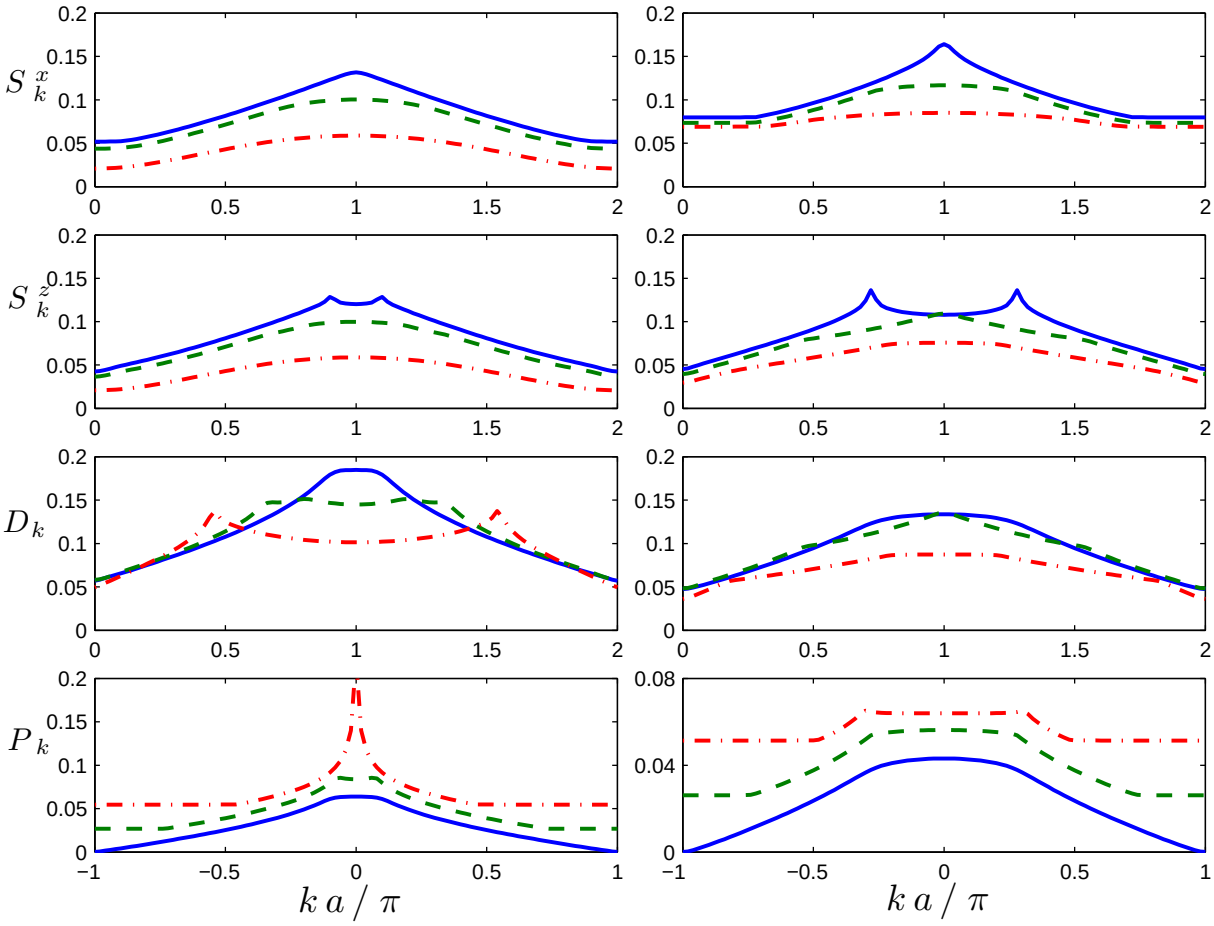

Figure 8.5: Spin, charge density and pairing correlation functions for the general Hubbard model at $U/t = -2$, $\delta g/t = -1$ and $\delta t/t = 2$. Difference in chemical potentials for spin-up and spin-down species are chosen to be $\delta\mu \equiv (\mu_\downarrow - \mu_\uparrow)/2 = 1.2t$ and $2.4t$ for the left and right column, respectively. The solid, dashed, and dash-dotted line shapes correspond to $\mu \equiv (\mu_\uparrow + \mu_\downarrow)/2 = -t$ (half-filling), $-2.5t$, and -3.3, respectively.

trap center (at half-filling), we have the FFLO state characterized by the peaks of P_k locating at non-zero momentum k. In the small polarization case (see Fig. 8.4(a)), one could get a fully paired superfluid in the wings, while in the large polarization case (see Fig. 8.4(b)) a fully polarized normal state is found near the trap edge. Therefore, in this case we have a similar two-shell structure as is obtained with the conventional Hubbard model. However, from the insets of Fig. 8.4(a) (at small polarization), we can see that the polarization is not monotone with the variation of particle density, which is different from the case in the conventional Hubbard model. Furthermore, in the case as shown in Fig. 8.4(a), in the trap center the spin polarization p is found to be about 0.118, which is noticeably higher than the critical polarization for the observation of a fully paired superfluid state in the wings in the conventional Hubbard model. More interestingly, the correlated tunneling in GHM could lead to a completely different shell structure, when the on-site interaction is not very strong (Fig. 8.5). In the trap center where the sites are half-filled by setting, the system shows a SDW order. By comparing the left and right column, we can observe that the SDW order in the core is more prominent for a higher magnitude of spin polarization. When moving toward the edge, we can see some remanence of the FFLO order characterized by tiny peaks at non-zero momentum in the momentum space pairing correlation. Further away from the center, in the low polarization case (left column in Fig. 8.5), the system is found to be a Luther-Emery liquid with fully paired superfluidity, while in the high polarization case (right column), in the wings one has a fully polarized normal state instead.

8.4 Chapter Summary

In summary, we numerically study the ground state properties of a spin-polarized general Hubbard model with particle assisted tunneling by using a TEBD algorithm. We have found that the correlated hopping could affect the FFLO order in different ways depending on the magnitude of the correlated hopping rates. We have also analyzed how the system would behave under an overall trap potential in optical lattice experiments based on the LDA assumption. Our results indicate that for the conventional Hubbard model the critical spin-polarization below which one could find fully paired superfluid toward the edge of the trap could be very small even with strong on-site attractive interaction, as opposed to the prediction from mean field calculation based on Gaudin model. Furthermore our calculations reveal that when the particle assisted tunneling rates are significant compared with the strength of the on-site interaction they could lead to a completely different shell structure with SDW in the core and either a Luther-Emery liquid or a fully polarized normal Fermi gas in the wings.

CHAPTER IX

Summary and Future Directions

9.1 Summary of Thesis

In the first part of this thesis, I presented our theoretical studies on quantum optical implementation of quantum information processing with optical cavity QED systems. With state-of-the-art control techniques, atoms can be confined in a tiny optical resonantor for seconds, during which strong coupling between atomic transitions of the trapped atoms and cavity field can be achieved. The atom-cavity system working in the strong coupling regime provides us a unique platform where coherent control at the single-particle (either atom or photon) level is possible.

We proposed to utilize a high finesse one-sided optial cavity with a single trapped atom as our resource to generate Schrödinger cat states in weak coherent optical pulses. According to our implementation scheme, the cat states can be obtained by simply scattering weak optical pulses prepared in coherent states at the single-atom cavity followed by projective measurement on the atomic state. To quantitively characterize the performance of our scheme, we developed a numerical method to solve the dynamics of the system. The effects of experimental imperfections, such as the output pulse shape distortion from the scattering process, the atomic spontaneous emission, the randomness of atom-cavity coupling strength due to thermal motion of

the atom, as well as the mode mismatching for the coupling between cavity and free space fields, were studied with our numerical solution. Our calculations reveal that our scheme is relatively insensitive to the noise due to atomic thermal motion. We also find that the pulse shape distortion can be suppressed by choosing optial pulses with smaller bandwidth, while the photon loss error due to the atomic spontaneous emission can be reduced by increasing the atom-cavity coupling rate. And according to our calculation, the scheme is relatively more sensitive to the mode matching inefficiency as compared with other sources of errors.

We presented a fault-tolerant scheme for the implementation of neutral atom gates, where the effective interaction between neutral atoms is mediated by cavity assisted scattering of single-photon pulse. With our basic scheme, by reflecting a single photon pulse from the cavity with two trapped atoms, a controlled phase flip gate on the atoms can be realized. The photon pulse remains unentangled with the atoms after the scattering and can be detected at a single-photon detector. By introducing the single photon detector, the photon loss errors, which can be significant in cavity QED experiments, will be automatically detected once happening. If the photon does register a click at the detector, we know that the gate operation is realized with high fidelity. These specific features make the scheme robust against photon loss errors as they only affect the success probability of the gate operation. Even though the failure probability can be very close to unity, nonetheless, efficient fault tolerant quantum computation is still possible. The basic scheme can also be readily extended to realize robust multi-qubit atomic Toffoli gates on atoms localized in a single cavity, as well as a nonlocal controlled phase flip gate on two atoms trapped in remote cavities. With a mode discretization method, we numerically solved the dynamics of the system and quantitatively evaluated the success probability and gate

fidelity of our gate scheme. Our calculations reveal that the scheme could allow high fidelity gate operations under typical experimental conditions.

We proposed a scheme to swap the quantum (polarization) states of optical pulse sequences conditional on the atomic state of a single atom trapped in a two-sided optical cavity. According to our scheme, when two sequences of single-photon pulses are incident toward cavity mirrors on two opposite sides, conditioned on the atom being in state $|0\rangle$ or $|1\rangle$ the pulses will be either directly reflected back or resonantly tunnel through the cavity, thereby effectively realizing a controlled SWAP unitary gate. We presented a theoretical model for the proposed system and analytically solved it to evaluate the performance of our scheme. The effects of the pulse shape distortion, the spontaneous emission of the trapped atom, and the random variation of the atom-cavity coupling rate were studied with our analytical solution to the dynamics of the system. We also presented two quantum circuits for the construction of optical controlled phase flip gate from the CSWAP gate and certain single qubit gate.

In the second part of this thesis, I presented our work on time evolving block decimation (TEBD) numercial studies of a general Hubbard model (GHM) in one-dimension. The ultracold atom experimental techniques have opened up possiblities of mimicing condensed matter physics with AMO systems under well-controlled configurations. Realization of various important model Hamiltonians, such as variations of the Hubbard model, in condensed matter physics and exploration of new physics with them are being actively pursued. Recently a general Hubbard model was proposed to describe the physics of strongly interacting fermions in an anisotropic optical lattice near a wide Feshbach resonance. To find out if anything new will be present in this GHM, we have implemented an infinite lattice version of the TEBD algo-

rithm and have tested its reliability extensively before applying it to the studies on GHM. The TEBD algorithm is an extension to DMRG and can be used to efficiently simulate dynamics as well as ground state properties of quantum lattice systems.

We studied ground state properties of the general Fermi-Hubbard model with repulsive on-site interaction and equal population for spin-up and spin-down species with our TEBD code. We have found that when hole-doped below half-filling the GHM system with significant particle assisted tunneling rates exhibits coexistence of quasi-long range superfluid and charge density wave orders, while close to half-filling spin orders are dominant at quasi-long range. This feature is qualitatively different from that of conventional Hubbard model, in which with repulsive on site interaction the dominant quasi-long range orders are always given by spin orders regardless of the filling fraction.

The general Hubbard model with attractive on-site interaction and unequal spin population was also studied with the TEBD algorithm. We have found that the particle assisted tunneling mechanisms in GHM could suppress the FFLO-type order which is supported by the conventional Hubbard model. At the same time, the particle assisted tunneling rates in GHM enhances the spin orders. Based on the local density approximation, we have also estimated the effect of particle density inhomogeneity on the system, which, for example, can be induced by the presence of an overall harmonic trapping potential in experiments. Our results indicate that the critical spin-polarization, below which one could find fully paired superfluid in the wings toward the edge of the trap, could be very small even with pretty strong on-site attractive interaction, as opposed to the prediction from the mean field calculation based on the Gaudin model.

The level of physical implementation of quantum information processing at current

stage is still far below the standard of large-scale fault-tolerant quantum computing, which is necessary for the execution of nontrivial tasks intractable with classical computers. There is no doubt that theoretical and experimental pursuance of suitable QIP systems and schemes will go on for many years to come. As for classical simulation of quantum many-body system, there are many interesting physics in one-dimensional systems for one to study with the TEBD algorithm. Moreover, to access more interesting and more abundant physics in two-dimensional systems, implementation and test of existing ideas for 2D simulation as well as design of new algorithms are all good ways to go. In the following section, I will discuss some specific possible future directions, which are derived from our work presented in this thesis.

9.2 Future Directions

9.2.1 Quantum Optical Implementation of Quantum Information Processing with Cavity QED

Many theoretical proposals have been made along this direction. Nonetheless, for most of them the experimental realizations have not been achieved yet. For example, a controlled phase gate on two photonic qubits is of great importance, but until now there is only one proof-of-principle demonstration with weak coherent optical pulses achieved more than 10 years ago. Recently, a promising novel scheme for a photonic controlled phase flip gate based on conditional photon scattering from an atom-cavity system was proposed [56]. In this thesis, we have also presented a CSWAP gate scheme with similar basic idea, from which in principle one can also construct a photonic CPF gate. However, both schemes require multiple scattering of photon pulses with cavity systems and coherent single-qubit operations on either trapped atom or photon pulses in between, which could impose a lot of extra complexities for experimental realization. Therefore a more direct design of photon-photon interac-

tion in optical cavity QED system is still in order to relax the stringent requirements on experimental techniques. Another possible direction would be theoretical proposals for simulating strongly correlated quantum many-body physics by engineering effective interactions between atoms or photons with arrays of cavities. If model Hamiltonians which can exhibit topological orders could be devised, one could even further pursue possibilities of topological quantum computation with cavity QED systems.

9.2.2 Efficient Classical Simulation of Quantum Many-body Physics

We have implemented a TEBD algorithm, which works efficiently in a reliable manner. However in this thesis we have only explored the ground state physics of the general Hubbard model in very limited parameter regimes. Therefore, the most direct further study along this direction would be applying the TEBD code (possibly together with other methods) to obtain the complete phase diagram for the 1D general Hubbard model as given by Eqs (7.1) and (8.1) [160, 161]. Furthermore, the TEBD algorithm is a powerful tool for simulation of quantum dynamics of lattice systems. For example, one could directly apply the algorithm to simulate the time evolution of interesting states of matter such as the FFLO state, etc in optical lattice systems. Finally, people are also very interested in strongly interacting quantum many-body systems with disorders. For example, in bosonic systems, disorders could lead to interesting glassy states of matter, while for fermionic systems, the Anderson localization due to disorder is of great interests. Fortunately, with some straightforward extension, the TEBD algorithm can be applied to study the effect of disorders on such systems in one-dimension.

With experiences in TEBD numerical simulations, one may further pursue implementations of more complicated two-dimensional algorithms proposed recently from

the perspectives of quantum information theory. The implementation of these algorithms could test the validity of their basic ideas and deepen our understanding on classifications of quantum entanglement, as well as allow important studies on certain interesting 2D physical systems. A long term goal along this direction would be to develop efficient classical algorithms which enable us to fully understand the physics of the 2D Hubbard model as well as the physics of fractional quantum Hall systems.

BIBLIOGRAPHY

BIBLIOGRAPHY

[1] R. P. Feynman, "Simulating physics with computers", *Int. J. Theor. Phys.* **21**, 467 (1982).

[2] P. W. Shor, "Algorithms for Quantum Computation: Discrete Logarithms and Factoring", In *Proc. 35th Annual Symposium on Foundations of Computer Science* (IEEE Press, New York, 1994).

[3] L. K. Grover, "Quantum mechanics helps in searching for a needle in a haystack", *Phys. Rev. Lett.* **79**, 325 (1997).

[4] C. H. Bennett and G. Brassard, "Public key distribution and coin tossing", in *Proceedings of the IEEE International Conference on Computers, Systems, and Signal Processing* (IEEE Press, New York, 1984).

[5] A. K. Ekert, "Quantum cryptography based on Bells theorem", *Phys. Rev. Lett.* **67**, 661 (1991).

[6] C. H. Bennett, "Quantum cryptography using any two nonorthogonal states", *Phys. Rev. Lett.* **68**, 3121 (1992).

[7] C. Monroe, "Quantum information processing with atoms and photons ", *Nature* **416**, 238 (2002).

[8] Y. Makhlin, Gerd Schön, A. Shnirman, "Quantum-state engineering with Josephson-junction devices", Rev. Mod. Phys. 73, 357 (2001).

[9] *Experimental Quantum Computation and Information*, edited by F. De Martini and C. Monroe (IOS Press, Amsterdam, 2002).

[10] G. Vidal, "Efficient Classical Simulation of Slightly Entangled Quantum Computations", *Phys. Rev. Lett.* **91**, 147902 (2003).

[11] G. Vidal, "Efficient simulation of one-dimensional quantum many-body systems", *Phys. Rev. Lett.* **93**, 040502 (2004).

[12] A. J. Daley, C. Kollath, U. Schollwöck, and G. Vidal, "Time-dependent density-matrix renormalization-group using adaptive effective Hilbert spaces", *J. Stat. Mech.: Theor. Exp.*, P04005 (2004).

[13] F. Verstraete and J. I. Cirac, "Renormalization algorithms for quantum-many body systems in two and higher dimensions", arXiv:cond-mat/0407066 (2004).

[14] Y. Y. Shi, L. M. Duan, and G. Vidal, "Classical simulation of quantum many-body systems with a tree tensor network", *Phys. Rev. A* **74**, 022320 (2006).

[15] G. Vidal, "Classical simulation of infinite-size quantum lattice systems in one spatial dimension", *Phys. Rev. Lett.* **98**, 070201 (2007).

[16] G. Vidal, "Simulation of time evolution with multiscale entanglement renormalization ansatz", *Phys. Rev. A* **77**, 052328 (2008).

[17] J. Jordan, R. Orus, G. Vidal, F. Verstraete, J. I. Cirac , "Classical simulation of infinite-size quantum lattice systems in two spatial dimensions", arXiv:cond-mat/0703788 (2007).

[18] A. S. Holevo, "Some estimates for information quantity transmitted by quantum communication channel", *Probl. Pereda. Inf.* **9**, 3 (1973).

[19] D. P. DiVincenzo, "Two-bit gates are universal for quantum computation", *Phys. Rev. A* **51**, 1015 (1995).

[20] C. H. Bennett, G. Brassard, C. Crépeau, R. Jozsa, A. Peres, and W. K. Wootters, "Teleporting an unknown quantum state via dual classical and Einstein-Podolsky-Rosen channels", *Phys. Rev. Lett.* **70**, 1895 (1993).

[21] C. Bennett and S.J. Wiesner, "Communication via one- and two-particle operators on Einstein-Podolsky-Rosen states", *Phys. Rev. Lett.* **69**, 2881 (1992).

[22] A. Einstein, B. Podolsky, and N. Rosen, "Can Quantum-Mechanical Description of Physical Reality Be Considered Complete?",*Phys. Rev.* **47**, 777 (1935).

[23] J.S. Bell, "On the Einstein-Poldolsky-Rosen paradox", *Physics* **1**, 195 (1964).

[24] R. F. Werner, "Quantum states with Einstein-Podolsky-Rosen correlations admitting a hidden-variable model", *Phys. Rev. A* **40**, 4277 (1989).

[25] M. Horodecki, P. Horodecki, R. Horodecki, "Separability of mixed states: necessary and sufficient conditions", *Phys. Lett. A* **223**, 1 (1996).

[26] C. H. Bennett, H. J. Bernstein, S. Popescu, B. Schumacher, "Concentrating partial entanglement by local operations", *Phys. Rev. A* **53**, 2046 (1996).

[27] V. Vedral and M. B. Plenio, "Entanglement measures and purification procedures", *Phys. Rev. A* **57**, 1619 (1998).

[28] J. Eisert and M. B. Plenio, "Introduction to the basics of entanglement theory in continuous-variable systems", *Int. J. Quant. Inf.* **1**, 479 (2003).

[29] W. H. Zurek, "Decoherence and the transition from quantum to classical - REVISITED", arXiv:quant-ph/0306072 (2003).

[30] P. W. Shor, "Fault-tolerant quantum computation", in *Proc. 35th Ann. Symp. on Fundamentals of Computer Science* (IEEE Press, Los Alamitos, 1996).

[31] A. M. Steane, "Multiple particle interference and quantum error correction", *Proc. Roy. Soc. London A* **452**, 2551 (1996).

[32] D. Gottesman, "Class of quantum error correcting codes saturating the quantum Hamming bound", *Phys. Rev. A* **54**, 1862 (1996).

[33] A. R. Calderbank, E. M. Rains, P. W. Shor, and N. J. A. Sloane, "Quantum error correction via codes over GF(4)", *IEEE Trans. Inform. Theory* **44**, 1369 (1998).

[34] E. Knill, R. Laflamme, and W. H. Zurek, "Resilient quantum computation", *Science* **279**, 342 (1998).

[35] L.-M. Duan and G.-C. Guo, "Preserving coherence in quantum computation by pairing quantum bits", *Phys. Rev. Lett.* **79**, 1953 (1997).

[36] E. Farhi, J. Goldstone, S. Gutmann, J. Lapan, A. Lundgren, and D. Preda, "A Quantum Adiabatic Evolution Algorithm Applied to Random Instances of an NP-Complete Problem", *Science* **292**, 472 (2001).

[37] E. Farhi, J. Goldstone, S. Gutmann, and M. Sipser, "Quantum Computation by Adiabatic Evolution ", arXiv:quant-ph/0001106 (2000).

[38] S. Das Sarma, M. Freedman, C. Nayak, S. H. Simon, A. Stern, "Non-Abelian anyons and topological quantum computation", arXiv:0707.1889 (2007).

[39] L. M. K. Vandersypen, M. Steffen, G. Breyta, C. S. Yannoni1, M. H. Sherwood, and I. L. Chuang, "Experimental realization of Shor's quantum factoring algorithm using nuclear magnetic resonance", *Nature* **414**, 883 (2001).

[40] L. M. K. Vandersypen and M. Steffen, "Implementation of a three-quantum-bit search algorithm", *Appl. Phys. Lett.* **76**, 646 (2000).

[41] K. A. Brickman, P. C. Haljan, P. J. Lee, M. Acton, L. Deslauriers, and C. Monroe, "Implementation of Grovers quantum search algorithm in a scalable system", *Phys. Rev. A* **72**, 050306 (2005).

[42] J. I. Cirac and P. Zoller, "Quantum computations with cold trapped ions", *Phys. Rev. Lett.* **74**, 4091 (1995).

[43] F. Schmidt-Kaler, H. Häffner, M. Riebe, S. Gulde, G.P.T. Lancaster, T. Deuschle, C. Becher, C.F. Roos, J. Eschner, and R. Blatt, "Realization of the Cirac-Zoller controlled-NOT quantum gate", *Nature* **422**, 408 (2003).

[44] D. Leibfried, B. DeMarco, V. Meyer, D. Lucas, M. Barrett, J. Britton, W.M. Itano, B. Jelenkovic, C. Langer, T. Rosenband, and D.J. Wineland, "Experimental demonstration of a robust, high-fidelity geometric two ion-qubit phase gate," *Nature* **422**, 412 (2003).

[45] B.B. Blinov, D.L. Moehring, L.-M. Duan, and C. Monroe, "Observation of entanglement between a single trapped atom and a single photon," *Nature* **428**, 153 (2004).

[46] J. M. Raimond, M. Brune, and S. Haroche, "Colloquium: Manipulating quantum entanglement with atoms and photons in a cavity", *Rev. Mod. Phys.* **73**, 565 (2001).

[47] Q. A. Turchette, C. J. Hood, W. Lange, H. Mabuchi, and H. J. Kimble, "Measurement of conditional phase shifts for quantum logic", *Phys. Rev. Lett.* **75**, 4710 (1995).

[48] X. X. Yi, X. H. Su, and L. You, "Conditional quantum phase gate between two 3-state atoms", *Phys. Rev. Lett.* **90**, 097902 (2003).

[49] L.-M. Duan, B. Wang, and H. J. Kimble, *Phys. Rev. A* **72**, 032333 (2005).

[50] I. H. Deutsch, G.K. Brennen, and P.S. Jessen, "Quantum computing with neutral atoms in an optical lattice", *Fortschr. Phys.* **48**, 925(2000).

[51] G. K. Brennen, C.M. Caves, P.S. Jessen, and I.H. Deutsch, "Quantum logic gates in optical lattices", *Phys. Rev. Lett.* **82**, 1060 (1999).

[52] D. Jaksch, J.I. Cirac, P. Zoller, S.L. Rolston, R. Cote, and M.D. Lukin, "Fast quantum gates for neutral atoms", *Phys. Rev. Lett.* **85**, 2208 (2000).

[53] D. Jaksch, H.-J. Briegel, J.I. Cirac, C.W. Gardiner, and P. Zoller, "Entanglement of atoms via cold controlled collisions", *Phys. Rev. Lett.* **82**, 1975 (1999).

[54] E. Knill, R. Laflamme, and G. Milburn, "A scheme for efficient linear optics quantum computation", *Nature* **409**, 46 (2001).

[55] D. Bouwmeester, J.-W. Pan, K. Mattle, M. Eibl, H. Weinfurter, and A. Zeilinger, "Experimental quantum teleportation", *Nature* **390**, 575 (1997).

[56] L.-M. Duan and H. J. Kimble, "Scalable photonic quantum computation through cavity-assisted interactions", *Phys. Rev. Lett.* **92**, 127902 (2004).

[57] D. Loss and D. DiVincenzo, "Quantum computation with quantum dots", *Phys. Rev. A* **57**, 120 (1998)

[58] J. A. Gupta, R. Knobel, N. Samarth, and D. D. Awschalom, "Ultrafast manipulation of electron spin coherence", *Science* **292**, 2458 (2001).

[59] X.-Q. Li, Y.-W. Wu, D. G. Steel, D. Gammon, T. H. Stievvator, D. S. Katzer, D. Park, C. Piermarocchi, and L. J. Sham, "An all-optical quantum gate in a semiconductor quantum dot", *Science* **301**, 809 (2003).

[60] M. Atatüre, J. Dreiser, A. Badolato, A. Högele, K. Karrai, and A. Imamoglu, "Quantum-dot spin-state preparation with near-unity fidelity", *Science* **312**, 551 (2006).

[61] J. M. Taylor, H.-A. Engel, W. Dur, A. Yacoby, C. M. Marcus, P. Zoller, and M. D. Lukin, " Fault-tolerant architecture for quantum computation using electrically controlled semiconductor spins", *Nature Physics* **1**, 177 (2005).

[62] Y. Nakamura, Y. A. Pashkin, and J. S. Tsai, "Coherent control of macroscopic quantum states in a single-Cooper-pair box", *Nature* **398**, 786 (1999).

[63] C. H. van der Wal, A. C. J. ter Haar, F.K. Wilhelm, R. N. Schouten, C. J. P. M. Harmans, T. P. Orlando, S. Lloyd, and J. E. Mooij, "Quantum superposition of macroscopic persistentcurrent states", *Science* **290**, 773 (2000).

[64] M. V. Gurudev Dutt, L. Childress, L. Jiang, E. Togan, J. Maze, F. Jelezko, A. S. Zibrov, P. R. Hemmer, and M. D. Lukin, "Quantum register based on individual electronic and nuclear spin qubits in diamond", *Science* **316**, 1312 (2007).

[65] R. Folman, P. Krueger, D. Cassettari, B. Hessmo, T. Maier, and J. Schmiedmayer, "Controlling cold atoms using nanofabricated surfaces: Atom chips", *Phys. Rev. Lett.* **84**, 4749 (2000).

[66] D. Stick, W. K. Hensinger, S. Olmschenk, M. J. Madsen, K. Schwab, and C. Monroe, "Ion trap in a semiconductor chip", *Nature Physics* **2**, 36 (2006).

[67] A. Sørensen and K. Mølmer, "Quantum computation with ions in thermal motion", *Phys. Rev. Lett.* **82**, 1971 (1999).

[68] L.-M. Duan "Scaling Ion trap quantum computation through fast quantum gates ", *Phys. Rev. Lett.* **93**, 100502 (2004).

[69] J. I. Cirac and P. Zoller, "A scalable quantum computer with ions in an array of microtraps", *Nature* **404**, 579 (2000).

[70] D. Kielpinski, C. Monroe, and D.J. Wineland, "Architecture for a large-scale ion-trap quantum computer", *Nature* **417**, 709 (2002).

[71] H. Haäfner, W. Hänsel, C. F. Roos, J. Benhelm, D. Chek-al-kar, M. Chwalla, T. Körber, U. D. Rapol, M. Riebe, P. O. Schmidt, C. Becher, O. Gühne, W. Dür, and R. Blatt, "Scalable multiparticle entanglement of trapped ions", *Nature* **438**, 643 (2005).

[72] *Cavity Quantum Electrodynamics*, edited by P. R. Berman (Academic Press, New York, 1994).

[73] D. Jaksch, C. Bruder, J. I. Cirac, C. W. Gardiner, and P. Zoller, "Cold bosonic atoms in optical lattices", *Phys. Rev. Lett.* **81**, 3108 (1998).

[74] M. Greiner, O. Mandel, T. Esslinger, T. W. Hänsch, and I. Bloch, "Quantum phase transition from a superfluid to a Mott insulator in a gas of ultracold atoms", *Nature* **415**, 39 (2002).

[75] J.-W. Pan, D. Bouwmeester, M. Daniell, H. Weinfurter, A. Zeilinger, "Experimental test of quantum nonlocality in three-photon Greenberger-Horne-Zeilinger entanglement", *Nature* **403**, 515 (2000).

[76] Z. Zhao, Y.-A. Chen, A.-N. Zhang, T. Yang, H. J. Briegel, J.-W. Pan, "Experimental demonstration of five-photon entanglement and open-destination teleportation", *Nature* **430**, 54 (2004).

[77] Cirac, J.I., P. Zoller, H.J. Kimble, and H. Mabuchi, "Quantum state transfer and entanglement distribution among distant nodes in a quantum network", *Phys. Rev. Lett.* **78**, 3221C3224 (1997).

[78] A. Sørensen and K. Mølmer, "Probabilistic generation of entanglement in optical cavities ", *Phys. Rev. Lett.* **90**, 127903 (2003).

[79] B. Wang and L.-M. Duan, "Implementation scheme of controlled SWAP gates for quantum fingerprinting and photonic quantum computation", *Phys. Rev. A* **75**, 050304 (2007).

[80] A. Kuhn, M. Hennrich, T. Bondo, and G. Rempe, "Controlled generation of single photons from a strongly coupled atom-cavity system", *Appl. Phys. B* **69**, 373 (1999).

[81] C. K. Law and H.J. Kimble, "Deterministic generation of a bit-stream of single-photon pulses", *J. Mod. Opt.* **44**, 2067 (1997).

[82] W. Lange and H.J. Kimble, "Dynamic generation of maximally entangled photon multiplets by adiabatic passage", *Phys. Rev. A* **61**, 063817 (2000).

[83] B. T. H. Varcoe, S. Brattke, M. Weidinger, and H. Walther, "Preparing pure photon number states of the radiation field", *Nature* **403**, 743 (2000).

[84] P. Bertet, S. Osnaghi, P. Milman, A. Auffeves, P. Maioli, M. Brune, J.M. Raimond, and S. Haroche, "Generating and probing a two-photon Fock state with a single atom in a cavity", *Phys. Rev. Lett.* **88**, 143601 (2002).

[85] A. Kuhn, M. Hennrich, and G. Rempe, "Deterministic single-photon source for distributed quantum networking", *Phys. Rev. Lett.* **89**, 067901 (2002).

[86] J. McKeever, A. Boca, A.D. Boozer, R. Miller, J.R. Buck, A. Kuzmich, and H.J. Kimble, "Deterministic generation of single photons from one atom trapped in a cavity", *Science* **303**, 1992 (2004).

[87] B. Wang and L.-M. Duan, "Engineering superpositions of coherent states in coherent optical pulses through cavity-assisted interaction", *Phys. Rev. A* **72**, 022320 (2005).

[88] U. Schollwöck, "The density-matrix renormalization group ", *Rev. Mod. Phys.* **77**, 259 (2005).

[89] S. R. White, "Density matrix formulation for quantum renormalization groups", *Phys. Rev. Lett.* **69**, 2863 (1992).

[90] A. Osterloh, Luigi Amico, G. Falci, and R. Fazio, "Scaling of entanglement close to a quantum phase transition", *Nature* **416**, 608 (2002).

[91] T. J. Osborne, M. A. Nielsen, "Entanglement in a simple quantum phase transition", *Phys. Rev.A* **66**, 032110(2002).

[92] T. R. Olivaira, G. Rigolin, and M. C. de Oliveira , "Genuine multipartite entanglement in quantum phase transitions", *Phys. Rev.A* **73**, 010305(R)(2006).

[93] J. I. Latorre, E. Rico, and G. Vidal, "Ground state entanglement in quantum spin chains", *Quantum Inf. Comput.* **4**, 48 (2004).

[94] B. Wang and L.-M. Duan, "Superfluidity of fermions with repulsive on-site interaction in an anisotropic optical lattice near a Feshbach resonance", *N. J. Phys.* **10**, 073007 (2008).

[95] B. Wang and L.-M. Duan, to be submitted.

[96] E. W. Carlson, V. J. Emery, S. A. Kivelson, and D. Orgad, "Concepts in high temperature superconductivity", in *The physics of superconductors* (Springer, Berlin, 2003).

[97] J. McKeever, J. R. Buck, A. D. Boozer, A. Kuzmich, H.-C. Nägerl, D. M. Stamper-Kurn, and H. J. Kimble, "State-insensitive cooling and trapping of single atoms in an optical cavity", *Phys. Rev. Lett.* **90**, 133602 (2003).

[98] C. J. Hood, T. W. Lynn, A. C. Doherty, A. S. Parkins, and H. J. Kimble, "The atom-cavity microscope: single atoms bound in orbit by single photons", *Science* **287**, 1447 (2000).

[99] T.W. H. Pinkse, T. Fischer, P. Maunz, and G. Rempe, "Trapping an atom with single photons ", *Nature* **404**, 365 (2000).

[100] R. Grimm, M. Weidemller, and Y. B. Ovchinnikov, "Optical dipole traps for neutral atoms", *Adv. At. Mol. Opt. Phys.* **42**, 95 (2000).

[101] J. Ye, D. W. Vernooy, and H. J. Kimble, "Trapping of single atoms in cavity QED", *Phys. Rev. Lett.* **83**, 4987 (1999).

[102] H. J. Kimble, "Strong interactions of single atoms and photons in cavity QED", *Phys. Scr.* **T76**, 127 (1998).

[103] C. J. Hood, M. S. Chapman, T. W. Lynn, and H. J. Kimble, "Real-time cavity QED with single atoms", *Phys. Rev. Lett.* **80**, 4157 (1998).

[104] E. T. Jaynes and F. W. Cummings, "Comparison of quantum and semiclassical radiation theory with application to the beam maser", *Proc. IEEE* **51**, 89 (1963).

[105] H. J. Kimble, "Structure and dynamics in cavity quantum electrodynamics", in Cavity Quantum Electrodynamics, P. Berman ed. (Academic Press, San Diego, 1994), pp. 203-266.

[106] D. J. Heinzen, J. J. Childs, J. E. Thomas, and M. S. Feld, "Enhanced and inhibited visible spontaneous emission by atoms in a confocal resonator", *Phys. Rev. Lett.* **58**, 1320 (1987).

[107] S. E. Morin, C. C. Yu, and T. W. Mossberg, "Strong atom-cavity coupling over large volumes and the observation of subnatural intracavity atomic linewidths", *Phys. Rev. Lett.* **73**, 1489 (1994).

[108] E. Schrödinger, "Quantum theory and measurement", *Naturwiss.* **23**, 807 (1935).

[109] C. Monroe, D.M. Meekhof, B.E. King, D.J. Wineland, "A "Schrödinger cat" superposition state of an atom", *Science* **272**, 1131 (1996).

[110] V. Buzek, A. Vidiella-Barranco, and P. L. Knight, "Superpositions of coherent states: Squeezing and dissipation", *Phys. Rev. A* **45**, 6570 (1992).

[111] T. C. Ralph, A. Gilchrist, and G. J. Milburn, "Quantum computation with optical coherent states", *Phys. Rev. A* **68**, 042319 (2003).

[112] H. Jeong, M. S. Kim, and J. Lee, "Quantum-information processing for a coherent superposition state via a mixedentangled coherent channel", *Phys. Rev. A* **64**, 052308 (2001).

[113] S. J. van Enk and O. Hirota, "Entangled coherent states: Teleportation and decoherence", *Phys. Rev. A* **64**, 022313 (2001).

[114] S. Glancy, H. M. Vasconcelos, and T. C. Ralph, "Transmission of optical coherent-state qubits", *Phys. Rev. A* **70**, 022317 (2004).

[115] J. A. Dunningham and K. Burnett, and Stephen M. Barnett, "Interferometry below the Standard Quantum Limit with Bose-Einstein Condensates", Phys. Rev. Lett. 89, 150401 (2002).

[116] V. Buzek, and P. L. Knight, "Quantum interference, superposition states of light, and nonclassical effects", *Progress in Optics*, vol. **XXXIV**, edited by E. Wolf (North Holland, Amsterdam, 1995).

[117] G. M. D'Ariano, M. F. Sacchi, and P. Kumar, "Tomographic measurements of nonclassical radiation states", *Phys. Rev. A* **59**, 826 (1999).

[118] M. Brune, E. Hagley, J. Dreyer, X. Maître, A. Maali, C. Wunderlich, J. M. Raimond, and S. Haroche, "Observing the progressive decoherence of the "meter" in a quantum measurement", *Phys. Rev. Lett.* **77**, 4887 (1996).

[119] A. Ourjoumtsev, R. Tualle-Brouri, J. Laurat, and P. Grangier, "Generating Optical Schrödinger Kittens for Quantum Information Processing", *Science* **312**, 83 (2006).

[120] E. Solano, G. S. Agarwal, and H. Walther, "Strong-driving-assisted multipartite entanglement in cavity QED", *Phys. Rev. Lett.* **90**, 027903 (2003).

[121] S. J. van Enk, "Entanglement capabilities in infinite dimensions: multidimensional entangled coherent states", *Phys. Rev. Lett.* **91**, 017902 (2003).

[122] K. M. Gheri and H. Ritsch, "Single-atom quantum gate for light", *Phys. Rev. A* **56**, 3187 (1997).

[123] S. Song, C. M. Caves, and B. Yurke, "Generation of superpositions of classically distinguishable quantum states from optical back-action evasion", *Phys. Rev. A* **41**, 5261 (1990).

[124] A. P. Lund, H. Jeong, T. C. Ralph, and M. S. Kim, "Conditional production of superpositions of coherent states with inefficient photon detection", *Phys. Rev. A* **70**, 020101(R) (2004).

[125] J. McKeever, A. Boca, A. D. Boozer, J. R. Buck, H. J. Kimble, "Experimental Realization of a One-Atom Laser in the Regime of Strong Coupling", *Nature* **425**, 268 (2003).

[126] G. R. Guthöhrlein, M. Keller, K. Hayasaka, W. Lange, and H. Walther, "A single ion as a nanoscopic probe of an optical field ", *Nature* **414**, 49 (2001).

[127] J. Wenger, M. Hafezi, F. Grosshans, R. Tualle-Brouri, and P. Grangier, "Maximal violation of Bell inequalities using continuous-variable measurements", *Phys. Rev. A* **67**, 012105 (2003).

[128] D. Gottesman, A. Kitaev, J. Preskill, "Encoding a qubit in an oscillator", *Phys.Rev. A* **64**, 012310 (2001).

[129] D. F. Walls and G. J. Milburn, *Quantum Optics* (Springer-Verlag, Berlin, 1994).

[130] L.-M. Duan, A. Kuzmich, H. J. Kimble, "Cavity QED and quantum-information processing with "hot" trapped atoms", *Phys. Rev. A*, **67**, 032305 (2003).

[131] T. Pellizzari, S. A. Gardiner, J. I. Cirac, and P. Zoller, "Decoherence, continuous observation, and quantum computing: a cavity QED model", *Phys. Rev. Lett.* **75**, 3788 (1995).

[132] J. A. Sauer, K. M. Fortier, M. S. Chang, C. D. Hamley, and M. S. Chapman, "Cavity QED with optically transported atoms", *Phys. Rev. A* **69**, 051804 (2004).

[133] P. Maunz, T. Puppe, I. Schuster, N. Syassen, P. W. H. Pinkse, G. Rempe, "Cavity cooling of a single atom", *Nature* **428**, 50 (2004).

[134] J. McKeever, J. R. Buck, A. D. Boozer, and H. J. Kimble, Phys. Rev. Lett. **92**, 143601 (2004).

[135] A. Boca, R. Miller, K. M. Birnbaum, A. D. Boozer, J. McKeever, and H. J. Kimble, "Observation of the vacuum Rabi spectrum for one trapped atom", *Phys. Rev. Lett.* **93**, 233603 (2004).

[136] P. Maunz, T. Puppe, I. Schuster, N. Syassen, P. W. H. Pinkse, and G. Rempe, "Normal-mode spectroscopy of a single-bound-atomCcavity system", *Phys. Rev. Lett.* **94**, 033002 (2005).

[137] M. Keller, B. Lange, K. Hayasaka, W. Lange, and H. Walther, "Continuous generation of single photons with controlled waveform in an ion-trap cavity system ", *Nature* **431**, 1075 (2004).

[138] A. Kreuter, C. Becher, G. P. T. Lancaster, A. B. Mundt, C. Russo, H. Häffner, C. Roos, J. Eschner, F. Schmidt-Kaler, and R. Blatt, "Spontaneous emission lifetime of a single trapped $\mathbf{Ca}^+$ ion in a high finesse cavity", *Phys. Rev. Lett.* **92**, 203002 (2004).

[139] M.A. Rowe, A. Ben-Kish, B. DeMarco, D. Leibfried, V. Meyer, J. Beall, J. Britton, J. Hughes, W.M. Itano, B. Jelenkovic, C. Langer, T. Rosenband, and D.J. Wineland, "Transport of quantum states and separation of ions in a dual RF ion trap", *Quant. Inf. Comp.* **2**, 257 (2002).

[140] S. Kuhr, W. Alt, D. Schrader, I. Dotsenko, Y. Miroshnychenko, W. Rosenfeld, M. Khudaverdyan, V. Gomer, A. Rauschenbeutel, and D. Meschede, "Coherence properties and quantum state transportation in an optical conveyor belt", *Phys. Rev. Lett.* **91**, 213002 (2003).

[141] L.-M. Duan and R. Raussendorf, "Efficient quantum computation with probabilistic quantum gates", *Phys. Rev. Lett.* **95**, 080503 (2005).

[142] S. D. Barrett and P. Kok, "Efficient high-fidelity quantum computation using matter qubits and linear optics", *Phys. Rev. A* **71**, 060310(R) (2005).

[143] D. Schrader, I. Dotsenko, M. Khudaverdyan, Y. Miroshnychenko, A. Rauschenbeutel, and D. Meschede, "Neutral Atom Quantum Register", *Phys. Rev. Lett.* **93**, 150501 (2004).

[144] M.A. Nielsen and I.L. Chuang, *Quantum Computation and Quantum Information* (Cambridge University Press, Cambridge, 2000).

[145] H. Buhrman, R. Cleve, J. Watrous, and R. de Wolf, "Quantum fingerprinting", *Phys. Rev. Lett.* **87**, 167902 (2001).

[146] D. Gottesman and I. Chuang, "Quantum digital signatures", arXiv:quant-ph/0105032 (2001).

[147] A. Imamoglu, D. D. Awschalom, G. Burkard, D. P. DiVincenzo, D. Loss, M. Sherwin, and A. Small, "Quantum information processing using quantum dot spins and cavity QED", *Phys. Rev. Lett.* **83**, 4204 (1999).

[148] E. Waks and J. Vuckovic, "Dipole induced transparency in drop-filter cavity-waveguide systems", *Phys. Rev. Lett.* **96**, 153601 (2006).

[149] A. Badolato, K. Hennessy, M. Atatüre, J. Dreiser, E. Hu, P. M. Petroff, and A. Imamoglu, "Deterministic coupling of single quantum dots to single nanocavity modes ", *Science* **308**, 1158 (2005).

[150] J. P. Reithmaier, G. Sęk, A. Löffler, C. Hofmann, S. Kuhn, S. Reitzenstein, L. V. Keldysh, V. D. Kulakovskii, T. L. Reinecke, and A. Forchel, "Strong coupling in a single quantum dot-semiconductor microcavity system", *Nature* 432, 197 (2004).

[151] T. Yoshie, A. Scherer, J. Hendrickson, G. Khitrova, H. M. Gibbs, G. Rupper, C. Ell, O. B. Shchekin, D. G. Deppe, "Vacuum Rabi splitting with a single quantum dot in a photonic crystal nanocavity", *Nature* **432**, 200 (2004).

[152] J. Vučković, D. Fattal, C. Santori, G. S. Solomon, Y. Yamamoto, "Enhanced single-photon emission from a quantum dot in a micropost microcavity", *Appl. Phys. Lett.* **82**, 3596 (2003).

[153] L-M. Duan, J.I. Cirac, P. Zoller, and E. S. Polzik, "Quantum communication between atomic ensembles using coherent light", *Phys. Rev. Lett.* **85**, 5643 (2000).

[154] E. Knill, R. Laflamme, and G. J. Milburn, "Thresholds for linear optics quantum computation", arXiv:quant-ph/0006120 (2000).

[155] W. M. C. Foulkes, L. Mitas, R. J. Needs, and G. Rajagopal, "Quantum Monte Carlo simulations of solids", *Rev. Mod. Phys.* **73**, 33 (2001).

[156] M. P. A. Fisher, P. B. Weichman, G. Grinstein, and D. S. Fisher, *Phys. Rev. B* **40**, 546 (1989).

[157] M. Suzuki, "General decomposition theory of exponential operators", in *Quantum Monte Carlo methodsin condensed matter physics* edited by M. Suzuki (World Scientific, Singapore, 1993).

[158] J. K. Chin, D. E. Miller, Y. Liu, C. Stan, W. Setiawan, C. Sanner, K. Xu, W. Ketterle, "Evidence for superfluidity of ultracold fermions in an optical lattice ", *Nature* **443**, 961 (2006).

[159] T. Stöferle, H. Moritz, K. Günter, M. Köhl, and T. Esslinger, "Molecules of fermionic atoms in an optical lattice", *Phys. Rev. Lett.* **96**, 030401 (2006).

[160] L.-M. Duan, "Effective Hamiltonian for fermions in an optical lattice across a feshbach resonance", *Phys. Rev. Lett.* **95**, 243202 (2005).

[161] L.-M. Duan, "General Hubbard model for strongly interacting fermions in an optical lattice and its phase detection", arXiv:0706.2161 (2007).

[162] V.W. Scarola, E. Demler, S. Das Sarma, "Searching for a supersolid in cold-atom optical lattices", *Phys. Rev. A* **73**, 051601(R) (2006).

[163] X.-L. Gao, M. Rizzi, M. Polini, R. Fazio, M. P. Tosi, V. L. Campo, Jr., and K. Capelle, "Luther-Emery phase and atomic-density waves in a trapped fermion gas", *Phys. Rev. Lett.* **98**, 030404 (2007).

[164] F. K. Pour, M. Rigol, S. Wessel, and A. Muramatsu, "Supersolids in confined fermions on one-dimensional optical lattices", *Phys. Rev. B* **75**, 161104(R) (2007).

[165] A. Feiguin and F. Heidrich-Meisner, "Pairing states of a polarized Fermi gas trapped in a one-dimensional optical lattice", *Phys. Rev. B* **76**, 220508(R) (2007).

[166] J. E. Hirsch, "Bond-charge repulsion and hole superconductivity", *Physica C* **158**, 326 (1989).

[167] R. Strack and D. Vollhardt, "Hubbard model with nearest-neighbor and bond-charge interaction: exact ground-state solution in a wide range of parameters", *Phys. Rev. Lett.* **70**, 2637 (1993).

[168] L. Arrachea and A. A. Aligia, "Exact solution of a Hubbard chain with bond-charge interaction", *Phys. Rev. Lett.* **73**, 2240 (1994).

[169] S. R. White and A. E. Feiguin, "Real-time evolution using the density matrix renormalization group", *Phys. Rev. Lett.* **93**, 076401 (2004).

[170] P. Jordan and E. Wigner, "Über das Paulische 'Aquivalenzverbot"', *Z. Phys.* **47**, 631 (1928).

[171] E. H. Lieb and F. Y. Wu, "Absence of Mott transition in an exact solution of the short-range, one-band model in one dimension", *Phys. Rev. Lett.* **20**, 1445 (1968).

[172] H. J. Schulz, "Correlated fermions in one dimension", *Int. J. Mod. Phys. B* **5**, 57 (1991).

[173] H. J. Schulz, "Correlation exponents and the metal-insulator transition in the one-dimensional Hubbard model", *Phys. Rev. Lett.* **64**, 2831 (1990).

[174] L. -M. Duan, "Detecting correlation functions of ultracold atoms through Fourier sampling of time-of-flight images", *Phys. Rev. Lett.* **96**, 103201 (2006).

[175] P. Fulde, and R. A. Ferrell, "Superconductivity in a strong spin-exchanged field", *Phys. Rev.* **135**, A550 (1964).

[176] A. I. Larkin, and Yu. N. Ovchinnikov, "Inhomogeneous state of superconductors (Production of superconducting state in ferromagnet with Fermi surfaces, examining Green function)", *Sov. Phys. JETP* **20**, 762 (1965).

[177] G. Sarma, "On the influence of a uniform exchange eld acting on the spins of the conduction electrons", *J. Phys. Chem. Solids*, **24**, 1029 (1963).

[178] M. W. Zwierlein, A. Schirotzek, C. H. Schunck, and W. Ketterle, "Fermionic superfluidity with imbalanced spin populations", *Science* **311**, 492 (2006).

[179] M. W. Zwierlein, C. H. Schunck, A. Schirotzek, and W. Ketterle, "Direct observation of the superfluid phase transition in ultracold Fermi gases", *Nature* **442**, 54 (2006).

[180] Y. Shin, M. W. Zwierlein, C. H. Schunck, A. Schirotzek, and W. Ketterle, "Observation of phase separation in a strongly interacting imbalanced Fermi gas", *Phys. Rev. Lett.* **97**, 030401 (2006).

[181] G. B. Partridge, W.-H. Li, R. I. Kamar, Y.-A. Liao, and R. G. Hulet, "Pairing and phase separation in a polarized Fermi gas ", *Science* **311**, 503 (2006).

[182] G. B. Partridge, W.-H. Li, Y.-A. Liao, R. G. Hulet, M. Haque, and H. T. C. Stoof, "Deformation of a trapped Fermi gas with unequal spin populations", *Phys. Rev. Lett.* **97**, 190407 (2006).

[183] K. Yang, "Inhomogeneous superconducting state in quasi-one-dimensional systems", *Phys. Rev. B* **63**, 140511(R) (2001).

[184] H. Hu, X.-J. Liu, and P. D. Drummond, "Phase diagram of a strongly interacting polarized fermi gas in one dimension", *Phys. Rev. Lett.* **98**, 070403 (2007).

[185] G. Orso, "Attractive fermi gases with unequal spin populations in highly elongated traps ", *Phys. Rev. Lett.* **98**, 070402 (2007).

[186] M. Tezuka and M. Ueda, "Density-Matrix Renormalization Group study of trapped imbalanced fermi condensates", *Phys. Rev. Lett.* **100**, 110403 (2008).

[187] M. Rizzi, M. Polini, M. A. Cazalilla, M. R. Bakhtiari, M. P. Tosi, and R. Fazio, "Fulde-Ferrell-Larkin-Ovchinnikov superfluidity in one-dimensional optical lattices", *Phys. Rev. B* **77**, 245105 (2008).

[188] G. G. Batrouni, M. H. Huntley, V. G. Rousseau, and R. T. Scalettar, "Exact numerical study of pair formation with imbalanced fermion populations", *Phys. Rev. Lett.* **100**, 116405 (2008).